ISSN : 2717 - 5022

JOURNAL ON GEOINFORMATICS

Nepal

Number: 25 Jestha 2083 (May 2026)

Annual Publication of Survey Department, Government of Nepal

Delegation members from Nepal and India during 7th the Boundary Working Group (BWG) meeting held in New Delhi, India

Training provided to Armed Police Force officers by the Survey Department at the APF Boundary Training Center, Nawalparasi (West)

Honourable Minister Prativa Rawal visiting the Survey Department

Delegation members from Nepal and India during 12th SOC meeting held in Kathmandu, Nepal, from 2-4 February 2026

Felicitation of Retired Officials of the Survey Department on the Occasion of the Department's 68th Anniversary

Deputy Director General Susheel Dangol participated in the Space2Earth Summit 2025, held in Tokyo, Japan, from 7-10 July 2025, as a representative of National Mapping Agency of Nepal.

Journal on Geoinformatics

Nepal

Number : 25

Jestha 2083 BS

May 2026 AD

Annual publication of Survey Department, Government of Nepal

Published by:
Government of Nepal
Ministry of Land Management, Cooperatives, Federal Affairs and General Administration
Survey Department
Min Bhawan, Kathmandu
Nepal

No. of copies : 400

FOREWORDS

It is with great pride and honor that the Survey Department presents the 25th Issue (Silver Jubilee Edition) of the Journal on Geoinformatics Nepal, the Department's respected annual publication. Marking twenty-five years since its inaugural publication in 2002, this commemorative issue celebrates the journal's continuous contribution to the advancement of geoinformatics, surveying, mapping, and spatial sciences in Nepal. Over the past quarter century, the journal has grown into a respected platform for knowledge exchange and scientific dissemination, documenting the evolution of Nepal's geospatial sector and strengthening the nation's geospatial knowledge base.

Geoinformatics has advanced rapidly, transforming how geospatial data is collected, analyzed, and applied in planning, environmental management, disaster response, and infrastructure development. As Nepal embraces digital transformation, geospatial technology has become essential for evidence-based decision-making and innovation. In this context, the Survey Department, as the National Mapping Agency, remains committed to strengthening Nepal's geospatial foundation through modern land information systems, large-scale topographic mapping, and advanced technologies such as LiDAR, UAV, CORS, and digital geospatial platforms.

This Silver Jubilee Issue presents a rich collection of articles contributed by distinguished experts, researchers, and professionals. The papers featured in this edition reflect current developments and practical innovations in land surveying, GIS, remote sensing, spatial data management, land use planning, and emerging geospatial technologies. Together, these contributions reaffirm our shared commitment to scientific excellence, technological innovation, and sustainable development through geoinformatics.

On this special occasion, I extend my sincere gratitude to all who have contributed to the success and continuity of this journal over the past twenty-five years. I acknowledge the dedication of editors, editorial boards, authors, reviewers, readers, and well-wishers, whose collective support has shaped Journal on Geoinformatics Nepal into a valued academic and professional publication.

As we celebrate this occasion, we also look ahead with renewed commitment. I encourage researchers, professionals, and readers to continue contributing to this journal and to the wider growth of geoinformatics in Nepal and beyond.

Thank you for your continued support and invaluable contributions over these remarkable twenty-five years.

Enjoy Reading!
Thank you!

Prakash Joshi
Director General
lightjoshiji@gmail.com

EDITORIAL

Dear Readers,

Welcome to the 25th Issue (Silver Jubilee Edition) of the Journal on Geoinformatics Nepal.

The publication of this twenty-fifth issue marks a significant milestone in the journey of the journal. Since its inception in 2002, the journal has served as a dedicated platform for scholarly exchange, technical insight, and professional dialogue in the field of geoinformatics. Over the past twenty-five years, it has steadily documented the growth of geospatial science and contributed to the advancement of knowledge, innovation, and practice in discipline.

This Silver Jubilee Edition celebrates both continuity and progress. Over the years, the journal has recorded the transformation of geoinformatics—from conventional surveying and cartography to digital mapping, remote sensing, GIS, and emerging geospatial technologies. As the National Mapping Agency, the Survey Department has remained closely engaged in this transformation through mapping, land information modernization, and the adoption of modern geospatial technologies. In this context, the journal continues to serve as an important platform for documenting progress and encouraging professional discourse.

This issue presents articles from professionals, researchers, and academicians covering digital land administration, GIS applications, remote sensing, land use planning, and related innovations. These contributions reflect the growing relevance of geoinformatics in supporting national development and addressing contemporary challenges.

We extend our sincere gratitude to all the advisory board members, authors, reviewers, editorial team members, and readers who have contributed to the continuity and credibility of this journal over the past twenty-five years. We also acknowledge the continued support of the Survey Department in sustaining this publication as a valued platform for knowledge sharing and professional engagement.

As we celebrate this milestone, we reaffirm our dedication to strengthening this journal as a space for research, collaboration, and innovation in geoinformatics. We invite our readers to engage with this special edition and continue contributing to the growth of geospatial knowledge in Nepal.

Warm regards,

Karuna K.C.
Editor-in Chief,
Jestha, 2083 (May 2026)

Advisory Council

Prakash Joshi
Chairperson

Karuna K.C.
Member

Susheel Dangol
Member

Krishna Prasad Sapkota
Member

Narayan Regmi
Member

Editorial Board

Karuna K.C.
Editor-in-Chief

Kamal Ghimire
Member

Dayanand Joshi
Member

Bikash Kumar Karna (Ph.D.)
Member

Tina Baidar
Member

Journal on
GEOINFORMATICS
Nepal

Jestha 2083, May 2026
Number 25

Product Price

Cover Concept
Activities of Survey Department

Features

Articles

Contents

Contents

Contents

AI-Driven Window Detection and Semantic Segmentation from Street View Imagery Using Grounding DINO and DeepLabV3 for Digital Twin Modeling

Sumeer Koirala[1], Prof. Dr. Xiaoxiang Zhu[2], Dr.-Ing. Yao Sun[3], Mr. Alejandro Rueda Segura[2],
mailtosumeer@gmail.com, xiaoxiang.zhu@tum.de, yao.sun@dlr.de, alejandro.rueda@tum.de
[1]Survey department, [2]Technical University of Munich, [3]German Aerospace Center,

KEYWORDS

Deep learning, Semantic segmentation, Grounding DINO, DeepLabV3, Digital twins

ABSTRACT

AI-driven automated generation of façade information using street view images can be a vital step toward large-scale urban digital twin generation. Traditional approaches rely on rule-based methods and manual annotation, which poses a significant time lag and is difficult on a large scale. This study focused on a state-of-the-art AI-based pipeline for window detection from street view images and semantic segmentation for windows parameter generation. The proposed workflow consists of image rectification(correcting perspective distortion in street view images). Secondly, window regions are detected using a zero-shot object detection model(GroundingDINO) followed by semantic segmentation using a fine-tuned DeepLabV3 model trained on the WinSyn dataset. Through systematic experimentation with different parameters and hyperparameters, the optimization of label classes from 11 to 3 classes significantly improved segmentation performance. The refined model achieved a mean Intersection over Union (mIoU) of 80.74%, representing an improvement of 44.31% compared to the baseline performance of 36.43% obtained using four classes. This class optimization reduced ambiguity among window components and improved segmentation consistency. Segmentation outputs are further refined using morphological operations to improve frame continuity and remove noise in window panes. Geometric parameters such as pane arrangement, frame thickness, and window layout are extracted from the refined masks and structured into a parametric representation. The proposed pipeline demonstrates the potential of combining zero-shot detection and semantic segmentation for automated façade analysis from street-view imagery. The extracted window information can support applications in urban digital twin generation, building energy modeling, and large-scale architectural analysis.

1. INTRODUCTION

Window detection and reconstruction from street-view images is very challenging. There is a lot of complexity in architecture, design, and structure, and real-world styles. Traditional window reconstruction techniques like Laser scanning, surveying, and photogrammetry are quite time-consuming and costly. On

the other hand, traditional object detection and segmentation techniques require a large volume of data and annotated labels for desired performance, and it could be time-consuming and costly for training data creation or training data collection. CityGML 3.0 is an essential standard for the generation of high-quality and realistic digital twins of urban environments. Window reconstruction is one of the critical components for CityGML 3.0 data. On the other hand, a city like Munich is still utilizing CityGML 2.0 and looking forward to an upgrade. Although the upgrade is critical, manual ways of window extraction is labor intensive process when dealing with large city areas. Furthermore, existing methods are constrained by the need for a large amount of training labels and limited ability to handle the complex and diverse nature of real-world data/ images.

1.1 Research gap

Despite having AI-driven techniques for façade detection and segmentation, several limitations persist:

Dependence on Synthetic Data: Several methods heavily rely on large volumes of high-quality synthetic or procedural datasets, limiting scalability and reliability in complex, real-world environments (Kelly, et al., 2024).

Lack of Domain-Specific Frameworks: General object detection models exist, but frameworks tailored for window detection and reconstruction are scarce, especially for unlabeled or complex real-world data (Pang & Biljecki, 2022).

Simplified 2D-to-3D Window Models: Existing 2D-to-3D approaches often oversimplify window structures, failing to capture detailed geometries for accurate digital twins (Hu et al., 2022).

Limited Use of Street-View Imagery: Low-resolution street-view images are underutilized for 3D reconstruction, leaving opportunities to develop image-to-mesh pipelines for real-world window geometries.

2. STATE OF THE ART

Object detection and semantic segmentation are two strongly correlated tasks for visual recognition. These tasks are strongly correlated, but they are resolved as separate tasks using entirely different techniques (Dong, et al. 2014). Object detection is the task of formulating a bounding box to enclose an object of interest (Felzenszwalb, et al. 2009), whereas semantic segmentation assigns a label to each pixel from predefined classes or predefined labels (Carreira, et al. 2012). In this research, I am interested in applying object detection methods for detecting window frames in street view images utilizing the detected windows, labeling each pixel with Windows classes, and generating 3d Windows. Semantic segmentation and object detection are highly correlated tasks and can be used for mutually beneficial tasks like windows detection from street view images, semantically semantic images, and reconstruction of geometry.

On one hand object detection provides prior knowledge to object (e.g., Windows), which can be later used for refining semantic segmentation. On the other hand, semantic segmentation is capable of providing both local and global semantic information from detected

object (e.g., windows detected from street view image) (Peng, Nan et al. 2020).

2.1. Zero-shot object detection

Object detection can be termed as computer vision technique, which identifies objects, labels items within images, videos, or even live footage. The main task of object detection is to identify and locate single or multiple objects with reference to predefined categories from images. (Tang, Feng et al. 2017).

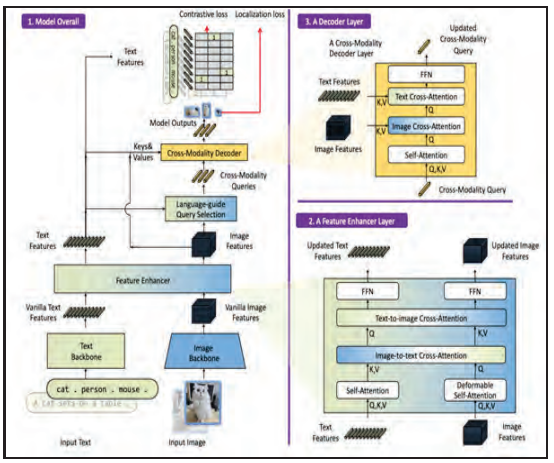

Figure 1: GroundingDINO architecture.

Zero shot learning (ZSL) is technique of identifying objects, even though training sets are not available. ZSL significantly tackles problem of data scarcity (Wang, Zhang et al. 2020). This approach mostly focuses on feature identification using concept of classification problem. Some of the significant challenges of ZSL are a) most of the ZSL benchmarks datasets mostly focuses on single dominant object in single image. Secondly, most of the ZSL are based on zero-shot classification method, which is not convenient to apply directly in the entire scene. Finally, ZSL fails to consider occlusion and clutters in real world scenarios (Li, Yao et al. 2019) Whereas Zero shot object detection (ZSoD) is techniques of simultaneously detection and localization of novel categories of object classes, even without the visual presence of those classes during the training phase. ZSoD can be utilized in variety of application ranging from ovel object localization, tracking and retrieval of object to determination of relationship of object with its environment only using either object name or natural language description (Rahman, et al. 2020).

2.2. You Only Look Once (YOLO) model

YOLO is an objection detection paradigm that works on the modality of utilizing object detection as regression problem, using spatially separated bounding boxes and associated class probabilities to detect objects. Whereas prior object detection model utilized repurpose classifiers to perform detection. YOLO model utilizes single neural network to predict bounding box around object of interest and predicts class probabilities directly using full image in single evaluation. Having the full detection pipelines using single network, hence it can be optimized directly on end-to end detection performance (Redmon 2016)

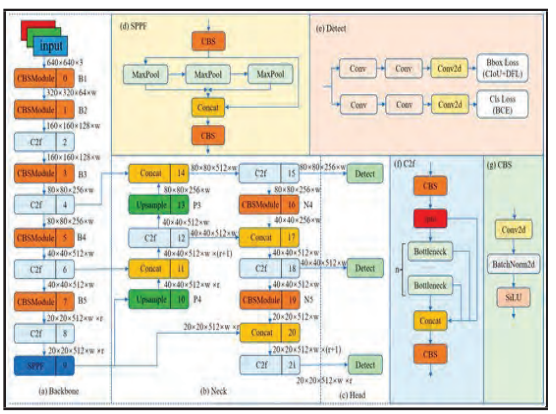

Figure 2: YOLOV8 model architecture. Source:(Wang, Chen et al. 2023)

2.3. Semantic segmentation

Semantic Segmentation (SS) can be defined as process of scene labelling, which is intended to assign a semantic label to each image pixel. One of the major challenges of SS is presence of multiple classes with higher degree of similarity between them (Yu, et al. 2018). SS provides category labels to each pixel, it is very beneficial for variety of tasks including self-driving, pedestrian detection, defect detection also geometry generation.(Hao, et al. 2020). SS was first termed in 1970 by (Ohta, et al. 1978) emphasizing on generation of semantically meaningful semantic regions. Lately, with advancement of deep learning techniques, research on SS has significantly advanced. Accuracy of segmentation has significantly increased with introduction of pioneering fully convolution network (FCN) by (Long, et al. 2015)

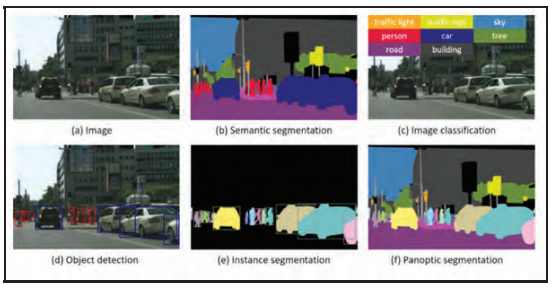

Figure 3: Different computer vision tanks. source : (Hao, et al. 2020)

2.4. Deeplabv3plus

Deeplabv3plus model is based on encoder-decoder method. This method uses different network forms and pyramid pooling modules to improve the accuracy of the network. Furthermore, representative algorithm is composed of Deeplab series(Liu, et al. 2024) and pyramid scene parsing network (PSPNet) (Sun and Wang 2018). Deeplab module perform spatial pyramid pooling at several grid scales or apply numerous atrous convolutions with varying rates. First component of deeplabv3plus network(Yang, et al. 2020) is backbone network. Backbone network extracts feature semantic information.(Wang, Li et al. 2019)

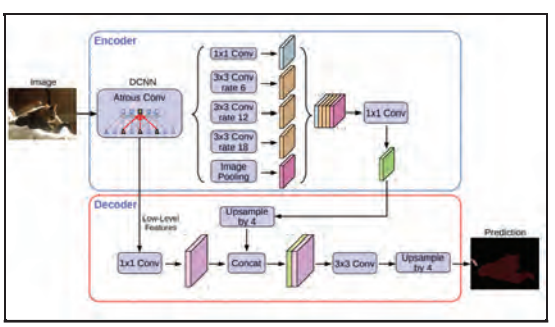

Figure 4: Deeplabv3plus model. Source:(Chen, Zhu et al. 2018)

3. METHODOLOGY

The proposed pipeline combines zero-shot object detection and semantic segmentation to automatically extract window information from street-view imagery. The workflow consists of image rectification, window detection, semantic segmentation, mask refinement, pane arrangement, and geometric parameter extraction. The resulting data can support urban digital twin generation, building energy modeling, and architectural analysis.

3.1. Window segmentation

3.1.1. Semantic segmentation

Semantic segmentation had been implemented using the DeepLabV3 model. This section provides in detail the process of training the DeepLabV3 model on the WinSyn dataset.

The window segmentation process consists of key parameters such as model architecture, class weights, learning rate, and the specific classes involved in the segmentation task. The

approach ensures that the model effectively learned the necessary features for detecting

and segmenting windows in different settings, and the choice of the most appropriate settings is intended at the end of this process. SS was carried out in the WinSyn datasets (Kelly, et al. 2024).

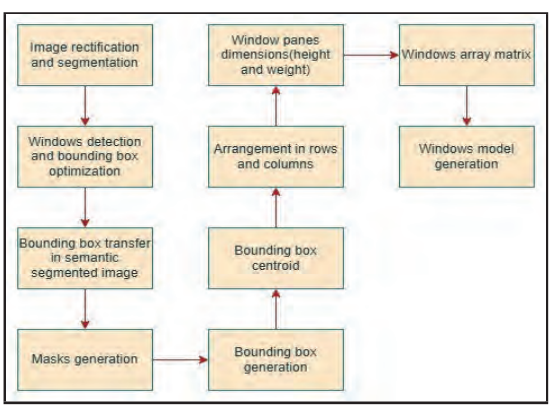

Figure 5: Overall methodology

Semantic segmentation was carried out using following subtasks:

3.1.2. Image Rectification

Street-view images from the WinSyn dataset were first rectified using a homographic transformation (Sasank, 2020) to correct perspective distortion and align window structures. Homography matrices were computed and applied to both segmented

masks and ground truth images to ensure consistency in subsequent analysis.

Bounding Box Generation and Transfer: Bounding boxes were generated around windows in rectified images to correct segmentation errors, with multiple boxes distinguished using color coding. These coordinates were then transferred to the segmented images, and pixels outside the boxes were reclassified as walls to improve segmentation accuracy.

3.1.3. Mask Generation and Refinement

HSV-based red and green masks were created to differentiate window panes and frames. Morphological operations, including opening with a 5×5 kernel, were applied to remove noise and connect fragmented components. Contours corresponding to individual panes were filtered by area, eliminating small or spurious detections.

Pane Arrangement: Bounding box centroids were calculated to arrange panes into rows and columns. Grouping thresholds of 15 pixels in both x and y directions were used, and dimensions within a 5-pixel tolerance were normalized to ensure consistent layout.

Window Matrix Construction and Frame Thickness: Panes were encoded into a 2D matrix representing spatial arrangement and inter-pane relationships. Frame thickness was calculated as the average Euclidean distance from five key points on the frame to the nearest pane edges. All extracted parameters—including row and column counts, pane dimensions, frame thickness, and spatial topology—were saved in JSON format for visualization, parametric analysis, and digital twin integration.

3.2. Windows detection

The window detection process utilized the GroundingDINO model. GroundingDINO model combines images and natural language processing to detect objects in an image and generate a bounding box. GroundingDINO model was utilized with the framework mentioned in figure1.

In the first step of window detection, street view images were fed into the GroundingDINO

model along with the text prompt "Window" to specifically focus the model on detecting windows in the street view images. Secondly, GroundingDINO, a transformer-based object detection model, combines the image and text prompts together. It focuses on different segments of the image and correlates these segments with the text prompt "window". The model checks the shape, structure, and appearance of each region in the street view image, distinguishing windows from other structures like façades, doors, and rooftops. It then determines a confidence score for each detected segment. Thirdly, each detected window segment is encapsulated by a bounding box. This bounding box is generated using four coordinates: x-min, x-max, y-min, and y-max, which represent the top, bottom, left, and right edges of the detected image. Fourthly, visualizations of the generated images show that, in some cases, the bounding boxes narrowly capture the windows' edges in the street view images. To address this issue, a 10-pixel margin was added to each side of the detected image bounding box:

$x_{min} = x_{min} - 10$, $y_{min} = y_{min} - 10$, $x_{max} = x_{max} + 10$, $y_{max} = y_{max} + 10$.

Finally, after expanding the bounding boxes and creating a buffer around the detected

windows, the windows are clipped.

Post-Training Evaluation:

Post training evaluation of the model was carried using standard segmentation metrics

Intersection over Union (IoU) and pixel accuracy. These metrics depicted how well the

model segmented the windows and its constituent structures. Once the model reached

satisfactory performance, inference was done on to real-world street view images, providing pixel-level classification of windows and their components, which was used for 3D

window reconstruction.

Accuracy Assessment of Segmentation:

The accuracy assessment of the semantic segmentation task was performed by comparing the segmentation results with the ground truth. The ground truth data used for this assessment came from the Windows labels in the Winsyn dataset, which contained a total of 452 images. These labels were divided into three classes: window panes, window frames, and walls.

Optimized Parameters for Semantic segmentation:

Semantic segmentation was performed using a fine-tuned DeepLabV3 model on the WinSyn dataset. Key optimization parameters included:

- **Image and Crop Size:** Input images were resized and cropped to ensure uniform processing and preserve window details.
- **Model Training:** A pre-trained backbone was fine-tuned with selective freezing of layers to leverage learned features while maintaining stability.
- **Iterations and Learning Rate:** Training iterations and learning rate were tuned for optimal convergence. Class weights were applied to mitigate class imbalance.
- **Class Selection:** The original WinSyn dataset contained 11 label classes, but using all classes resulted in suboptimal performance. Segmentation was optimized to focus on four key categories critical for window reconstruction:
    1. **Window Pane** – glass portions of the window
    2. **Window Frame** – surrounding structural elements
    3. **Wall** – areas surrounding the window
    4. **Background** – all remaining regions

This optimization from 11 to 4 classes reduced ambiguity, improved segmentation consistency, and ensured accurate extraction of window geometry for downstream analyses.

4. RESULTS AND DISCUSSION

4.1. Semantic segmentation

The impact of class selection on semantic segmentation performance is illustrated in Figure 6. Initial experiments using the full 11-class WinSyn dataset revealed significant challenges. Classes such as blinds, shutters, bars, and miscellaneous objects exhibited high visual similarity to panes and frames, leading to frequent misclassification and a maximum mIoU of only 36.43%. Segmentation masks were often noisy, with window components partially merged or misidentified, demonstrating that the high number of classes introduced unnecessary complexity for the model.

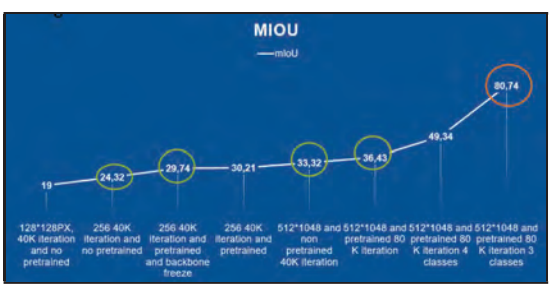

Figure 6: Segmentation optimization

To address this, the number of classes was reduced to four key categories: window pane, window frame, wall, and background. This simplification improved class separability and reduced ambiguity, raising the mIoU to 49.34%. While performance improved considerably, misclassification between blinds and panes persisted due to similar color and texture characteristics. These results indicate that even moderate reductions in class number can significantly improve segmentation accuracy but may still be insufficient when visually overlapping features exist.

The final optimization combined similar

classes, resulting in a three-class setup: window pane, window frame, and wall. This configuration prioritized the most critical components for window reconstruction and minimized distractions from redundant classes. With the same pretrained backbone and 80K training iterations, the model achieved a maximum mIoU of 80.74%. Segmentation masks under this configuration were markedly cleaner, with clear separation between panes, frames, and surrounding walls. Fine details such as narrow frame boundaries and individual panes were accurately captured, demonstrating the effectiveness of the combined strategy of class simplification, fine-tuning, and sufficient iterations.

Table 1: Segmentation accuracy.

Metric	**Value (%)**
Overall Accuracy	93.29 %
Precision (Wall)	96.89 %
Precision (Frame)	77.61 %
Precision (Panes)	90.29 %
Recall (Wall)	94.22 %
Recall (Frame)	81.33 %
Recall (Panes)	95.86 %
F1-Score (Wall)	95.18 %
F1-Score (Frame)	77.82 %
F1-Score (Panes)	92.14 %
Mean Intersection over Union (mIoU)	81.56 %
Metric	**Value (%)**

Table 1 complements these visual findings by providing quantitative performance metrics. The model achieved high overall accuracy (93.29%), with strong precision for walls (96.89%) and panes (90.29%) and slightly lower precision for frames (77.61%), reflecting the challenge of consistently detecting narrow frame structures. Recall values were similarly high for walls (94.22%) and panes (95.86%), while frames achieved 81.33%, indicating that most window components were correctly identified. The F1-scores further confirm consistent performance, with walls (95.18%) and panes (92.14%) outperforming frames (77.82%). The overall mIoU of 81.56% reflects robust segmentation quality across all classes and supports the pipeline's suitability for accurate window parameter extraction.

Overall, these results demonstrate that semantic segmentation performance is highly sensitive to both the number of classes and hyperparameter selection. Class simplification, combined with fine-tuning pretrained models and optimized training iterations, provides a reliable approach to segmenting complex window structures from street-view imagery. These optimized segmentation masks form the foundation for downstream processing, including bounding box extraction, pane arrangement, frame thickness calculation, and spatial encoding, enabling precise reconstruction of window geometry for digital twin modeling and large-scale architectural analysis. Figure 7 shows the semantic segmentation of images in their original form, which contains the geometric distortion. Homographic transformation was used to rectify the image depicted in Figure 8.

Figure 7: Semantic segmentation on original images

4.2. Windows detection

Window detection from street-view imagery was performed using two state-of-the-art object detection models: YOLOv8 and Grounding DINO. The goal was to identify the most suitable model for complex urban environments with diverse window architectures, varying lighting conditions, occlusions, and camera angles. Both models were evaluated based on precision, recall, mean average precision (mAP), bounding box alignment, and detection speed.

Figure 8: Semantic segmentation results(rectified)

4.2.1. YOLOv8 window detection

The YOLOv8 model, known for its speed and efficiency in single-stage object detection, was fine-tuned on annotated street-view images containing window locations. Under a 50% Intersection over Union (IoU) threshold, YOLOv8 achieved a precision of 91.4% and recall of 91.0%, indicating strong detection performance. Most missed detections were caused by occlusions, complex camera angles, or objects obstructing the view, such as trees and vehicles.

YOLOv8 produced reasonably accurate bounding boxes and maintained high inference speed, making it suitable for real-time applications and large-scale image inference. However, the model struggled with windows on slanted images or highly occluded façade s, limiting its reliability for complex urban scenes. Figures 6.12 and 6.13 illustrate training performance, loss reduction, and qualitative detection results, showing accurate predictions for vertical images but reduced performance for slanted or partially obscured windows.

Figure 9: Windows detection using YOLO V8 model

4.2.2. Grounding DINO window detection

Grounding DINO, a transformer-based object detection model integrating visual and textual prompts, was employed with the following parameters: TEXT_PROMPT = "window", BOX_THRESHOLD = 0.25, and TEXT_THRESHOLD = 0.25. The model demonstrated superior detection in challenging conditions, including small, misaligned, or occluded windows in complex façade s. Bounding box alignment was highly accurate,

and the model effectively handled diverse architectural styles, low-resolution images, and non-standard window geometries

The integration of textual prompts enabled Grounding DINO to detect windows missed by YOLOv8, providing a significant advantage in comprehensive detection tasks. While inference speed was slightly slower than YOLOv8, the model's robustness in challenging scenarios outweighed the speed trade-off.

Figure 10: Windows detection (Grounding DINO model)

4.2.3 Comparison and model selection

Table 2: Results comparison.

Model	Precision (%)	Recall (%)	mAP50 (%)	Bounding Box Accuracy	Inference Speed	Notes
YOLOv8	91.4	91.0	90.5	Good	High	Missed occluded/ slanted windows
Grounding DINO	93.2	94.1	92.8	Excellent	Moderate	Robust detection for complex/ occluded windows

Table 2 summarizes the comparative performance of YOLOv8 and Grounding DINO:

YOLOv8 excelled in inference speed and performed well for vertical, unobstructed images, but struggled under occlusions or non-standard angles. Grounding DINO, in contrast, achieved higher overall detection completeness and bounding box alignment for complex urban façades, making it more suitable for applications prioritizing detection accuracy over speed.

For this study, complete and reliable window detection was essential for downstream segmentation and parameter extraction. Therefore, Grounding DINO was selected as the preferred model, as it required no task-specific training and provided consistent detection across diverse street-view images.

4.3. Discussion

The results demonstrate that the proposed pipeline effectively integrates zero-shot window detection, optimized semantic segmentation, and parametric 3D modeling to reconstruct windows from street-view images. Several key observations can be drawn from the experiments:

Semantic Segmentation: Simplifying the label classes from 11 to three—window pane, window frame, and wall—was critical in reducing ambiguities between visually similar components. The optimized model achieved a mean Intersection over Union (mIoU) of 80.74%, with an overall accuracy of 93.29%, indicating robust delineation of window components. Fine-tuning pretrained models and increasing training iterations to 80K allowed the network to capture fine details that were previously lost with smaller crop sizes (128 px). Morphological operations further enhanced mask quality by connecting fragmented frames and removing noise, demonstrating the importance of post-processing in achieving high-quality segmentation.

Window Detection: Comparison between YOLOv8 and Grounding DINO highlighted the trade-offs between speed and detection robustness. While YOLOv8 achieved high precision (91.4%) and recall (91.0%) with fast inference, it struggled with occluded or slanted windows. Grounding DINO, using visual and textual prompts, was able to detect complex, misaligned, or partially occluded windows with higher completeness and bounding box accuracy, making it more suitable for urban façades with diverse architectural styles.

Challenges and Limitations: Despite promising results, the pipeline faces limitations when handling very low-resolution images, arched or non-rectangular windows, and extreme occlusions. The image rectification model depends on sufficient vanishing points; insufficient points can reduce rectification quality. YOLOv8, while fast, may miss occluded windows, limiting its applicability in comprehensive urban analyses.

Implications: The study shows that combining zero-shot detection with optimized semantic segmentation provides a scalable framework for façade analysis. It reduces reliance on large annotated datasets, supports diverse window styles, and enables accurate parameter extraction for 3D modeling. This modular approach is adaptable to various urban environments and can be extended for other façade components.

5. CONCLUSION

The proposed modular pipeline successfully integrates zero-shot object detection, semantic segmentation, and parametric 3D reconstruction to automate window modeling from street-view imagery. Key outcomes and contributions include:

1. **High-Accuracy Segmentation:** Optimizing class labels and fine-tuning pretrained models achieved a mean IoU of 80.74%, clearly distinguishing window panes, frames, and walls.
2. **Robust Detection with Grounding DINO:** Zero-shot detection outperformed YOLOv8 for occluded and complex façades, highlighting the effectiveness of vision-language models in architectural analysis.
3. **Enhanced Image Rectification and Mask Refinement:** Vanishing-point-based rectification and morphological operations ensured accurate geometry and spatial consistency.
4. **Parametric 3D Modeling:** Extracted parameters (rows, columns, pane dimensions, frame thickness) enabled scalable and accurate 3D reconstruction using Blender, preserving topological and spatial relationships.
5. **Modularity and Scalability:** The pipeline is adaptable to different window architectures and can be extended for additional façade elements or urban-scale digital twin generation.

Future Work: To further enhance applicability, future research should focus on low-resolution and non-rectangular windows, complex occlusions, lighting variations, and multi-view integration. Extending the pipeline to fully automate diverse façade modeling will increase its value for urban digital twin frameworks and architectural analysis.

In summary, this study demonstrates that combining zero-shot detection, optimized semantic segmentation, and parametric modeling provides a scalable and accurate solution for automated window reconstruction, bridging the gap between street-view imagery and urban digital twins.

REFERENCES

Carreira, J., Caseiro, R., Batista, J., & Sminchisescu, C. (2012). Semantic segmentation with second-order pooling. In *European conference on computer vision* (pp. 430-443). Berlin, Heidelberg: Springer Berlin Heidelberg.

Dong, J., Chen, Q., Yan, S., & Yuille, A. (2014). Towards unified object detection and semantic segmentation. In *European Conference on Computer Vision* (pp. 299-314). Cham: Springer International Publishing.

Felzenszwalb, P. F., Girshick, R. B., McAllester, D., & Ramanan, D. (2009). Object detection with discriminatively trained part-based models. *IEEE Transactions on Pattern Analysis and Machine Intelligence*, 32(9), 1627-1645..

Hao, S., Zhou, Y., & Guo, Y. (2020). A brief survey on semantic segmentation with deep learning. *Neurocomputing*, 406, 302-321..

Hu, H., Zhang, Y., & Zhu, Q. (2022). Efficient procedural modelling of building façades based on windows from sketches. *The Photogrammetric Record*, *37*(179), 272–295.

Kelly, T., Femiani, J., & Wonka, P. (2024). Winsyn: A high resolution testbed for synthetic data. In *Proceedings of the IEEE/CVF Conference on Computer Vision and Pattern Recognition* (pp. 22456-22465).

Liu, Y., Bai, X., Wang, J., Li, G., Li, J., & Lv, Z. (2024). Image semantic segmentation approach based on DeepLabV3 plus network with an attention mechanism. *Engineering Applications of Artificial Intelligence*, 127, 107260.

Long, J., Shelhamer, E., & Darrell, T. (2015). Fully convolutional networks for semantic segmentation. In *Proceedings of the IEEE conference on computer vision and pattern recognition* (pp. 3431-3440).

Ohta, Y. I., Kanade, T., & Sakai, T. (1978, November). An analysis system for scenes containing objects with substructures. In *Proceedings of the Fourth International Joint Conference on Pattern Recognitions* (pp. 752-754). Piscataway: Institute of Electrical and Electronics Engineers Incorporated.

Pang, Y., & Biljecki, F. (2022). End-to-end building façade reconstruction from panoramic street view images. *ISPRS Journal of Photogrammetry and Remote Sensing*, 187, 146–163.

Rahman, S., Khan, S. H., & Porikli, F. (2020). Zero-shot object detection: Joint recognition and localization of novel concepts. *International Journal of Computer Vision*, 128(12), 2979-2999.

Redmon, J., Divvala, S., Girshick, R., & Farhadi, A. (2016). You only look once: Unified, real-time object detection. In *Proceedings of the IEEE conference on computer vision and pattern recognition* (pp. 779-788).

Sasank, C., & Mittal, A. (2020). Rectification of building façades using a deep learning-based vanishing point detection. In *Proceedings of the IEEE/CVF Winter Conference on Applications of Computer Vision* (WACV).

Sasank, C., & Mittal, A. (2020). Rectification of building façades using a deep learning-based vanishing point detection. *Proceedings of the IEEE/CVF Winter Conference on Applications of Computer Vision (WACV)*.

Sun, W., & Wang, R. (2018). Fully convolutional networks for semantic segmentation of very high resolution remotely sensed images combined with DSM. *IEEE Geoscience and Remote Sensing Letters*, 15(3), 474-478.

Wang, Y., Li, S., & Li, W. (2019). Deep learning-based backbone network for feature extraction in semantic segmentation. *IEEE Access*, 7, 12345-12356.

Yang, Z., Peng, X., & Yin, Z. (2020). Deeplab_v3_plus-net for image semantic segmentation with channel compression. In *2020 IEEE 20th International Conference on Communication Technology (ICCT)* (pp. 1320-1324). IEEE.

Yu, H., Yang, Z., Tan, L., Wang, Y., Sun, W., Sun, M., & Tang, Y. (2018). Methods and datasets on semantic segmentation: A review. *Neurocomputing*, 304, 82-103..

Author's Information

Name	:	Sumeer Koirala
Academic Qualification	:	MSc Geographic information system and science, MSc Land management and Geospatial sciences
Organization	:	Survey Department
Current Designation	:	Chief Survey Officer

Cadastral Boundary Delineation Using Transfer Learning Approach

Er. Helina Shrestha[1], Er. Amrit Karmacharya[2], Er. Prabesh Shrestha[3]
helysian.2@gmail.com, dosamritkarma@gmail.com, prabeshrestha07@gmail.com
[1]Ministry of Land Management, Co-operatives, Federal Affairs and General Administration,
[2]NAXA, [3]Survey Department

KEYWORDS

UNET, Cadaster, Deep learning, Visible boundary delineation, Nepal

ABSTRACT

The adoption of Fit-for-Purpose Land Administration aims at providing a flexible and low-cost alternativev for cadastral boundary delineation that emphasizes visible boundaries derived from earth observation imagery. Recent advances show that deep learning can support the automatic delineation of visible cadastral boundaries. However, applications remain constrained by limited, small-scale datasets and weak understanding of which cadastral characteristics are identifiable. This study investigates the use of a transfer learning-based U-Net model to extract visible cadastral boundaries from high-resolution UAV imagery in a study area covering 200 hectares in Banepa Municipality, Nepal. The U-shaped model, pre-trained on agricultural field boundaries in Cambodia and Vietnam, and fine-tuned on 30 cm satellite imagery of the Terai region, was applied as a fixed classifier t o UAV orthophotos at 3 cm, 15 cm, and 30 cm resolutions. A patch-based pipeline splits imagery into 512 X 512 tiles, predicts boundary masks, and converts them into vector polylines via morphological operations, skeletonization, and graph-based line extraction. Results indicate that coarser resolutions produce more generalized and cadastral-like parcel shapes, while finer resolutions capture detailed man-made features but suffer from over-segmentation. The 15 cm resolution yields the best overall performance, particularly in sub-urban areas, though the model struggles to form closed and complete polylines. Predicted boundaries align closely with visible features such as roads, fences, and cultivation edges. The outcomes suggest that deep learning-based workflows can generate preliminary boundary maps that can assist image-based cadastral mapping, reducing reliance on manual digitization and field visits, thus supporting the concept of fit-for-purpose approach in countries with incomplete and outdated cadastres.

1. INTRODUCTION

Land tenure security is fundamental to achieving the Sustainable Development Goals (SDGs) related to poverty reduction, food security, and gender equality (Unger et al., 2021). Despite its importance, approximately 75% of the world's population lacks access to formal land administration systems, a gap most prevalent in developing nations where traditional systems remain unaffordable (Enemark et al., 2014; Zevenbergen et al., 2013). The absence of formal recognition to land leads to increased tenure insecurity, reduced investment, and stagnant economic development (Brasselle et al., 2002; Lawry et al., 2014).

Traditionally, cadastre—the central component of land administration—has relied on ground-based surveying using Total Stations (TS) and Global Navigation Satellite Systems (GNSS) to capture high-precision coordinates (UNECE, 1996; Williamson, 2002). While accurate, these methods are labor-intensive, expensive, and slow. Estimates suggest that at current rates, achieving full cadastral coverage in many countries would take centuries (Zevenbergen et al., 2013). Consequently, land administration experts advocate for Fit-for-Purpose Land Administration (FFPLA), a shift in focus from high-precision mapping to flexible, affordable, and scalable coverage (Enemark et al., 2014; Williamson, 2008).

The spatial framework of FFPLA emphasizes image-based mapping, leveraging the fact that many cadastral boundaries coincide with visible features like roads, fences, and cultivation edges (Luo et al., 2017). The broader adoption of FFPLA has encouraged innovative technologies, such as the use of Unmanned Aerial Vehicles (UAVs) to accelerate the mapping processes. The fit for purpose approach to map cadastral boundaries predominantly included participatory mapping using on-screen visual interpretation approaches, which despite being a viable alternative to fieldwork, is often tedious and prone to human inconsistencies (Crommelinck et al., 2018). To improve efficiency, researchers initially explored Object-Based Image Analysis (OBIA) and rule-based workflows, such as Multi-Resolution Segmentation (MRS) and Mean-Shift segmentation (Kohli et al., 2017; Y. A. Wassie et al., 2018). However, these methods often struggle with parameter selection and varying geographic terrains (Hossain & Chen, 2019).

Recent studies demonstrate that the fusion of earth observation and deep learning algorithms provides promising opportunities in automated visible parcel boundary delineation where the study areas are large and a large amount of datasets have to be processed (Crommelinck et al., 2019; Fetai et al., 2021; Grift et al., 2023). Among deep learning techniques, Convolutional Neural Networks (CNNs) are popularly used in image interpretation tasks and object detection and offer higher accuracy in delineating cadastral boundaries than traditional edge detection and image segmentation approaches (Xia et al., 2019; Fetai et al., 2022).

Within the deep learning domain, the task of cadastral boundary delineation is formulated as a semantic segmentation problem, as it requires the assignment of class labels at the pixel level to identify boundary regions. Fully Convolutional Network (FCN), first introduced by Long et al. (2015), adapts CNN architectures by replacing fully connected layers with convolutional layers, enabling dense, pixel-wise predictions for inputs of arbitrary size. The encoder–decoder structure, combined with skip connections, facilitates the preservation and recovery of spatial information, making FCNs particularly effective for semantic segmentation tasks.

Among FCN architectures, U-Net, proposed by Ronneberger et al. (2015), has been extensively adopted in cadastral and field boundary extraction studies. U-Net offers a good balance between segmentation accuracy and computational efficiency. Its symmetric encoder–decoder design with skip connections supports precise spatial localization, which is critical for accurate pixel-level delineation of cadastral boundaries.

Despite the significance of such architectures, challenges in widespread application remains. High-quality cadastral benchmark datasets are scarce, and the performance of these algorithms across different geographic locations is not well understood (Grift et al., 2023). Transfer learning—the process of taking a model trained on a data-rich source and fine-tuning it for a new task—offers a way to overcome data scarcity and speed up automation (Bashath et al., 2022).

Building upon this paradigm, this study employs a U-Net architecture previously trained on a large agricultural benchmark dataset AI4Small Farms created by Persello

et al. (2023), and fine-tuned on a visible boundary dataset from the Terai region of Nepal. This transfer-learning based model is utilized to extract visible cadastral boundaries in Banepa Municipality using UAV imagery at three resolutions—3 cm, 15 cm, and 30 cm. By testing these different resolutions, the study investigates how varying image resolutions and local geographic characteristics influence the transferability and accuracy of deep learning models, while qualitatively assessing their ability to identify visible boundaries in urban and sub-urban areas.

2. MATERIALS AND METHODS

2.1. Image data

Literature indicates that deep learning methods exhibit higher performance in regions with visible cadastral boundaries, which are predominantly found in rural and semi-urban settings. For this study, we have selected a 200-hectare site (Figure 1) within ward 10 of Banepa Municipality of Kavrepalanchok District. This area encompasses diverse topographic variations such as low land, gentle slopes to steep hills, and mixed land use types including residential, agricultural and forested zones.

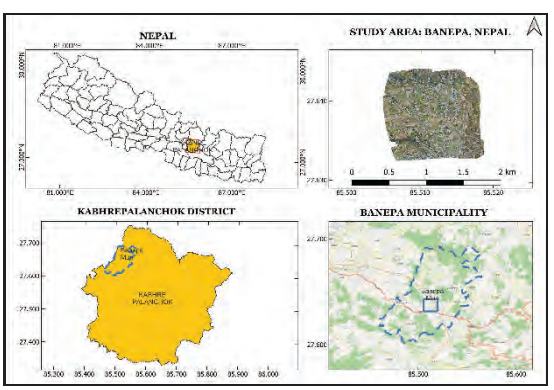

Figure 1. Study area

The UAV images were captured using a DJI Mavic Pro drone at a flight altitude of 100 m, with 70% overlap between images. The data were processed in Pix4D mapper to create an ortho-mosaic (with a spatial resolution of 3 cm and a digital elevation model (DEM) at 10 cm resolution derived from a photogrammetric point cloud. An ortho-mosaic was produced using the DEM. Horizontal and vertical accuracies were assessed by comparing coordinates of five ground control points (GCPs) and three independent checkpoints, surveyed via static differential global positioning system (DGPS) observations with Trimble R 7 receivers. Raw GNSS data were post-processed in Trimble Business Center software, yielding a root mean square error (RMSE) of 0.006 m during ortho-mosaic georeferencing.

The UAV orthophoto was further down-sampled to 30 cm and 15 cm resolutions using average resampling, as the original model was trained on 30cm imagery. This allowed testing transfer learning performance on resolutions differing from the training data; 15 cm was selected as an intermediate value between the original resolution 3 cm and 30 cm.

2.2. Transfer learning approach

In the context of transfer learning, pre-trained models are trained on benchmark datasets that combine images with corresponding labels. This strategy is used extensively to address two major requirements of deep learning models—1) vast amounts of labeled datasets and 2) resource-intensive computational resources—to train models effectively. Common approaches include using the pre-trained model directly as a classifier (no retraining needed); as a feature extractor (freezing convolutional layers while retraining the classifier); or via fine-tuning (retraining some or all layers for the new task) (Elgendy, 2020). In this study, we used the pre-trained model solely as a classifier to delineate visible boundary features in UAV imagery that potentially correspond to cadastral boundaries.

2.3 Model and weights

The model architecture employed in this study is a modified U-Net designed specifically for satellite image segmentation. The model was pre-trained on the AI4SmallFarms dataset by Persello et al. (2023), which comprises high-resolution Google Maps imagery and 439,001 agricultural field polygons spanning diverse agricultural landscapes in Vietnam

and Cambodia. The network was fine-tuned on a 30 cm resolution satellite imagery dataset of visible cadastral boundaries, digitized by experts to represent cadastral features in Nepal's Terai region.

2.4 Model pipeline

The processing pipeline consists of four key steps implemented via dedicated Python modules (Table 1).

Table 1. Pipeline modules and description

Step	Module	Description
1	patch.py	Split study area image into 512 * 512 pixel patches
2	data_generator.py	Load images/masks with on-the-fly augmentation (flip, rotate)
3	georeferenced_predictions.py	Generate geo-referenced raster predictions
4	polygonize.py	Skeletonize → graph extraction → vector polylines

Key components:

Config.py manages central configuration including data paths, hyperparameters (BATCH_SIZE=2, EPOCHS=100, LEARNING_RATE=0.0001), and training models (FROM SCRATCH or PRETRAINED_WEIGHTS).

data_generator.py implements a DataGenerator class extending tf.keras.utils.Sequence for efficient batch loading, with augmentations: horizontal/vertical flips, 0-360° rotations) and normalization options (min-max, z-score, or log).

models/satellite_unet.py deploys keras_unet.models.satellite_unet, supporting training from scratch or fine-tuning, optimized with Jaccard Loss and metrics (Recall, Precision, F1 score, IoU)

2.5 Vectorization pipeline

The polygonize.py module converts binary segmentation masks into GIS-compatible vectors through morphological operations (dilation to connect fragments, erosion to remove artifacts), skeletonization to one-pixel lines, graph-based extraction using sknw (pixels as nodes, adjacency as edges), and Douglas-Peucker simplification (0.6 m tolerance).

2.6 Experimental setup

The model was implemented using a robust hardware and software stack. The hardware configuration includes a high-performance computing system equipped with an **Intel Core i7-13700H CPU** (13th Gen, 20 threads, 2.4GHz) and **32 GB of RAM**. To handle the intensive computational requirements of the transfer learning model, an **NVIDIA GeForce RTX 4060 GPU** was utilized.

The model inference was performed on **Windows 11** operating system using Python 3.10.1 in a **virtual environment (venv)**, with **TensorFlow 2.10.1**. To leverage the GPU capabilities, **CUDA 11.2** and **cuDNN 8** were configured as the parallel computing platform and deep neural network library, respectively.

TensorFlow 2.10.1
virtual environment (venv) for dependency management
Python 3.10.1
Windows 11 operating system
cuDNN 8
CUDA 11.2
NVIDIA GeForce RTX 4060 GPU and 13th Gen Intel Core 17-13700H CPU (20 threads, 2.4GHz) and 32 GB of RAM.

3. RESULTS AND DISCUSSION

The classifier generated georeferenced vector polylines from binary masks. Figure 2 shows predicted boundaries overlaid on UAV orthophotos at 3 cm, 15 cm, and 30 cm resolutions across 17 representative tiles. Due to unavailable reference cadastral data, evaluation relied on qualitative visual assessment focusing on boundary alignment, completeness, and processing efficiency.


UAV 3cm
UAV 15cm
UAV 30cm


UAV 15cm
UAV 30cm

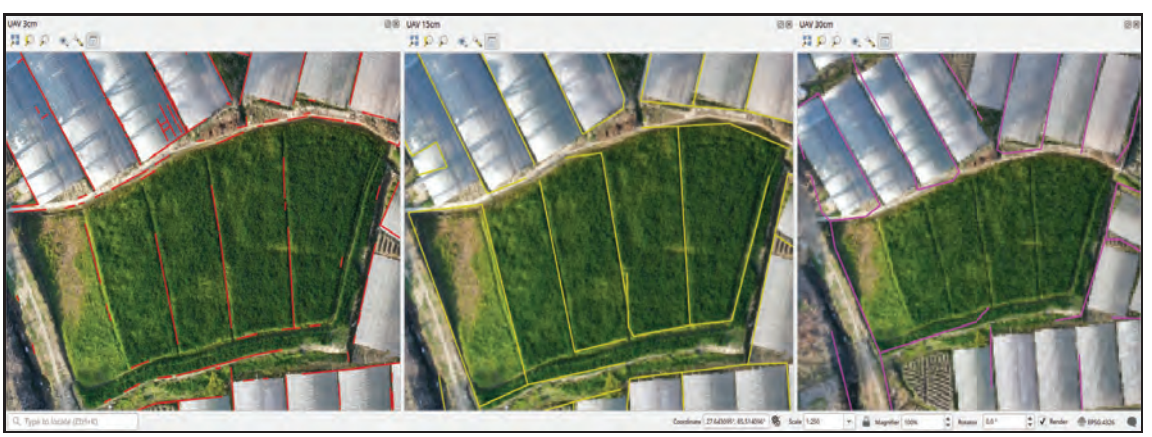
UAV 3cm
UAV 15cm
UAV 30cm

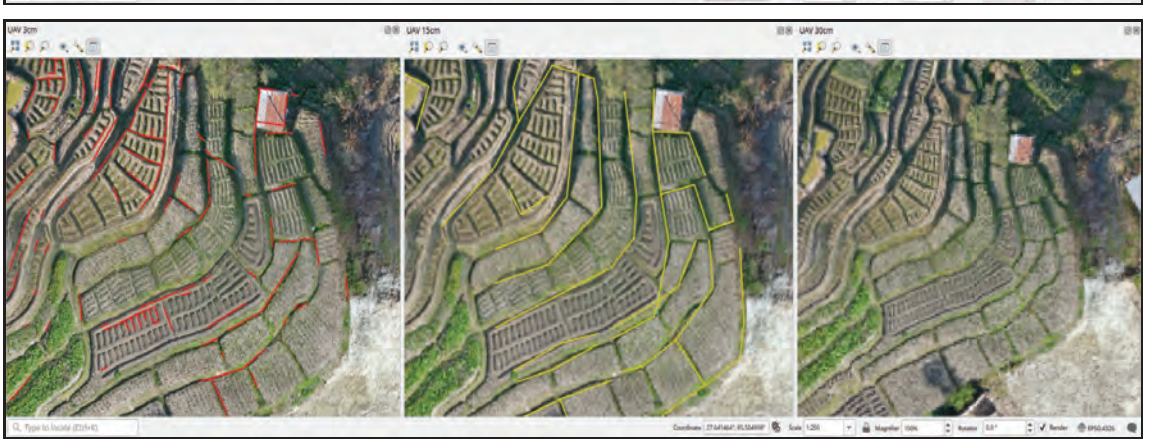
UAV 3cm
UAV 15cm
UAV 30cm

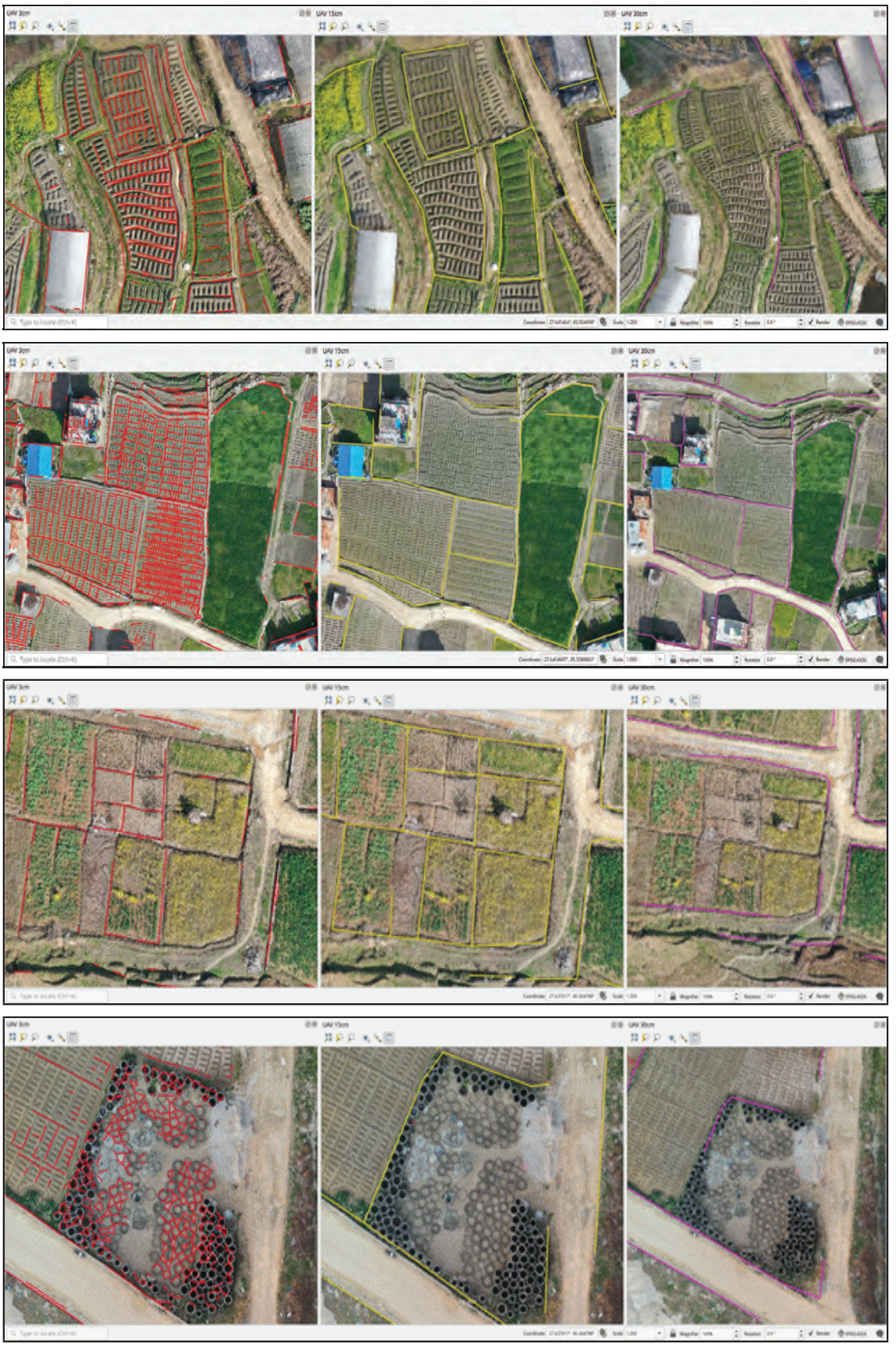
UAV 3cm
UAV 15cm
UAV 30cm


UAV 3cm
UAV 15cm
UAV 30cm

Figure 2. Predicted boundary polylines (colored overlays) generated by the classifier, shown overlaid on UAV orthophotos at 3 cm, 15 cm, and 30 cm resolutions

The 3 cm UAV imagery required the longest processing time, with the full pipeline completing in 2 hours and 55 seconds. At this resolution, the model predicted clear, man-made boundaries, such as fences and well-structured plots. However, a drawback of the model was that it frequently interpreted minor spatial variations such as temporary agricultural divisions and subtle textural changes as parcel boundaries. This resulted in over-segmentation, producing fragmented parcel divisions that deviated from real cadastral representations.

The 30 cm UAV imagery achieved the fastest processing time, completing the entire pipeline in approximately 40 seconds. At this resolution, the model generated more generalized parcel representations, emphasizing the dominant land-cover classes. Linear features such as roads were identified more effectively compared to other resolution.

The 15 cm UAV imagery provided a balance between spatial detail and generalization, yielding the most promising overall results. The pipeline completed in 4 minutes and 6 seconds, significantly faster than the 3cm data while offering more details than the 30 cm imagery. Nevertheless, the model had some limitations. The model tended to generate extra segments around buildings, and while boundary segments were often detected, complete parcel polylines were not consistently formed. The extraction quality was also strongly influenced by land cover: green land cover patches were typically extracted as complete and closed polylines, whereas bare land cover patches were extracted only as partial segments.

Comparing the length of the extracted line segments, the model made more predictions on 3cm imagery. At 15 cm and 30 cm resolutions, longer and continuous line segments were produced. This suggests that higher imagery resolution limits the model's ability to delineate and connect linear features.

Table 2. Processing times and segment lengths by resolution

Resolution	Processing Time	Total Segment Length (km)
3 cm	2h 55m	258,447
15 cm	4m 6s	132,072
30 cm	40 s	74,163

3.1. Interpretation

The visual assessment reveals that predicted polylines align closely with physically visible features (fences, cultivation edges, roads, etc.) across resolutions. The authors interpret the model outputs as a reflection of current ground reality better than potentially outdated official records, which often include legal constructs without physical markers. A basic observation suggests that at different resolutions different granularity is observed.

3cm	15cm	30cm
Plots	Farms	Roads

The predicted boundaries can support Nepal's UAV-based cadastral mapping by automating the initial delineation of visible cadastral boundaries. Addition of an automated step in the pre-survey phase could offer several practical advantages.

1. First, it helps field teams start with a clearer visual reference, reducing uncertainty and speeding up the adjudication process.
2. Second, it allows technical staff to shift effort from drawing parcel boundaries by hand to verifying and adjusting model outputs, which is generally faster and less error-prone.
3. Third, it helps to maintain consistency across different survey areas and survey teams.

This approach aligns with contemporary research on cadastral data maintenance.

Fetai et al. (2022) suggest that automatically detected visible physical boundaries can serve as preliminary digital spatial boundaries, which field teams can subsequently refine through either manual adjustment using UAV imagery or ground surveys. However, it should be understood that deep learning excels where visible boundaries predominate but it cannot capture legal cadastral constructs lacking physical expression such as fragmented administrative divisions or outdated records without ground markers. Multiple studies confirm this fundamental limitation and suggest that deep learning is effective only for visible boundaries (Y. Wassie et al., 2016); there is a need to quantify visible vs. invisible boundary proportions in benchmarks, as legal cadastral data often diverges from topographical reality (Grift et al., 2023).

3.2 Limitations

1. Due to the lack of reference data for quantitative comparison, evaluation metrics namely, precision, recall and F-score are not computable.
2. This study used the pre-trained model as a classifier, fine-tuning with a locally representative dataset can enhance the output.
3. The UAV orthophoto contained shadowed areas caused by variations in illumination and object height. These shadows may have affected the spectral characteristics of certain features, leading to potential misclassification and reduced accuracy in shaded regions.
4. The model was trained on a representative dataset for flat terrain in Cambodia, Vietnam and fine-tuned in the dataset of Chitwan, so it is not able to detect terraces in hilly areas, although terrace features are visible features in UAV images. Fine-tuning the model on a representative terrace dataset should result in better model prediction.

4. CONCLUSION

The results show that the transfer learning–based U-Net model, used as a fixed classifier, can extract visible cadastral boundaries from UAV imagery. Resolutions of 3 cm, 15cm and 30 cm were tested, with 15 cm offering the best balance between detail and generalization. Processing times range from 40 seconds for 30 cm resolution to 2h55m for 3 cm resolution across the tested resolutions, offering substantial gain in terms of time consumed over manual digitization. These exploratory qualitative findings demonstrate the utility of automated preliminary mapping within Nepal's image-based cadastral re-surveying workflows, particularly by providing field teams with clear visual references and reduce manual digitization effort. This approach aligns with and supports the spatial framework of Fit-for-Purpose Land Administration for regions with incomplete/outdated cadastral coverage.

REFERENCES

Bashath, S., Perera, N., Tripathi, S., Manjang, K., Dehmer, M., & Streib, F. E. (2022). A data-centric review of deep transfer learning with applications to text data. *Information Sciences*, *585*, 498–528. https://doi.org/10.1016/j.ins.2021.11.061

Brasselle, A.-S., Gaspart, F., & Platteau, J.-P. (2002). Land tenure security and investment incentives: Puzzling evidence from Burkina Faso. *Journal of Development Economics*, *67*(2), 373–418. https://doi.org/10.1016/S0304-3878(01)00190-0

Crommelinck, S., Höfle, B., Koeva, M. N., Yang, M. Y., & Vosselman, G. (2018). Interactive cadastral boundary delineation from UAV data. *ISPRS Annals of the*

Photogrammetry, Remote Sensing and Spatial Information Sciences, *IV–2*, 81–88. https://doi.org/10.5194/isprs-annals-IV-2-81-2018

Crommelinck, S., Koeva, M., Yang, M. Y., & Vosselman, G. (2019). Application of Deep Learning for Delineation of Visible Cadastral Boundaries from Remote Sensing Imagery. *Remote Sensing*, *11*(21), 2505. https://doi.org/10.3390/rs11212505

Elgendy, M. (2020). Transfer learning. *In Deep learning for vision systems* (pp. 147–192). Manning.

Enemark, S., Bell, K., Lemmen, C., & Mclaren, R. (2014). *Fit-For-Purpose Land Administration*.

Fetai, B., Grigillo, D., & Lisec, A. (2022). Revising Cadastral Data on Land Boundaries Using Deep Learning in Image-Based Mapping. *ISPRS International Journal of Geo-Information*, *11*(5), 298. https://doi.org/10.3390/ijgi11050298

Fetai, B., Račič, M., & Lisec, A. (2021). Deep Learning for Detection of Visible Land Boundaries from UAV Imagery. *Remote Sensing*, *13*(11), 2077. https://doi.org/10.3390/rs13112077

Grift, J., Persello, C., & Koeva, M. (2023). *Cadastral Boundary Delineation using Deep Learning and Remote Sensing Imagery: State of the Art and Future Developments*.

Hossain, M. D., & Chen, D. (2019). Segmentation for Object-Based Image Analysis (OBIA): A review of algorithms and challenges from remote sensing perspective. *ISPRS Journal of Photogrammetry and Remote Sensing*, *150*, 115–134. https://doi.org/10.1016/j.isprsjprs.2019.02.009

Kohli, D., Crommelinck, S., Bennett, R., Koeva, M., & Lemmen, C. (2017). *Object-based image analysis for cadastral mapping using satellite images*. https://doi.org/10.1117/12.2280254

Lawry, S., Samii, C., Hall, R., Leopold, A., Hornby, D., & Mtero, F. (2014). The Impact of Land Property Rights Interventions on Investment and Agricultural Productivity in Developing Countries: A Systematic Review. *Campbell Systematic Reviews*, *10*(1), 1–104. https://doi.org/10.4073/csr.2014.1

Long, J., Shelhamer, E., & Darrell, T. (2015). *Fully Convolutional Networks for Semantic Segmentation* (arXiv:1411.4038). arXiv. https://doi.org/10.48550/arXiv.1411.4038

Luo, X., Bennett, R., Koeva, M., Lemmen, C., & Quadros, N. (2017). Quantifying the Overlap between Cadastral and Visual Boundaries: A Case Study from Vanuatu. *Urban Science*, *1*(4), 32. https://doi.org/10.3390/urbansci1040032

Persello, C., Grift, J., Fan, X., Paris, C., Hänsch, R., Koeva, M., & Nelson, A. (2023). AI4SmallFarms: A Dataset for Crop Field Delineation in Southeast Asian Smallholder Farms. *IEEE Geoscience and Remote Sensing Letters*, *20*, 1–5. https://doi.org/10.1109/LGRS.2023.3323095

Ronneberger, O., Fischer, P., & Brox, T. (2015). *U-Net: Convolutional Networks for Biomedical Image Segmentation* (arXiv:1505.04597). arXiv. https://doi.org/10.48550/arXiv.1505.04597

UNECE (Ed.). (1996). *Land administration guidelines: With special reference to countries in transition*. United Nations.

Unger, E.-M., Bennett, R. M., Lemmen, C., & Zevenbergen, J. (2021). LADM for sustainable development: An exploratory

study on the application of domain-specific data models to support the SDGs. *Land Use Policy*, *108*. Scopus. https://doi.org/10.1016/j.landusepol.2021.105499

Wassie, Y. A., Koeva, M. N., Bennett, R. M., & Lemmen, C. H. J. (2018). A procedure for semi-automated cadastral boundary feature extraction from high-resolution satellite imagery. *Journal of Spatial Science*, *63*(1), 75–92. https://doi.org/10.1080/14498596.2017.1345667

Wassie, Y., Koeva, M., & Bennett, R. (2016). Towards automated detection of visual cadastral boundaries: Initial investigation of imagery, algorithms and perceptions. *GIM International*, *30*, 23.

Williamson, I. P. (2002). *The Cadastral "Tool Box" – a Framework for Reform*.

Williamson, I. P. (2008). *Using Cadastres to Support Sustainable Development*.

Xia, X., Persello, C., & Koeva, M. (2019). Deep Fully Convolutional Networks for Cadastral Boundary Detection from UAV Images. *Remote Sensing*, *11*(14), 1725. https://doi.org/10.3390/rs11141725

Zevenbergen, J., Augustinus, C., Antonio, D., & Bennett, R. (2013). Pro-poor land administration: Principles for recording the land rights of the underrepresented. *Land Use Policy*, *31*, 595–604. https://doi.org/10.1016/j.landusepol.2012.09.005

Author's Information

Name	:	Helina Shrestha
Academic Qualification	:	Master of Science in Geo-Information Science and Earth observation
Organization	:	Ministry of Land Management, Cooperatives, Federal Affairs and General Administration
Current Designation	:	Survey Officer

Comparative Evaluation of Image Compression Techniques for High-Resolution Orthophoto Imagery

Tina Baidar[1], Prabesh Shrestha[1], Sanjeevan Shrestha[2]
tina.baidar13@gmail.com, prabeshrestha07@gmail.com, shr.sanjeevan@gmail.com
[1]Survey Department
[2]Ministry of Land Management, Co-operatives, Federal Affairs and General Administration

KEYWORDS

High-resolution imagery, LiDAR orthophotos, Image compression, Lossless and lossy compression, JPEG 2000, ECW

ABSTRACT

The rapid growth of high-resolution data from UAV, LiDAR, and satellite platforms has significantly improved the accuracy and applicability of geospatial analysis, while simultaneously creating challenges related to large data volumes, storage, transmission, and computational efficiency. Image compression plays a critical role in addressing these challenges by reducing data size while maintaining acceptable visual and analytical quality. This study presents a comparative analysis of three widely used image compression techniques—JPEG2000 (lossless and lossy) and Enhanced Compression Wavelet (ECW)—applied to high-resolution LiDAR orthophotos. Compression performance was evaluated in terms of output size, compression ratio, and processing time, while image quality was assessed through both qualitative parameters (edge sharpness, spatial detail, color fidelity, radiometric consistency, texture, and geometric integrity) across multiple interpretation scales and quantitative approaches (MSSSIM, PSNR, ERGAS, and RASE metrics). Results indicate that JPEG2000 lossless preserves complete radiometric and spatial fidelity, making it ideal for high-precision analytical applications, although it offers limited compression efficiency. JPEG2000 lossy demonstrates the best overall balance, achieving high compression ratios with lower processing time while maintaining strong structural and spectral integrity, as evidenced by consistently high MSSSIM and PSNR values and low error metrics. In contrast, ECW achieves the highest compression ratios and smallest file sizes, making it highly efficient for storage and transmission; however, it exhibits greater variability, higher computational cost, and reduced performance in high-detail features. Overall, JPEG2000 lossy emerges as the most suitable compression method for general remote sensing applications, while JPEG2000 lossless is recommended for high-accuracy tasks and ECW for storage-efficient visualization and data dissemination.

1. INTRODUCTION

The rapid advancement of remote sensing technologies has led to an unprecedented increase in the availability of high-resolution geospatial data. Improvements in satellite sensors, Light Detection and Ranging (LiDAR) systems, and Unmanned Aerial Vehicle (UAV) platforms have enabled the acquisition of

imagery with spatial resolutions ranging from sub-meter to centimeter levels (Yao et al., 2019; Dong & Chen, 2017). As a result, geospatial analysis has become more precise and reliable, significantly enhancing applications in topographic mapping, urban planning, disaster management, and environmental monitoring. The growing demand for accurate, large-scale, and frequently updated spatial information has further accelerated the adoption of high-resolution datasets in both scientific research and operational practices.

Digital image processing plays a central role in extracting meaningful information from high-resolution geospatial datasets in Nepal. Fundamental techniques—including image enhancement, filtering, segmentation, feature extraction, and classification—are essential for transforming raw sensor data into usable geospatial products (Schowengerdt, 2012). In the context of Nepal, high-resolution orthophotos derived from UAV and LiDAR platforms have become increasingly important for large-scale mapping, cadastral updating, infrastructure planning, and disaster risk assessment. These geometrically corrected images remove distortions caused by rugged terrain, sensor tilt, and perspective effects, thereby ensuring uniform scale and enabling accurate map-based measurements (Sestras et al., 2025). However, Nepal's highly heterogeneous landscape—characterized by steep topography, fragmented land parcels, mixed land cover, and rapid urban expansion—poses significant challenges for automated image classification. As a result, visual interpretation continues to be the primary method for feature extraction in many operational applications. Even where automated approaches are applied, extensive manual validation and editing are required to achieve the level of accuracy demanded by national mapping and land administration activities.

Despite the widespread use of high-resolution datasets across various domains, they also introduce significant challenges related to data volume. Large file sizes increase the burden on storage systems, transmission bandwidth, and computational resources, particularly for institutions with limited infrastructure. These constraints can hinder efficient data sharing, processing, and long-term management. To address these challenges, image compression has become an essential component of geospatial data handling. Compression techniques reduce data size while attempting to preserve the visual and analytical quality required for specific applications. In remote sensing workflows, effective compression enables faster data transfer, reduces storage costs, and supports web-based and cloud-enabled geospatial services.

Image compression methods are broadly categorized into lossless and lossy approaches. Lossless compression ensures exact reconstruction of the original data but typically achieves limited reduction in file size. In contrast, lossy compression attains significantly higher compression ratios by removing redundant or less perceptually important information, albeit at the cost of some data degradation (Singh et al., 2016). Given the increasing reliance on high-resolution orthophotos for both visual interpretation and analytical tasks, it is essential to evaluate how different compression techniques affect image quality and usability.

Therefore, the primary objective of this study is to comparative evaluate the performance of commonly used image compression techniques for high-resolution LiDAR orthophotos, with a focus on balancing compression efficiency, radiometric integrity, and visual interpretability for geospatial applications.

2. IMAGE COMPRESSION TECHNIQUES

Image compression techniques are generally classified into lossless and lossy methods,

based on whether the original image can be perfectly reconstructed after decompression. Lossless compression preserves all original pixel values. In contrast, lossy compression reduces file size by eliminating perceptually or statistically redundant information. Although this approach introduces some level of data loss, it significantly decreases storage and transmission requirements. (Singh et al., 2016).

Common lossless algorithms include Run-Length Encoding (RLE), Lempel–Ziv–Welch (LZW), Deflate (ZIP-based compression), and JPEG 2000 operating in lossless mode (Gupta et al., 2017). RLE is particularly effective for images containing large homogeneous regions, while LZW is widely implemented in TIFF formats. Deflate is commonly used in PNG and other ZIP-based formats. JPEG 2000 in lossless mode employs reversible wavelet transforms, enabling higher compression efficiency compared to traditional lossless techniques. Although lossless methods typically achieve lower compression ratios than lossy approaches, they guarantee complete preservation of the original data.

For lossy compression, widely used algorithms include the Discrete Cosine Transform (DCT) and the Discrete Wavelet Transform (DWT). DCT forms the basis of standard JPEG compression, whereas DWT underpins JPEG 2000 lossy compression and ECW format (Gautam, 2010). These methods achieve higher compression ratios by reducing data precision and removing redundancy; however, excessive compression can introduce artifacts and degrade both spatial and spectral information. Consequently, selecting an appropriate compression method requires careful consideration of the trade-off between file size reduction and data quality.

1.1 JPEG 2000

JPEG 2000 (ISO/IEC 15444) is an international image compression standard based on wavelet transform coding, designed to deliver high compression efficiency, scalability, and both lossless and lossy encoding (Marcellin et al., 2000). It is widely used in remote sensing and geospatial applications for preserving spatial detail, handling large raster datasets, and integrating georeferencing and metadata within the file. The standard employs the Discrete Wavelet Transform (DWT) to decompose images into multi-resolution frequency sub-bands, followed by Embedded Block Coding with Optimized Truncation (EBCOT), which combines quantization and context-based arithmetic coding (Rabbani & Joshi, 2002). This enables efficient compression, precise rate control, and progressive reconstruction by quality or resolution. In lossy mode, irreversible wavelet filters and quantization achieve high compression while maintaining visual quality, whereas lossless mode uses reversible integer transforms without quantization to allow exact image reconstruction and full radiometric preservation (Rabbani & Joshi, 2002).

1.2 Enhanced Compression Wavelet (ECW)

Enhanced Compression Wavelet (ECW) is a proprietary wavelet-based raster compression format developed by Hexagon for efficient storage, transmission, and visualization of large geospatial datasets, including orthophotos, satellite imagery, and digital elevation models (Hexagon, 2025). ECW supports rapid visualization at different spatial scales without fully decompressing the file and thus, addresses the challenges of big geospatial data by offering high compression ratios, fast access, and flexible data handling. ECW uses DWT to decompose images into frequency sub-bands, separating low-frequency components that capture overall structure from high-frequency components that encode fine details such as edges and textures (Demirel & Anbarjafari, 2011). The wavelet coefficients are then quantified and entropy-coded, where the quantization level

determines the compression ratio and balances file size against radiometric fidelity. ECW files retain embedded georeferencing and projection metadata, including coordinate reference system (CRS), pixel resolution, and spatial extents, enabling seamless integration into GIS workflows and preserving spatial alignment with other raster or vector layers without requiring auxiliary world files.

3. METHODOLOGY

3.1 Image datasets

For this study, orthomosaic imagery with a ground sampling distance (GSD) of 15 cm produced by the Survey Department under the LiDAR Surveying and Mapping Program (2022) was used (Joshi & Koirala, 2020). A total of 67 RGB orthoimage tiles were acquired in GeoTIFF format. The orthophotos had been preprocessed as part of the original mapping project and provided as color-balanced mosaics. They were orthorectified using a high-resolution digital elevation model (DEM) generated from the LiDAR project, ensuring minimal geometric distortion and radiometric inconsistencies. As a result, the dataset is readily usable for downstream analysis without the need for additional photogrammetric correction or image enhancement.

3.2 Compression formats and platforms

For this study, two widely used wavelet-based image compression formats were applied to the LiDAR-orthophotos. ECW compression was performed using ERDAS IMAGINE, which supports efficient handling of large, high-resolution geospatial datasets and provides progressive, multi-resolution access. JPEG 2000 was implemented in a GIS environment, applying both lossless and lossy modes to evaluate the trade-off between compression ratio and data fidelity. The choice of these platforms allowed direct comparison of commonly used remote sensing compression workflows under realistic operational conditions, reflecting typical data processing and analysis scenarios in geospatial applications.

3.3 Experimental setup

All image compression processes were carried out on a computing system equipped with Intel(R) Xeon(R) W-2145 CPU operating at 3.70GHz, 64 GB of RAM and 2 GB AMD graphics card.

3.4 Evaluation of compression performance and compressed images

The evaluation of compression performance and the quality of compressed images was carried out using a combination of computational performance analysis, qualitative visual assessment, and quantitative statistical metrics, ensuring a comprehensive and multi-dimensional comparison of the applied compression techniques (JPEG2000 lossless, JPEG2000 lossy, and ECW).

For compression performance analysis, key indicators including compressed file size, compression ratio, and processing time were measured for each dataset. The compressed output size was compared against the original input to assess storage efficiency, while the compression ratio was calculated to quantify the degree of data reduction achieved by each method. Additionally, compression time was recorded to evaluate computational efficiency and processing overhead. These metrics were analyzed comparatively across all test images to identify trade-offs between storage optimization and processing requirements.

The qualitative assessment focused on evaluating the perceptual and interpretative quality of the compressed images. Key parameters assessed included edge sharpness, spatial detail preservation, color fidelity, radiometric consistency, texture representation, and geometric integrity. Representative features

such as building edges, roads, vegetation, water bodies, and small urban objects were examined to understand how compression affects both high-detail and homogeneous regions. Evaluation was performed using a matrix of representative image clips from both the original and compressed datasets, enabling side-by-side visual comparison.

For quantitative assessment, widely recognized image quality metrics were employed to objectively evaluate the fidelity of compressed images relative to the original datasets. These included Multi-Scale Structural Similarity Index (MSSSIM), Relative Average Spectral Error (RASE), Peak Signal-to-Noise Ratio (PSNR), and Erreur Relative Globale Adimensionnelle de Synthèse (ERGAS) (Table 1). Furthermore, statistical analysis was performed to assess central tendencies, variability, and robustness of each compression method.

4. RESULTS AND ANALYSIS

4.1 Compression performance analysis

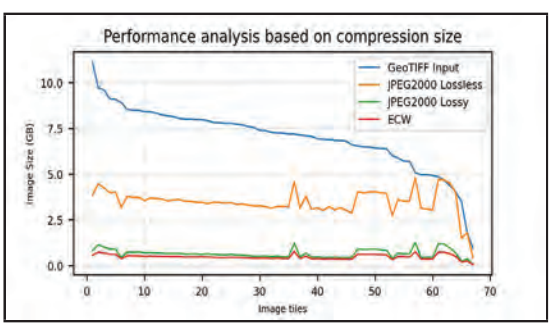

Figure 1: Input vs output compressed size (JPEG2000 lossless vs JPEG2000 lossy vs ECW)

The comparative evaluation of JPEG2000 lossless, JPEG2000 lossy, and ECW compression techniques in terms of compressed output file size (in Figure 1) demonstrates that ECW consistently achieved the highest compression, compared to both JPEG2000 variants. JPEG2000 lossy provided compression near to ECW, while JPEG2000 lossless resulted in output sizes closer to the original input, as expected due to its non-destructive nature.

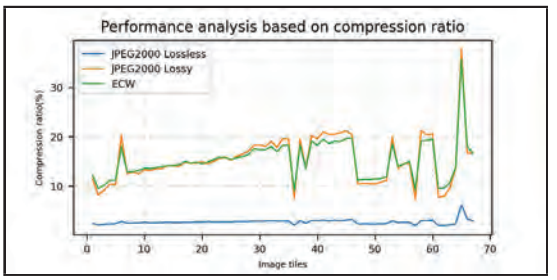

Figure 2: Compression ratio comparison among JPEG2000 lossless, JPEG2000 lossy, and ECW

Similarly, compression ratio analysis (in Figure 2) further reinforced these observations. ECW exhibited the highest compression ratios across most test images, followed by JPEG2000 lossy, while JPEG2000 lossless maintained relatively low and stable ratios. However, ECW also showed variability in performance, with occasional spikes in compression ratio for highly homogeneous images, indicating sensitivity to image content.

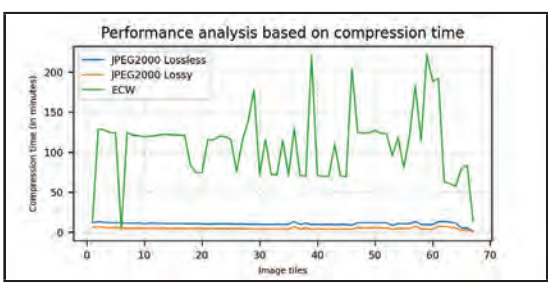

Figure 3: Compression time comparison among JPEG2000 lossless, JPEG2000 lossy, and ECW

In terms of computational performance (in Figure 3), JPEG2000 lossy demonstrated the most efficient balance between compression ratio and processing time, achieving relatively high compression at significantly lower processing times. JPEG2000 lossless exhibited moderate processing times with consistent behavior across datasets. In contrast, ECW required substantially higher compression times,

Table 1: Quantitative Evaluation Metrics with Variable Definitions

Metric	Formula	Notations	Measures	Value Range and interpretation
MSSSIM (Multi-Scale Structural Similarity)	$MSSSIM = [l_m(x,y)^{\alpha_M} . \prod_{j=1}^{M} [c_j(x,y)]^{\beta_j} [s_j(x,y)]^{\gamma_j}$	x,y: reference and test images; M: number of scales; $l_m(x,y)$: luminance comparison at coarsest scale $c_j(x,y)$: contrast comparison at scale j; $s_j(x,y)$: structure comparison at scale j; $\alpha_M, \beta_j, \gamma_j$: weighting factors	Structural Similarity (perceptual quality)	Value range: 0-1 Interpretation: Higher is better
RASE (Relative Average Spectral Error)	$RASE = \frac{100}{\mu} \sqrt{\frac{1}{N} \sum_{i-1}^{N} (RMSE_i)^2}$	N: number of spectral bands;μ: mean radiance of all band; $RMSE_i$: root mean square error of band i	Spectral radiometric error	Value range:>= 0 Interpretation: Lower is better
PSNR (Peak Signal-to-Noise Ratio)	$PSNR = 20 * log_{10} \left(\frac{MAX}{\sqrt{MSE}} \right)$	MAX : maximum pixel value; MSE : Mean square error	Pixel error (signal fidelity)	Value range: 0 – inf (dB) Interpretation: higher is better
ERGAS (Erreur Relative Globale Adimensionnelle de Synthèse	$ERGAS = 100. \frac{h}{l} \sqrt{\frac{1}{N} \sum_{i-1}^{N} \left(\frac{RMSE_i}{\mu_i} \right)^2}$	h/l: resolution ratio; $RMSE_i$: RMSE of band i; μ_i: mean of band I; N : number of band	Global relative spectral error	Value range: >= 0 Interpretation: lower is better

particularly for large or complex images, indicating a higher computational overhead despite its superior compression efficiency.

Overall, the comparative evaluation of JPEG2000 lossless, lossy, and ECW compression techniques demonstrates clear tradeoffs between compression efficiency, processing time, and storage optimization.

4.2 Qualitative assessment

A qualitative evaluation was conducted to assess the perceptual impact of selected compression techniques across multiple spatial scales and feature types, including edge sharpness, spatial detail preservation, color fidelity, radiometric consistency, texture, and geometric integrity. The chosen scales follow established remote sensing principles that relate object size to spatial resolution for accurate feature interpretation (Lechner et al., 2009; Blaschke, 2010). The selection of interpretation scales was based on the relationship between feature size and spatial resolution, where smaller and more detailed features require larger scales to ensure accurate representation, while larger and homogeneous features can be effectively interpreted at smaller scales without significant loss of information.

The qualitative evaluation shows that lossless JPEG2000 compression preserves image quality almost identical to the original across all parameters, including edge sharpness, spatial detail, color fidelity, radiometric consistency, texture, and geometric integrity. In contrast, lossy JPEG2000 introduces slight blurring, minor detail loss, and subtle color shifts, while ECW lossy compression provides efficient storage but results in slight smoothing, reduced texture, and minor geometric distortions. High-detail features such as vehicles, building edges, and urban textures are relatively affected, whereas larger homogeneous features like vegetation and water bodies remain relatively stable. However, it is important to acknowledge that qualitative assessment is inherently limited by human visual perception and may not capture subtle pixel-level distortions relevant to automated analysis workflows.

4.3 Quantitative assessment

The comparative quantitative evaluation of compression performance using four widely used statistical analysis in image quality metrics – MSSSIM, RASE (%), PSNR (dB), and ERGAS reveals across three compression methods: JPEG2000 (lossless), JPEG2000 (lossy) and ECW. It is important to note that JPEG (lossless) consistently demonstrated perfect values for all images across all evaluated metrics; therefore, it was excluded from the boxplot analysis to avoid graphical saturation and preserve interpretability.

As illustrated in Figure. 4, Both JPEG (lossy) and ECW methods achieve high MSSSIM (>0.98), indicating strong structural preservation. However, JPEG2000 achieve slightly higher MSSSIM median values and exhibit a tighter IQR, indicating superior preservation of structural information and more consistent perceptual quality. However, few outlier exist for both cases.

In terms of spectral fidelity, JPEG2000 demonstrates lower median RASE values with a tighter interquartile range, whereas ECW exhibits greater dispersion and several high-value outliers (up to 7%), suggesting less consistent performance.

Similarly, PSNR results show that JPEG2000 generally attains higher reconstruction quality, with median values exceeding those of ECW and fewer low-quality outliers. The upper whisker for JPEG2000 extends beyond 40 dB, indicating excellent quality in best cases while

Table 2: Parameter-based qualitative evaluation of compression techniques (JPEG2000 lossless vs JPEG 2000 lossy vs ECW)

Key Parameters	Description	Original Image	Lossless	Lossy	
			JPEG2000	JPEG2000	ECW
Edge Sharpness	Building Boundaries (1:10)	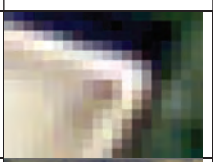	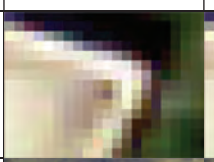	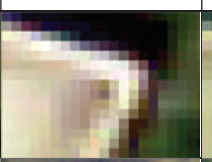	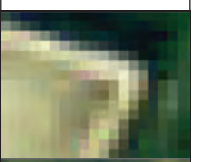
	Shoreline (water bodies) (1:100)	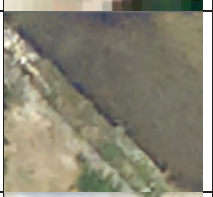	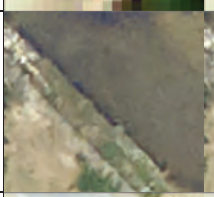	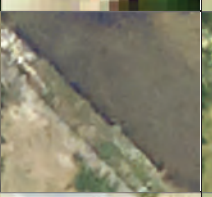	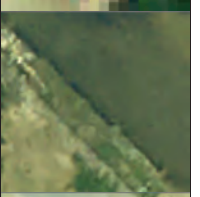
	Road (1:100)				
Spatial Detail Preservation	Single tree crown (1:100)				
	Vehicles (1:50)				
	Small house (1:100)				
Color Fidelity	Vegetation (1:500)				
	Building roofs (1:50)			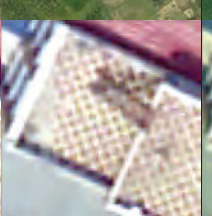	
	Roads (1:50)		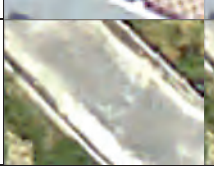	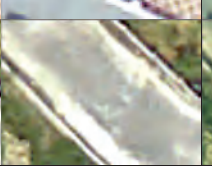	

Radiometric Consistency	Water bodies (1:100)	
	Homogeneous agricultural land (1:500)	
	Bare land (1:100)	
Texture	Vegetation (1:50)	
	Water Bodies (1:50)	
	Urban surface (1:50)	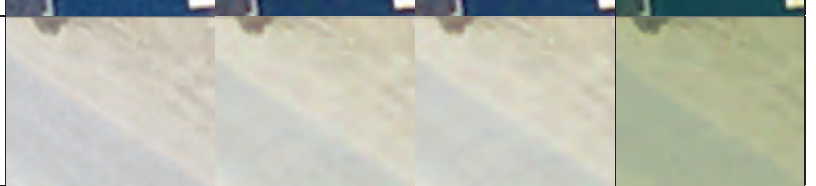
Geometric Integrity	Building Edges (1:10)	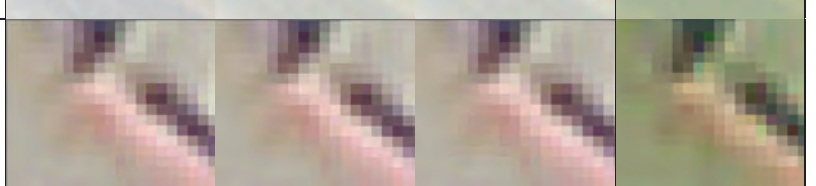
	Road Edges (1:10)	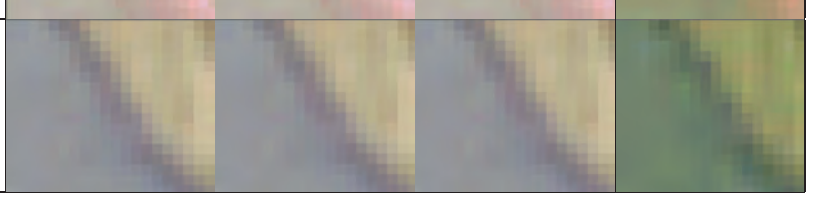

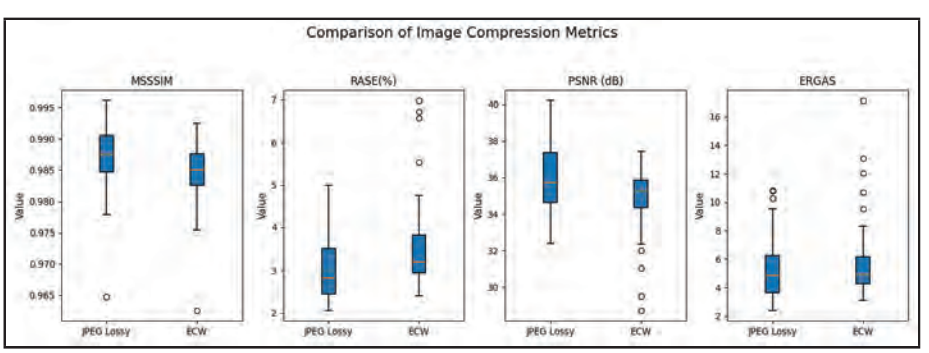

Figure 4: Boxplot for quantitative evaluation of compression techniques (JPEG2000 lossless vs JPEG 2000 lossy vs ECW

ECW shows more lower-end outliers (down to ~29 dB), suggesting occasional degradation.

For the ERGAS metric, although both methods present comparable central tendencies, ECW displays significantly higher variability and more extreme outliers (up to 17), indicating occasional degradation in global reconstruction accuracy.

Overall, JPEG2000 (lossy) not only provides better average performance across all evaluated metrics but also demonstrates greater robustness and stability, making it a more reliable choice for applications requiring high-fidelity image compression. However, ECW exhibits greater dispersion and more outliers, indicating less predictable performance.

5. DISCUSSION

The comparative assessment of JPEG2000 (lossless and lossy) and ECW compression methods highlights important trade-offs between compression efficiency, processing time, data fidelity and format interoperability, which directly influence their suitability for different remote sensing applications.

JPEG2000 lossless preserves original image quality and radiometric and spectral integrity, making it the most appropriate choice for high-precision tasks such as numerical analysis, automatic classification, and scientific studies. However, its lower compression efficiency limits its practicality for large-scale storage.

JPEG2000 lossy provides the best overall balance, achieving high compression ratios with low processing time while maintaining strong structural and spectral fidelity. Its consistent performance across MSSSIM, RASE, PSNR, and ERGAS metrics indicates that it is well-suited for a wide range of applications, including visual interpretation, numerical analysis, and automated classification.

ECW achieves the highest compression ratios and smallest file sizes, making it advantageous for data storage and transmission. ECW is more appropriate for visual interpretation, general visualization, and feature digitization, where storage efficiency and quick rendering are prioritized over fine analytical accuracy. However, its higher computational cost, low performance on high detailed features and greater variability and the presence of significant outliers across multiple metrics, along with observed smoothing and occasional distortions, reduce its reliability for detailed interpretation and analytical applications.

Overall, JPEG2000 lossy emerges as the most versatile option, offering a strong balance between compression efficiency, processing time, and data fidelity within an open and widely supported standard. JPEG2000 lossless remains essential for applications requiring complete data integrity, despite its lower compression efficiency. In contrast, although ECW provides superior compression and storage efficiency, it is a proprietary format with limited acceptance across image visualization and processing platforms, restricting its use in interoperable and analysis-driven workflows. Therefore, ECW is best suited for storage-efficient visualization and dissemination, while open-format JPEG2000 is preferable for analytical and cross-platform remote sensing applications.

These findings are largely consistent with existing literature, which generally recognizes JPEG2000 as a robust standard for remote sensing image and its product compression due to its superior rate-distortion performance and preservation of spectral fidelity (Ruzickova & Ruzicka, 2012; Zabala & Pons, 2010). Previous studies have demonstrated that lossless JPEG2000 maintains radiometric integrity for scientific applications, while its lossy variant achieves an effective balance between compression efficiency and image quality, particularly for

classification and interpretation tasks (Zabala & Pons, 2010). Similarly, although ECW is known for achieving high compression ratios and efficient data streaming, prior research and technical documentation have reported smoothing effects and reduced reliability in representing fine spatial details under higher compression levels (Hexagon, 2025).

6. CONCLUSION AND RECOMMENDATION

This study aimed to evaluate the performance of JPEG2000 (lossless and lossy) and ECW compression techniques for high-resolution LiDAR-derived orthophotos using both qualitative and quantitative assessment methods. The results showed that ECW achieved the highest compression ratios and smallest file sizes, while JPEG2000 lossy provided comparable compression with significantly lower processing time. JPEG2000 lossless preserved image quality and radiometric integrity almost identical to the original but with limited compression efficiency. Quantitative analysis further indicated that JPEG2000 lossy consistently achieved higher structural similarity and signal quality with lower error metrics compared to ECW, while ECW exhibited greater variability and the presence of outliers.

These findings indicate that, although all three methods effectively reduce data volume, their performance differs in terms of efficiency, consistency, and quality preservation. For practical applications, JPEG2000 lossless is recommended for high-precision analytical tasks requiring full data integrity, JPEG2000 lossy for general-purpose remote sensing workflows requiring a balance between quality and efficiency, and ECW for storage-efficient visualization and data dissemination where maximum compression is prioritized over analytical accuracy. Therefore, the selection of a compression technique should be guided by application requirements, particularly in balancing storage efficiency and data fidelity in high-resolution remote sensing workflows.

REFERENCES

Blaschke, T. (2010). Object-based image analysis for remote sensing.*ISPRS Journal of Photogrammetry and Remote Sensing*, 5(1), 2–16.

Demirel, H., & Anbarjafari, G. (2011). Discrete wavelet transform-based satellite image resolution enhancement. *IEEE Transactions on Geoscience and Remote Sensing*, 49(6), 1997 - 2004.

Dong, P., & Chen, Q. (2017). LiDAR remote sensing and applications. CRC Press.

Gautam, B. (2010). Image compression using discrete cosine transform and discrete wavelet transform (Bachelor Thesis).

Gupta, A., Bansal, A., & Khanduja, V. (2017). Modern lossless compression techniques: Review, comparison and analysis. Second International Conference on Electrical, Computer and Communication Technologies (ICECCT) (pp. 1-8). IEEE.

Hexagon. (2025). ERDAS ECW JP2 SDK 6.1: User Guide. Hexagon.

Joshi, A., & Koirala, S. (2020). Preparation of high-resolution DTM and orthophoto using LiDAR in Nepa. *Journal on Geoinformatics, Nepal*, 20(1), 75-80.

Lechner, A. M., Stein, A., Jones, S. D., & Ferwerda, J. G. (2009). Remote sensing of small and linear features: Quantifying the effects of pixel size on detection accuracy. *Remote Sensing of Environment*, 113(9), 1909–1921.

Marcellin, M., Gormish, M., Bilgin, A., & Boliek, M. (2000). An overview of JPEG-2000. Proceedings DCC 2000. *Data Compression Conference* (pp. 523-541)). IEEE.

Rabbani, M., & Joshi, R. (2002). An overview of the JPEG 2000 still image compression standard. *Signal processing: Image communication*, 17(1), 3-48.

Ruzickova, K., & Ruzicka, J. (2012). Comparison of mpact of JPEG 2000 Lossy Comparison with ECW Lossy Compression to Digital Terrain Model. The 33rd Asian Conference on Remote Sensing. Pattaya, Thailand.

Schowengerdt, R. A. (2012). Techniques for image processing and classifications in remote sensing. Academic Press.

Sestras, P., Badea, G., Badea, A. C., Salagean, T., Roșca, S., Kader, S., & Remondino, F. (2025). Land surveying with UAV photogrammetry and LiDAR for optimal building planning. *Automation in Construction*, 173, 106092.

Singh, M., Kumar, S., Chouhan, S. S., & Shrivasta, M. (2016). Various image compression techniques: lossy and lossless. *International Journal of Computer Applications*, 142(6), 23-26.

Yao, H., Qin, R., & Chen, X. (2019). Unmanned Aerial Vehicle for remote sensing applications—A Review. *Remote Sensing*, 11(12), 1443.

Zabala, A., & Pons, X. (2010). Effects of lossy compression on remote sensing image classification of forest areas. *International Journal of Applied Earth Observation and Geoinformation*, 43-51.

Author's Information

Name	:	Tina Baidar
Academic Qualification	:	MSc. in Geospatial Technologies
Organization	:	Survey Department
Current Designation	:	Chief Survey Officer

Evaluating the Effectiveness of Land Use Zoning in Preserving Agricultural Land for Food Security in Nepal

Tanka Prasad Dahal[1], Reshma Shrestha[2], Purna Bahadur Nepali[2]
tpdahal@gmail.com, reshma@ku.edu.np, purna@kusom.edu.np
[1]Land Management Training Center, [2]Kathmandu University, Nepal

KEYWORDS

Land use planning, Food security, Agricultural land, Sustainable development goal

ABSTRACT

About 673 million people experienced hunger in 2024, underscoring the immense challenge of achieving the SDG goal 2 "Zero Hunger" target by 2030. To combat this goal, security of food must be assured which are categorized in four components: access, availability, utilization and sustainability. Linking components of food security with land use planning, availability of food seems associated with production of food, which is dependent upon availability of agriculture land. Therefore, aim of this study is to evaluate the land use zoning implementation at local level focusing on preservation of the agriculture land considering the case of Banepa Municipality. The methodology adopted for this study is desk review and of key informant interview (KII) and focus group discussion (FGD). For desk review, research articles and policies related to food security and land use has been reviewed to understand its linkages. Freely available remote sensing imagery and maps were used to map the existing land use, while land use zoning guidelines developed by Banepa Municipality were referenced in the preparation of the zoning map. The comparison of existing land use and proposed land use zoning based on legal document reflects that there are bottlenecks in legal arrangements and intuitional arrangements for the land use zoning. Current policy provisions and institutional arrangement is unable to preserve agriculture land that directly impacts on food availability and ultimately affects food security. This study concludes that policy revision and local level capacity building is required to implement the land use zoning and planning for agricultural land preservation. It also recommended for effective implementation of land use policy for preservation of agricultural land and optimum utilization of land for food security.

1. INTRODUCTION

Now a day fertile agricultural lands are an irreplaceable natural resource (Paster, 2004). Considering the loss of agriculture land as a challenge of food security, the increase in population and aspirations impacts on land becomes scarce resource. Land is limited so there is conflict between the competing use of it with interests of individual land user and the common good. As highlighted by Ikerd (2011), land use planning is important for protection of agricultural land such that it contributes in combating food insecurity.

In addition, the study of (FAO, 1993) mentioned that Land use planning is complex subject that needs to be combining with physical, social and economic aspect. Therefore, it seems that land use planning and its implementation is must to protect the productive potential agricultural land for sustainable food systems. Land use planning is not easy task it is complex subject needs to combine physical, social and economic aspect of use with foreseen for future (FAO, 1993).

Land use planning is the process of carefully deciding how portions of the earth's surface should be used considering both present and future conditions based on established goals and criteria (Richardson, 1989). It involves assessing, regulating, and arranging land resources to balance competing demands, promote sustainable development, and maximize social, economic, and environmental benefits. Its purpose is to designate land for specific use: such as agriculture, residential areas, industry, infrastructure, recreation, and conservation for reducing conflicts and safeguarding natural resources (FAO, 1993).

Food security deals with the people's access to sufficient food based on physical and economic perspective for healthy life of them. There are various actors playing role in land use and food security system from local to global scale. The main actors are farmers, citizens in urban area, government institutions and thematic organizations as well as local institution, financial intuitions providing credits to agriculture or agribusiness, International institution like UN providing aid & advice, agriculture based enterprises, Non-government organizations, media (Mouël & Forslund, 2018).

In the global context, rapid population growth increases the demand for food as well as agricultural and forest products. Meeting food security needs using current farming methods is likely to intensify competition for natural resources, raise greenhouse gas emissions, and contribute to greater land degradation and deforestation (FAO, 2020). The challenges of food security and sustainable agriculture are; loss of arable land, limited land for agriculture, food and drought, rural poverty, increase food demand (Jia & Dosdogru, 2021).

Urbanization in Banepa Municipality increased gradually from 1992 to 2012, followed by a rapid surge that reached approximately 18% of the total land area by 2020, accompanied by a significant loss of agricultural land and other existing land uses (Twayana et al., 2020). Government of Nepal has been initiated the action for the protection of agricultural land through land use zoning based on land use policy 2015 but its effectiveness and impacts has not been analyzed yet. Hence, this study aims to evaluate the current land use zoning at local level and its outcome in terms of preserving the agriculture land considering the case of Banepa Municipality.

2. LITERATURE REVIEW

2.1. Land use and food security

World food summit 1996 defined food security as the situation where every person, at all times, has both physical and economic access to enough safe and nutritious food that fulfills their dietary requirements and food preferences, enabling an active and healthy life. Food security requires the consistent fulfillment of four interconnected dimensions: availability where sufficient food supply via production, stocks, and trade, access as households' ability to obtain food influenced by income, markets, and prices, utilization is effective nutrient use shaped by diet, care, and food preparation, and stability- reliable access despite shocks or disruptions (FAO, 2008).

Food security is the key contemporary challenge of the global community (Rockson et al., 2013).*The State of Food and Agriculture: Leveraging Food Systems for Inclusive Rural*

Transformation highlights that food systems encompass not only agricultural production but also processing, distribution, and consumption, all of which contribute significantly to employment and income generation in rural areas. It argues that the strengthening and modernization of these systems can foster inclusive rural transformation by integrating smallholder farmers, women, and youth into value chains, thereby reducing poverty and improving food security (FAO, 2017). The food security heavily depends on agricultural productivity growth (Baldos et al., 2014). Every piece of land need to utilize to feed 30 million citizen of Nepal (Bhattarai et al., 2023).

Land use is the dynamic phenomenon so need to have efficient land evaluation system during land use zoning (Pandey, 2023). There are several studies that emphasizes on combating food insecurity required preservation agriculture land. In this regards, Sustainable Land Management (SLM) theory emphasizes the coordinated and efficient use of land resources to satisfy present human needs while maintaining long-term land productivity and ecological health. It highlights the need to balance agricultural production with environmental protection and socio-economic development by promoting practices that reduce land degradation, improve soil fertility, and conserve water and biodiversity. The approach also advocates for adaptive, participatory, and context-specific land-use strategies that are responsive to local conditions and community priorities (Lininger et al., 2011). According to (Timilsina et al., 2019), in country like Nepal, land management practices had a substantial impact on soil quality and agricultural productivity. It also, highlighted the need for urgent interventions to curb land degradation while sustaining land productivity through the adoption of sustainable land management approaches including horizontal coordination and local level capacity building for local level land use planning is also highlighted in (Shrestha et al., 2021) Towards Sustainable Land Management : State of the Art in Land use Policies of Nepal.

2.2. Land use planning initiatives in Nepal (1990- 2015)

The concept of land use planning through land use zoning was initiated in Ninth Development plan of Nepal (1997-2002) in which focus has given to achieve sustainable land use by implementation of land use plan through zoning and aware people on role of land use plan in agriculture, environment and development activities (Nepal et al., 2020). The legal milestone on Implementation of land use plan, controlling fragmentation and encourage consolidation has been introduced during amend of Land Act 1964 in 2000. Nataional land use project was established in 2000 to carry out the land use plan of country. Land use planning through zoning at national and district level was initiated in land use policy 2001(Nepal et al., 2020). Provision of Central land use coordination council, land use program committee and central land use project at central level and land use action committee decided by government in 2000. The role of national land use project is to prepare land use plan of each VDC/Municipality based on District level land use plan (Oli, 2001) National land use policy was formulated in 2012 focused on sustainable socio-economic and environmental development through the optimum utilization of land resources. There is provision of classification agricultural, residential, commercial, and industrial, forest, public utility and other 7 zones.

2.3. Land use implementation initiatives (2015 onwards)

After devastating earthquake of 2015 and adaptation of new constitution of Nepal in 2015, realization for need of incorporating the risk and hazard of natural or manmade disaster during land use plan was incorporate in revised

Land Use Policy 2015. The policy is committed on the ideology for achieving sustainable, economic and environmental development through the optimum utilization of agricultural land and land resources (MoLRM, 2015). This policy aimed to formulation of federal, Provincial and local level land use plan and their implementation to protect agricultural land, forest area, religious and cultural area etc. Land Use Policy 2015 added 4 more land use zones and number of zones reached to 11.

The Land Use Policy 2015 proposed the responsibility of implementation to Ministry of land management, cooperative and poverty alleviation (Nepal et al., 2020). Implementation of land use is supported by institutional provision for federal to local level land use council (MoLRM, 2015).

Land Use Act, 2019 has been enacted with provision of classification of land, preparation land use zoning map and hand over those maps to local level for implementation of essence of land use policy 2015. The formation of institutional framework of federal to local level land use council including local level execution committee and their role and responsibility has been defined in the Act. Concept of land bank is also included in the act (Uprety, 2021).

Land Use Regulation, 2022 has been formulated and implemented for effective implementation of land use policy. The major provisions are focused on land use classification guidance (based on local need, data received from federal ministry and regulation annex-8), provisions of changing land use classes (zones), parcel fragmentation control & consolidation are included (NLC, 2023).

According to report of land ministry of Nepal-federal government prepared land use zoning maps of all local level in 1:10,000 scale including documents and handed over them to all 753 local governments in 2023. The Land Use Regulation, 2022, gave authority of updating those maps within six months were provided to respective local government. However, many local governments were unable to meet this deadline, prompting the government to extend the timeframe through amendments in 2023 and 2025. Despite technical support from the Survey Department, only around 350 local levels have completed land use zoning, others local level are unable to complete the process.

2.4. Land use & food security in Nepal

Nepal is facing declining in food security situation due to national and international crisis (Bista et al, 2013). In Nepal, the total area of agricultural holdings increased from 1.68 million hectares in 1961/62 to 2.65 million hectares in 2001/02. However, it declined to 2.52 million hectares in 2011/12 and further decreased to 2.22 million hectares by 2021/22 (GoN, 2023). There is urging for protection of agricultural land for production of food which triggered for the government policy that should be focused on protection of agriculture land. The research carried out by forest research and training center shows that the 26.31% crop land in 2000 decreases to 24.21% in 2019 (Aryal, 2022). This indicates that reduction of agriculture adversely affected the food security of country due to decrease in productivity.

Land management practices in Nepal have had a substantial impact on soil quality and agricultural productivity, highlighting the need for urgent interventions to curb land degradation while sustaining land productivity through the adoption of sustainable land management approaches (Timilsina et al., 2019). Expansion of agricultural area can be done by using fallow land in agriculture purpose (Paudel et al., 2019).

3. STUDY AREA

Banepa Municipality is situated approximately

21 km east of the capital, Kathmandu, in Kavrepalanchok District, Bagmati Province. It lies at 27°38' N and 85°31' E, about 1,500 m above sea level, covering an area of around 55 km² and divided into 14 administrative wards (MoFAGA, 2026). The Araniko Highway and well-connected local roads have enhanced accessibility, attracting businesses, tourists, and residents. The municipality hosts numerous religious and historical sites, educational institutions, and healthcare facilities, contributing to its social and economic development as well as tourism. Total population of Banepa is 55628 in 2011 census whereas 67,690 in 2021 Census, reflecting a population growth rate of 1.7–2 % per year and a 10-year growth of 17.3 %.

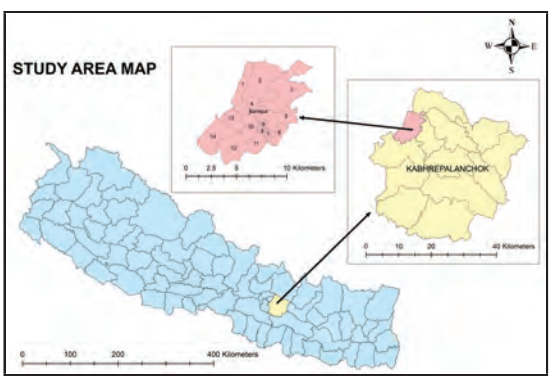

Figure 1: Study area map

4. METHODOLOGY

4.1. Data used

This study is based on mixed method approach using both primary and secondary data including literature review. The primary data used in this study are; Focus Group Discussion (FGD), Key informant interview (KII) whereas secondary data are; satellite imageries (Sentinal2A), administrative boundary data from national geoportal of Nepal. The land use zoning classification guideline approved from municipality has been used for preparation of proposed land use zoning classification map. Similarly, the literature related to land use and food security are collected from various web sources like Google Scholar, ResearchGate, ScienceDirect, JSTOR, SprinkLink, NepJOL, FAO, UNDP etc. The Policies, Act and Regulations related to land use are collected from website of Law commission and land Ministry of Nepal.

Primary data were collected through key informant interviews with members of the local-level land use council, policy experts (5) number. In addition, focus group discussions were conducted in Banepa Municipality wards no 2 and 6 including farmers and relevant stakeholders (ward representatives). Secondary data were obtained from the National Population Census 2011 and 2021, collected from the website of National Statistics Office (https://nsonepal.gov.np/). Administrative boundary data for local level and ward map of Banepa Municipality was downloaded from the National Geoportal (https://nationalgeoportal.gov.np), Survey Department of Nepal. Proposed land use zoning classification guidelines is sourced from the website of Banepa Municipality Office (https://banepamun.gov.np). Satellite imageries are collected form Copernicus website (https://dataspace.copernicus.eu/data-collections/copernicus-sentinel-missions/sentinel-2).

The literatures are search with key words- land policy, land use act, regulation, land use planning, institution related to land, responsibility of land management organization, food security, protection of agricultural land etc. A case study is carried out in Banepa Municipality to study the effectiveness of land use zoning classification practiced by local level focusing on agricultural land use change. The implementation status of land use zoning classification and bottlenecks on policy has been explored based on key informant interview and focus group discussion with members of local level land

use council and policy experts.

The tabular data analysis is done using MS Excel, whereas spatial analysis and mapping is carried out in GIS platform. Policy effectiveness assessment result is based in literature as well as KII (key informant interview) and focus group discussion (FGD).

5. RESULTS

The result of this study is subdivided in three dimensions as existing land use of study area, Proposed land use zoning, and Guidelines for land use zoning of study area;

5.1 Existing land use of the study area

Land use map of Banepa has been prepared based on the freely available satellite image (Sentinel-2) of 2024 and administrative boundary (shape file) downloaded from National geoportal, Survey Department of Nepal. **Figure-2**: shows the existing land use of Banepa Municipality in 2024 with major land use categories agricultural land, forest and residential or non-agricultural area.

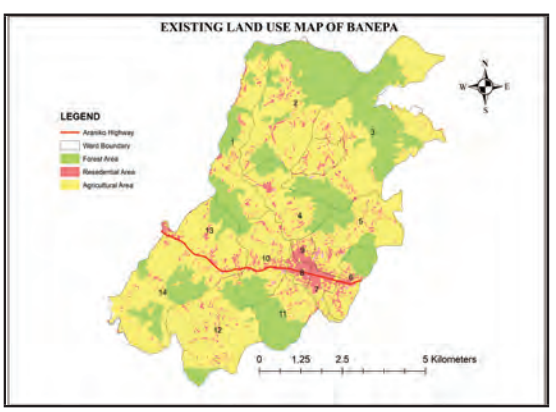

Figure 2: Existing land use map

The area of major land use categories is listed in **Table-1;** The total area of municipality is 5465.59 hectare where the coverage of major land use category are; agricultural land 3356.04 hectors (61.4%), forest area 1666.38 hectares (30.49%) and residential or non-agricultural area 284.34 hectares (5.20%).

Table 1: Existing Land use of study area

S.N.	Present land use category	Area (hectare)	Percentage
1	Agricultural	3356.03	61.40
2	Forest	1666.38	30.49
3	Residential or non-agricultural	284.34	5.20

5.2 Proposed land use zoning

Proposed Land use zoning map of Banepa Municipality is based on land use zoning guidelines approved by local level land use council. The proposed land use zoning map prepared in GIS environment is shown in **Figure-3**. During the mapping process there is complication due to inconsistent guidelines among the wards. Almost wards prepared the guidelines focused on the majority of land to be grouped in residential or non- agricultural land. The zoning criteria are mainly based on the buffer distance from roads.

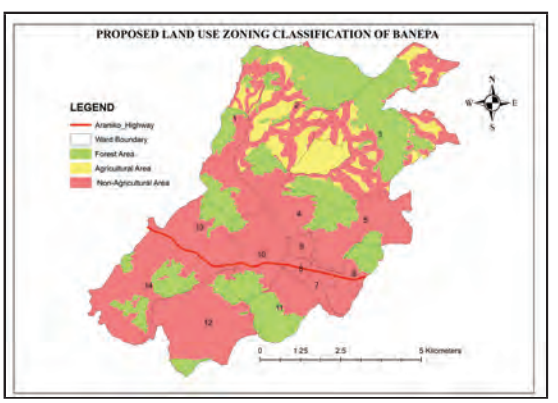

Figure 3: Proposed land use zoning classification map

Preparation of proposed land use zoning map is difficult due to unclear guidelines and conflicting provisions of the Local level land use council decision. Based on council's decisions the area of major land use classification zones are listed as; agricultural land (509.32 ha, 9.32%), forest area (1666.38 ha, 30.49%), and residential or non-agricultural land area (3289.88 ha, 60.19%). The area of major land use categories are shown in **Table-2**.

Table 2: Proposed Land use zoning

SN.	Land use zone category	Area (hectare)	Percentage
1	Agricultural	509.3247	9.32
2	Forest	1666.38	30.49
3	Non-agricultural/ Residential	3289.87	60.19

5.3. Guidelines of the land use zoning class of the case study area

The land use classification made by local land use council is based on the decisions received from the wards. The major criteria for classification is seem to be buffer distances from roads. Classification priority is residential rather than agricultural. The council decision is included in **Table-3** below;

Table 3: Proposed land use zoning guidelines of Banepa

Ward No	Local land use council decision
1	• Residential Area: Past Tukucha VDC ward no 1-4, Past Tukucha ward no 5: 100m from main road center, 50m from other road and river Residential • Remaining Agricultural
2	• Residential Area: 10m or more wider road either side 90m, 6-10m road either side 80m, 4-6m road either side 70m • Other area as present land use; Forest, water, tourism, School , commercial area • Remaining area agricultural
3	• Residential Area: Road 11m, 7m & 5m either side 150m, 100m, 30m • Other area as present land use; School, commercial, cultural, forest, water, Playground, tourism area • Remaining Agricultural area
4	• Up to *Dumtar ghatera dol* Agricultural area • Residential Area: *Akas devi* main road and *Rameshwor* road either side 100m
5	• Residential Area: Previous Banepa ward no 1& 2- residential area, main road 500m, 400m,300m either side • Other classes as present land use; Commercial, Forest, Public utility, river, cultural area etc.
6	• Commercial area: *Araniko* highway either side 150m • Other land use as present land use; Forest, Cultural • Remaining land focused to classify into residential area
7	• Residential area
8	• Residential area
9	• Residential area
10	• Commercial Area: *Arinako* highway 500m either side • Residential area: various road either side 300m/200m
11	• Residential area: Road either side 350m/300m/250m
12	• Non-agricultural/Residential area; Touches with road & river • Agricultural area: other than residential area
13	• Whole ward residential area
14	• Commercial: *Arinako* highway either side 700m • Commercial and Residential area: 500m either side of road

6. DISCUSSION

6.1. Comparison of existing and proposed land use

Based on the results obtained in section 5, a comparative analysis is conducted to understand the status of agriculture land that will be preserving. The **Table-4** shows comparison of existing land use and proposed land use zoning classification based on local level land use council decision.

Table 4: Comparison of existing and proposed land use zoning classes

SN	Land use zone	Existing Area (ha)	Proposed area (ha)	Difference area (ha)
1.	Agricultural	3356.03	509.3247	-2846.71
2.	Forest	1666.38	1666.38	0.0
3.	Residential or non-agricultural	284.34	3289.87	3005.53

It reveals that proposed land use zoning classification prepared based on the guidelines approved by the local level land use council shows that there is significant decrease of agricultural land area 2866.71 hectares (52%) in comparison with agricultural land area in existing land use of 2024. The residential land area- 3005.53 hectares in existing land use seems to be increased by 55% of total area in proposed land use zoning classification. It shows that the guidelines prepared by local level land use council is given priority to residential area rather than agricultural area without assessment of population growth & other parameters required for calculating demand of residential area. This reveals that land use zoning classification decisions has not followed the provisions of classification specified in existing legal provisions of land use policy, act and regulations. The focus has been given to classify lands into residential area due to high residential land value compared to agricultural land. This result shows that of major threat on the preservation of agricultural land in future. UN Food Security Atlas of Nepal, 2019 also highlighted the shrinking agricultural land results lower crop yield production reduces sufficiency of food, which affect the availability dimension of food security (NPC, 2019).

6.2. Challenges in protection of agricultural land

Referring to the Land Use Act, 2019 & Land Use Regulation, 2022-the Authority to updating and approval of land use zoning map and data prepared by federal government is delegated to local level land use council. The data from study area highlighted that the land use zoning classification carried out by local level is only focused on local needs whereas violating the provisions, land use map and data handed over from federal government & the guidelines of annex of land use regulation. In addition, the criteria formulated for preparation of land use zoning in land use regulation (2022) seems to have some technical flaws that has created room for maneuver to assign majority of land in non- agriculture categories. The study of (Timilsina et al., 2019) also mentioned that there were numerous flaws and negligence in the land use planning which in fact unable to access the land for agriculture purpose.

Considering the result obtained from FGD and KII, there is lack of control & monitoring mechanism during the approval process of the local level land use council led to misclassification and undermining the intent of the Land use policy, 2015. Lack of political commitment & proper alignment with coherence between sectorial policies—such as policy related to agriculture, forestry, urban development and food security has been seen unable to protect agricultural land. Limited technical capacity of local government & weak coordination among stakeholders; urban development, agriculture, climate involved in land use planning process is barrier for effective implementation of land use zoning which is also mentioned in (Subedi et al., 2025) present land use and land use zoning of Kushma Municipality . Lack of consistency between federal & local level land use plan is result of non-functionality of the federal and provincial land use council. Implementation of land use zoning faced lack of policy provision on institutional setup to check and approve final zoning carried out by local level land use council. It also highlighted unclear guidelines,

fragile environmental degradation due to unsystematic infrastructure development, more land value in residential land compared to cultivation land, influence of selfish group (mediator and plotter etc.), weak control provision for conversion of land use are major challenges in reduction of agricultural land impacting in food security to meet SDG goal 2.

The pertinent factors highlighted during KII is about political instability at the federal level, characterized by frequent government changes, created volatile policy environment that hinders long-term planning. Institutionally, local levels are hampered by weak capacity and poor coordination with higher tiers of government. This is compounded by a critical shortage of technical expertise, financial resources, and human resources. Furthermore, overlapping jurisdictions between local and federal governments, alongside a plethora of conflicting land-related policies, created legal complexities that stall the zoning process.

Similarly, other important factors highlighted during FGD and KII is the socio-economic issues and technical capacity is another major constraint for local governments to handle and update land use data. High population pressure, widespread poverty, and traditional land rights often conflict with formal zoning frameworks. The prevalence of informal settlements further complicates implementation and enforcement. Weak legal enforcement, low public awareness, and the absence of straightforward compensation mechanisms undermine compliance and foster resistance. These challenges are exacerbated by the compounding effects of climate change and rapid, unplanned urbanization, which made land use zoning task complex.

7. CONCLUSION

The evaluation of effectiveness of land use zoning carried out in the case study of Banepa Municipality during land use implementation showed that there is a major difference between the existing land use and the proposed land use zone around 52% agricultural land is allocated in non- agricultural area supports that the focus of land use zoning is to classify land into non-agricultural area and less priority has given to allocate land in agricultural category means unable to protect agricultural land in future.

The strategies for protection of agricultural land can be achieved by adding provision of control & approval of local level land use council decision by Province or Federal Council. Political awareness regarding land use planning for the members of local level land use council is also required. Assurance of participation of various stakeholders (Agriculture/Industry/Urban development etc.) including land use expert during update of land use zoning is required for effective implementation of land use zoning.

There is need of delegation of authority to district level organization dedicated to look over land use classification and implementation including technical support to local level. Need of coherence between various policies related to land should be established like; land policy, forest policy, agricultural policy, food security policy etc. The protection of agricultural land initiated by land use policy is essence of constitution of Nepal for food security (NLC, 2015). Proper implementation of land use policy can contribute in protection of agricultural land which is the base for SDG goal 2- Zero hunger.

REFERENCES

Aryal, R. R. (2022). National Land Cover Monitoring System for Nepal. In *Banko Janakari* (Vol. 32, Issue 1). https://doi.org/10.3126/banko.v32i1.45429

Baldos, U. L. C., & Hertel, T. W. (2014). Global food security in 2050: The role of agricultural productivity

and climate change. *Australian Journal of Agricultural and Resource Economics*, *58*(4), 554–570. https://doi.org/10.1111/1467-8489.12048

Bhattarai, K., Gautam, S. P., & Gyawali, B. R. (2023). Assessing Food Security Scenario at the Ward Level in Nepal: An Analysis of Caloric Needs from Diverse Crops Based on Location-Specific Factors and Policy Implications. *Nepal Public Policy Review*, *3*(1), 195–220. https://doi.org/10.59552/nppr.v3i1.63

Bista, D. R., Amgain, L. P., & Shrestha, S. (2013). Food security scenario, challenges, and agronomic research directions of Nepal. *Agronomy Journal of Nepal*, 3, 42-52.

FAO. (1993). Guidelines for land-use planning. In *FAO Development Series 1, ISSN 1020-0819, Food and Agriculture Organization of the United Nations Prepared* (Vol. 1).

FAO. (2008). An Introduction to the Basic Concepts of Food Security Food Security Information for Action. *EC - FAO Food Security Programme*, 1–3. http://www.fao.org/docrep/013/al936e/al936e00.pdf

FAO. (2017). The sate of food and agriculture, Liveraging food system for inclusive rural transformation. Food and Agriculture Organization of the United Nations, Rome.

FAO. (2020). Framework for integrated land use planning An innovative approach. *Food and Agricultural Organization of United Nations*, *February*, 16.

GoN. (2023). National Agricultural Census 2078. *National Statistics Office*. https://www.agricensusnepal.gov.np/post/10_64fc3705ded11

Jia, X., & Dosdogru, F. (2021). Sustainable land management for food security and sustainable agriculture through LDN response actions. *United Nations*, *30*(June), 0–20.

MoLRM. (2015). Land Use Policy 2015. *Ministry of Land Reform and Management, Government of Nepal*.

Mouël, C. Le, & Forslund, A. (2018). Land-use Change Trajectories in Existing Scenario Studies. In *Land Use and Food Security in 2050: a Narrow Road*.

NLC. (2015). The constitution of Nepal. *2015*. Nepal Law Commission, Government of Nepal.

NPC. (2019). *The Food Security Atlas of Nepal. Kathmandu*.National Planning Commision, Government of Nepal.

NLC. (2023). Land Use Rules, 2079. Nepal Law Commission, Government of Nepal.

Pandey, G. (2023). Land Use / Land use zoning Practice at Micro level in Nepal : An Assessment. *Voice of Teacher*, *8*(1), 23–42. https://scispace.com/pdf/land-use-land-use-zoning-practice-at-micro-level-in-nepal-an-4jaxuoz6dp.pdf

Paster, E. (2004). Preservation of Agricultural Lands through Land Use Planning Tools and Techniques. *Natural Resources Journal*, *44*(1). https://digitalrepository.unm.edu/nrj/vol44/iss1/9

Paudel, B., Zhang, Y., Yan, J., Rai, R., & Li, L. (2019). Farmers' perceptions of agricultural land use changes in Nepal and their major drivers. *Journal of Environmental Management*, *235*(January), 432–441. https://doi.org/10.1016/j.jenvman.2019.01.091

Richardson, N. (1989). *Land Use Planning and Sustainable Development in Canada*. Canadian Environmental Advisory Council Land.

Rockson, G., Bennett, R., & Groenendijk, L. (2013). Land Use Policy Land administration for food security : A research synthesis. *Land Use Policy*, *32*, 337–342. https://doi.org/10.1016/j.landusepol.2012.11.005

Shrestha, R., Nepali, P. B., & Dahal, T. P. (2021). Towards Sustainable Land Management : State of the Art in Land use Policies of Nepal. *IGI Global Scientific Publishing*, 351–369. https://doi.org/10.4018/978-1-7998-4372-6.ch018

Subedi, S., Pandit, R., Manoj, G. C., & Subedi, I. (2025). *Present Land Use and Land Use Zoning of Kushma Municipality : A Comparative Assessment with Cadastral Superimpose*. 77–92.

Timilsina, R. H., Ojha, G. P., Nepali, P. B., & U.Tiwari1. (2019). Agriculture land use in Nepal: Prospects and impacts on food security. *Journal of Agriculture and Forestry University*, *3*, 103–111.

Twayana, R., Bhandari, S., & Shrestha, R. (2020). Analyzing Urban Growth Pattern and Driving Factors Using Remote Sensing and GIS: A Case Study of Banepa Municipality, Nepal. *Journal on Geoinformatics, Nepal*, *20*(1), 9–18. https://doi.org/10.3126/njg.v20i1.39471

Author's Information

Name	:	Tanka Prasad Dahal
Academic Qualification	:	Master Degree in Geoinformatics, University of Twente, The Netherlands
Organization	:	Land Management Training Center
Current Designation	:	Director

CALENDAR OF INTERNATIONAL EVENTS

AGILE Conference 2026: Smart Data-Making Geospatial Data Actionable
Date: 16 – 19 June 2026
Country: Tartu, Estonia
Website: https://agile-gi.eu/conference-2026

14th EARSeL Workshop on Forest Fires 2026
Date: 25-26 June 2026
Country: Lisbon, Portugal
Website: https://forest-fires.earsel.org/workshop/14-FF-2026/homepage/

International Conference of Environmental Remote Sensing and GIS (ICERS)
Date: 01-03 July 2026
Country: Zagreb, Croatia
Website: https://alcar.geof.hr/icers-conference/

XXVth ISPRS Congress
Date: 04-11 July 2026
Country: Toronto, Canada
Website: https://www.isprs2026toronto.com/

Esri User Conference
Date: 13 – 17 July 2026
Country: San Diego, California
Website: https://www.esri.com/en-us/about/events/uc/overview

46th Scientific Assembly of the Committee on Space Research (COSPAR) and Associated Events
Date: 01-09 August 2026
Country: Florence, Italy
Website: https://www.cospar2026.org/

46th IGARSS 2026
Date: 9-14 August 2026
Country: Washington, D.C
Website: https://2026.ieeeigarss.org/

18th South East Asia Survey Congress
Date: 18-19 August 2026
Country: Kuala Lumpur, Malaysia
Website:https://seasc2026.aseanflag.org/?utm_source=conferenceindex&utm_medium=referral&utm_campaign=listing

3D GeoInfo | Smart Data Smart Cities | LADM & 3D
Date: 28 September - 02 October 2026
Country: Sofia, Bulgaria
Website: https://conference.gate-ai.eu/GeoSofia2026

ACRS 2026: 47th Asian Conference on Remote Sensing 2026
Date: 12-16 October 2026
Country: New Delhi, India
Website: https://acrs2026.in/

PHEDCS 2026: Geospatial Technologies, Photogrammetry and Remote Sensing for Sustainable Development in Environmental, Mining and Industrial Applications
Date: 22-23 October 2026
Country: Almaty, Kazakhstan
Website: https://www.phedcs.com/

FIG & UNECE WPLA International Conference
Date: 28-30 October 2026
Country: Istanbul, Turkey
Website: https://figcadastre.hkmo.org.tr/en/homepage

XXXVI International Symposium
Date: 5-6 November 2026
Country: Sofia, Bulgaria

9th International ISPRS Workshop Low-Cost 3D-Sensors, Algorithms, Applications
Date: 18-20 November 2026
Country: Braunschweig, Germany
Website: https://lc3d.fbk.eu/

WLF7: The 7th World Landslide Forum
Date: 23-27 November 2026
Country: Faridabad, India
Website: https://www.wlf7.org/

60th Photogrammetric Week
Date: 06-09 April 2027
Country: Stuttgart, Germany
Website: https://phowo.ifp.uni-stuttgart.de/

FIG Working Week
Date: 23-27 May 2027
Country: Stavanger, Norway

33rd International Cartographic Conference
Date: 18-23 July 2027
Country: Warsaw, Poland
Website: https://icaci.org/icc2027/

ISPRS Geospatial Week 2027
Date: 19-24 September 2027
Country: Warsaw, Poland
Website: https://www.gsw2027.pl/

Forest Fire Susceptibility Mapping Using Deep Neural Network

Ganesh Pandey[1], Bhoj Raj Ghimire[2]
ganeshpandey362@gmail.com1, bghimire@nou.edu.np[2]
Survey Department[1], Nepal Open University[2]

KEYWORDS

Forest fire, Susceptibility mapping, Machine learning, Deep learning, Kailali, Dang

ABSTRACT

Forest fires are an increasing environmental problem in Nepal, threatening biodiversity, ecosystem stability, and the livelihoods of forest-dependent communities. In recent years, both the frequency and intensity of fires have increased, highlighting the need for accurate forest fire susceptibility mapping to support effective management and risk reduction. This study develops a forest fire susceptibility model for Kailali District using a deep learning approach, integrating twelve explanatory variables related to topography, climate, vegetation, and human influence. Historical fire data from NASA's VIIRS archive (2012–2024) were used for training and validation, with trend analysis indicating peak fire events in 2016 and the lowest in 2020. The dataset was split into 70% training and 30% testing, and model performance was evaluated using accuracy, precision, recall, and F1-score, while the trained model was also applied to Dang District. The susceptibility map generated using the DNN model was classified into five risk zones from very low to very high, achieving accuracy, precision, recall, and F1-score values of 0.93, 0.92, 0.93, and 0.93, respectively. Overlay analysis of forest fire susceptibility map and historical fire occurrence showed that about 91% of observed fire events in Kailali and 88% in Dang District occurred within susceptible zones. This study demonstrates that integrating geospatial data with deep learning can effectively improve forest fire risk assessment in Nepal. The resulting susceptibility maps provide useful information for early warning systems, disaster preparedness, and sustainable forest management.

1. INTRODUCTION

Forest ecosystems provide essential ecological, economic, and social services, including biodiversity conservation, carbon sequestration, soil stabilization, and livelihood support for millions of people (Shi & Zhang, 2023). Despite their importance, forests are increasingly threatened by frequent and severe forest fires driven by climate change, land-use transformation, and anthropogenic activities (B. Mishra et al., 2023; Sharma & Khanal, 2024). In Nepal, forest fires occur predominantly during the dry pre-monsoon season (March–May), causing extensive damage to forest resources, wildlife habitats, air quality, and human health(FRA, 2015) (Parajuli et al., 2023). Forest fires in Nepal

are a newly explored area, and the importance of such studies is not fully acknowledged. There are not many detailed studies available on forest fires. With the acceleration of urbanization and increasingly inevitable human activities, the problems of forest ecological management are increasingly prominent (Mohajane et al., 2021, Vecín-Arias et al., 2016). Forest fire susceptibility maps are essential for understanding and predicting potential hazards in forest ecosystems. They support land-use planning, reduce vulnerability, and improve ecological risk management decisions(Banjade & Dhungana, 2025; Bouhissi et al., 2020). Developing these maps requires a forest fire inventory as the target variable, along with multiple explanatory factors. GIS and RS can be play crucial role in proper assessment, planning and management of forest fire hazard (Bouhissi et al., 2020; Eugenio et al., 2016; Mohajane et al., 2021) . These systems by utilizing the geospatial data can help in mapping the risk zone by identifying vulnerable areas and evaluating risks at various scales from global to community levels.

More recently, machine learning and deep learning approaches have been applied in environmental hazard mapping, offering higher predictive accuracy compared to conventional statistical methods (Tuyen et al., 2021; Aarich et al., 2024). Artificial intelligence (AI) and machine learning (ML) are frequently employed to map and track forest fire susceptibility in different parts of the globe (Ahmed et al., 2022) (Rihan et al., 2023) (Mohajane et al., 2021) (Tuyen et al., 2021). In Nepal, research on forest fires is still quite limited and most existing studies have used traditional approach (B. Mishra et al., 2023) (Parajuli et al., 2023). Traditional forest fire risk assessment methods in Nepal have largely relied on expert-based approaches and multi-criteria decision analysis techniques such as the Analytical Hierarchy Process (AHP). While these methods are useful, they often involve subjective weighting schemes and limited ability to capture complex nonlinear interactions among variables. Recent advancements in machine learning (ML) and deep learning (DL) offer powerful alternatives capable of learning complex patterns from large geospatial datasets. Deep Neural Networks (DNNs), in particular, have shown superior performance in hazard susceptibility mapping due to their ability to model high-dimensional, nonlinear relationships. Hence, this research aims to prepare wildfire susceptibility map of Kailali district by deep learning technique.

2. STUDY AREA

Kailali District is located in the southwestern Terai region of Nepal within Sudurpashchim Province. The district covers an area of approximately 3,235 km² and exhibits diverse topographic conditions, ranging from flat lowland plains to the hilly terrain of the Chure range. Elevation varies from 109 m to 1,950 m above sea level. Approximately 63% of the district is covered by forest, making it highly vulnerable to forest fire incidents. The climate of Kailali ranges from tropical to subtropical, with an average annual rainfall of around 1,840 mm. Dang District, selected for model transferability assessment, shares similar biophysical and socio-economic characteristics, making it suitable for comparative analysis.

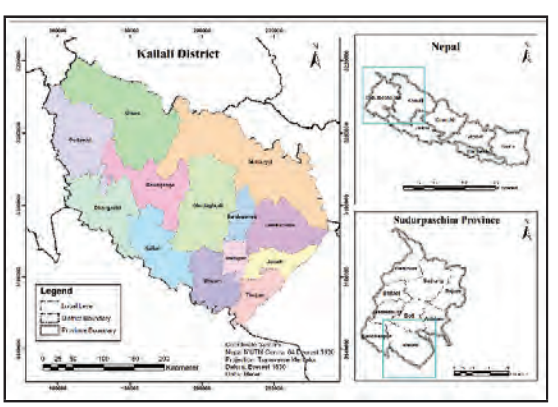

Figure 1: Kailali district

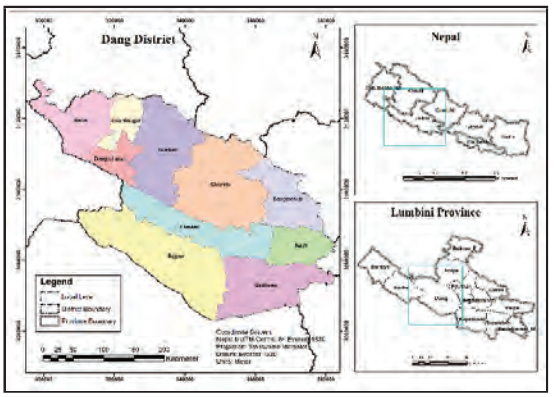

Figure 2: Dang district

3. MATERIAL AND METHODS

3.1 Datasets and software

This study integrated multiple geospatial datasets representing topographic, climatic, vegetation, and anthropogenic factors influencing forest fire occurrence. All these factors were selected based upon previous studies (Joshi et al., 2025; B. Mishra et al., 2023; Parajuli et al., 2020, 2023) . Elevation, slope, and aspect were derived from the Shuttle Radar Topography Mission (SRTM) Digital Elevation Model. Vegetation condition was represented using the Normalized Difference Vegetation Index (NDVI) derived from Landsat-8 imagery processed in Google Earth Engine (GEE). Land surface temperature (LST) and precipitation variables were obtained from satellite-based datasets, while anthropogenic factors such as distance to roads, settlements, rivers, and population density were derived from OpenStreetMap and national census data.

Table 1: Datasets

S. N.	Data	Resolution/ scale	Source
1	Administrative Boundary		Survey Department
2	Digital Elevation Model	30 meters	SRTM USGS Earth Explorer
3	Population Density	Excel ward level data	National Statistics Office
4	River Network	~1 cm at equator	OpenStreetMap (OSM)
5	Road Network	~1 cm at equator	OpenStreetMap (OSM)
6	Settlement	1:25000	Survey Department
6	Precipitation	30 sec	WorldClim
7	Landsat-8 Image	30 meter	USGS EarthExplorer via GEE
8	LST	30 meter	USGS EarthExplorer via GEE
9	NDVI	30 meter	USGS EarthExplorer via GEE
10	Land cover	30 meter	ICIMOD
11	WildFire Occurrence Data		FIRMS-VIIRS S-NPP 375m.

Historical forest fire occurrence data from 2012 to 2024 were collected from the NASA Fire Information for Resource Management System (FIRMS) VIIRS product. Equal numbers of fire and non-fire sample points were generated to construct a balanced dataset. All numerical variables were standardized using the StandardScaler technique, and categorical land cover data were encoded using one-hot encoding. A feedforward Deep Neural Network was developed using Python and TensorFlow. Following software's and tools were used in the analysis:

a) GIS and RStudio for spatial analysis and mapping.

b) Cloud computing platform to write

and execute Python for Landsat images processing, analysis, model training and testing.

c) Python packages (pandas, numpy, rasterio, sklearn, tensorflow).

d) R packages (dplyr, Kendall, lubridate)

3.2 Methodology

This study adopts a data-driven approach to model forest fire susceptibility using a deep neural network (DNN). The methodology comprises planning and literature review, data collection and pre-processing, trend analysis using the Mann-Kendall (MK) test, dataset preparation, susceptibility modelling, model evaluation, and spatial mapping. The overall methodology used for susceptibility mapping followed shown Figure 3 below.

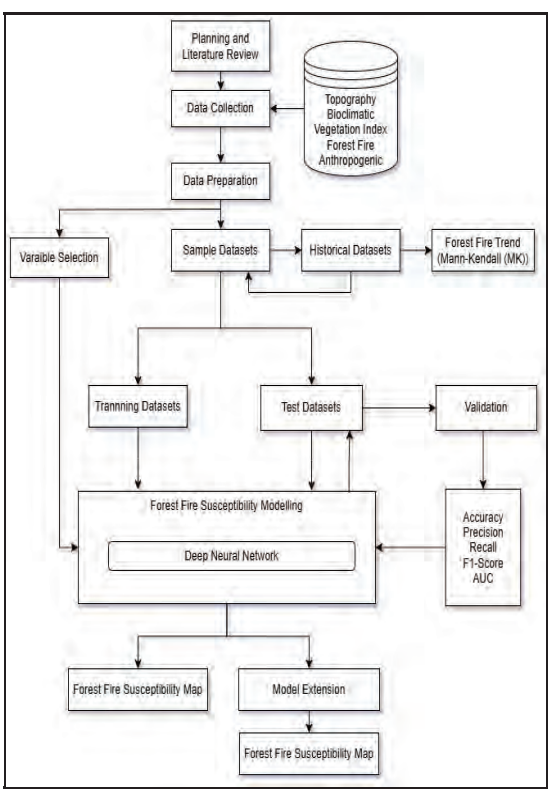

Figure 3: Forest fire susceptibility mapping

3.2.1 Data preparation

Collected data were projected to a common coordinate system UTM Zone 44N, WGS 84 datum and clipped to the administrative boundary of Kailali and dang district. The raster datasets were resampled to a consistent resolution having cell size 30m, and vector datasets (roads, rivers, settlements, population density) were converted to proximity raster's using Euclidean distance. NDVI and LST were derived from Landsat-8 imagery using Google Earth Engine (GEE). Historical forest fire occurrence data from 2012 to 2024 were collected from the NASA Fire Information for Resource Management System (FIRMS) VIIRS product. Equal numbers of fire and non-fire sample points were generated to construct a balanced dataset. For each sampled point Predictor and Target Variables were used. NDVI, LST, precipitation, elevation, slope, aspect, population density, distances to roads/rivers/settlements, and land cover class were used as input variables whereas Fire occurrence data were used as Target Variable. Each parameter that were used in susceptibility mapping were normalized by using standerscaler. All numerical variables were normalized by transforming the original data linearly. By using StandardScaler, each numeric feature was transformed to have zero mean and unit variance, ensuring that all features contribute equally to the model training process. Each value was then changed using following formula. The resulting data will have value ranging from 0 to 1.

$$Xscaled = \frac{x-\mu}{\sigma} \quad \ldots\ldots\ldots\ldots\ldots(1)$$

Where, X represents the original data value, μ represents the mean of the feature and σ is the standard deviation. Xscaled represents normalized data value. The OneHotEncoder from the scikit-learn library was used to convert categorical values into binary vectors, allowing algorithms to interpret them numerically without implying any ordinal relationship. The encoder was fitted to the land cover data and transformed it into a binary

matrix. The datasets were divided into training and testing sets. 70% of all the data points were used to train the deep learning model, while 30% were used to assess how well the model performed. A 70%–30% data split is used because it has been widely adopted in previous studies and consistently provides a good balance between model training and reliable validation performance (Chen et al., 2015; B. Mishra et al., 2023; Mohajane et al., 2021; Pham et al., 2020). To do this, the train_test_split() function was used to randomly split the datasets into training and testing parts.

3.2.2 Trend analysis

Trend analysis of historical fire data is essential in forest fire susceptibility mapping because it reveals spatiotemporal patterns of past fires, which are directly used to model and predict fire-prone areas in susceptibility assessments (Kumar & Kumar, 2022; M. Mishra et al., 2024; Tariq et al., 2021; Zhang et al., 2024). Mann-Kendall (MK) trend test method was used for the trend analysis for 2012–2023 time duration. This non-parametric test identifies the presence and direction of significant trends in fire frequency over time. The test results help contextualize whether wildfire frequency is increasing, decreasing, or stable. This approach is especially useful when working with time series data that isn't normally distributed, meaning the data might have outliers or follow a nonlinear pattern. A MK test with a 90% confidence level was used to check for a monotonic trend. During the test, the null hypothesis (H0) states that there is no trend in the population that the dataset comes from. The alternative hypothesis (H1) suggests there is a trend present. The null hypothesis is rejected if the p-value is less than or equal to 0.1 (Partal & Kahya, 2006) (Karpouzos et al., 2010) (Poudel & Shaw, 2016).

3.2.3 Forest fire susceptibility modelling

3.2.3.1 Deep neural network model

A feedforward DNN model was developed to predict the occurrence of forest fires based on the input variables. First of all, selection of input variables was performed for the collected dependent and independent data. The Variance Inflation Factor (VIF) was calculated by removing variables with the largest VIF value one at a time until all remaining variables have a VIF less than defined limit, typically less than 10 (Campo-Bescós et al., 2013) (B. Mishra et al., 2023). VIF was applied to remove correlated metrics. The correlation among the different variables selected after VIF applied is shown in Figure 4 below.

TensorFlow and Keras libraries were used for developing the model. This model was designed to perform binary classification, where the target variables indicate the presence and absence of fire. TensorFlow is an open-source machine learning framework widely used for deep learning applications. Keras, which is integrated within TensorFlow, offers a high-level API for constructing and training neural networks (Truong et al., 2023; A et al., 2024).

The model was designed using a sequential architecture with 3 hidden and 1 output layer.

- Input layer: In this layer number of input features were defined.
- Hidden layer: Three layers were used as hidden layers. The first hidden layer contains 64 neurons and ReLU activation function. The second hidden layer contains 32 neurons and ReLU as activation function. The third hidden layer contains 16 neurons and ReLU as activation function.
- Output layer: The output layer contains a single neuron with a sigmoid activation function. The output of this function is between 0 and 1.

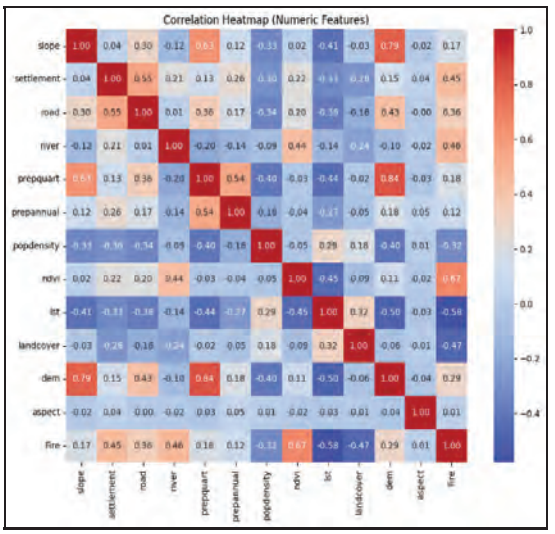

Figure 4: Correlation heatmap of variables

After defining the layers model was compiled by specifying the optimiation strategy, loss function, and evaluation matrix. Adam (Adaptive Moments Estimation) optimizer was selected for training the model. This algorithm was defined by Kingma and Ba (2014) for DNN model optimization. Adam is widely used because it works well and is efficient. It uses information from past gradients and changes the learning rate for each parameter on its own. This makes the model learn quicker and prevents issues like getting stuck in parts where learning slows down. Adam takes the best parts of two other optimization techniques, AdaGrad and RMSProp. It is also good at handling noisy data and can be applied with various types of networks structures and tasks (Wang et al., 2019). The binary_ crossentropy was used as loss function. This function is commonly used as loss function for binary classification problems. It measures the difference between the predicted probabilities and the actual binary labels.

3.2.3.1 Model validation

To evaluate the performance of the DNN model, popular matrixes precision, recall, accuracy, and F1-score were employed. The forest fire susceptibility map generated through modeling was validated using the historical fire occurrence data. Overlay analysis of forest fire susceptibility map and historical fire occurrence was done in ArcGIS. This spatial overlay process provided both visual and quantitative insights into the model's predictive performance and served as a foundational step for subsequent validation and analysis.

3.2.4 Forest fire susceptibility mapping

Using the trained DNN, a pixel-wise prediction was applied across the entire study area using the geospatial input layers. For this first all 12 variables were converted to raster. Raster file of all variables aspect, slope, elevation, distance from road, river, settlement, annual precipitation, precipitation of direst quarter, land surface temperature, landcover, population density, NDVI were imported in google colab environment and their CRS, resolution and extent were checked and ensured they have same coordinate reference system, resolution and extent. Then all the individual raster layers were stacked into a single multi-band raster file. Then the stacked raster was reshaped, StandardScaler and OneHotEncoder were applied as fitted on the training data, and DataFrame was created for prediction. This process is essential for integrating various spectral bands or thematic layers into a unified dataset, which can then be used for further modeling.

Stacking raster facilitate multi-band analysis and enhance the interpretability of geospatial data. After stacking raster, prediction was made. The data was the feed into the model to obtain the predicted outcomes for each pixel in the raster. After generating predictions for each pixel using the trained machine learning model, the results were reshaped and saved as a raster file in GeoTIFF format. Subsequently, the spatial distribution of predicted outcomes was visualized and analyzed using GIS software. The binary classification map was

further classed into five zones as Very low, low, moderate, high and very high.

3.2.5 Extension of DNN model

The trained DNN model was applied to the prepared predictor layers from Dang District. Kailali and Dang districts share similar Climatic zones (Tropical/Subtropical), vegetation types (Sal Forest, grasslands), Socioeconomic influences (agriculture, settlement encroachment), Fire ignition sources (human-induced) (ICIMOD,2023; Rokaya et al., 2024; Shakya et al., 2007) . Thus, using a model trained on Kailali for Dang is a valid application of spatial generalization in machine learning, enhancing scalability and operational use in data-scarce regions.

Similar data were collected for dang district as well. Topographical data, land cover and vegetation data, temperature and precipitation data, Euclidean distance from settlement, roads and rivers networks were projected to a common coordinate system (UTM Zone 44N, WGS 84 datum) and clipped to the administrative boundary of Dang district. The raster datasets were resampled to a consistent resolution (30m), and vector datasets (roads, rivers, settlements, population density) were converted to proximity raster's using Euclidean distance. NDVI and LST were derived from Landsat-8 imagery using Google Earth Engine (GEE).

4. RESULTS AND DISCUSSION

4.1. Result

The Mann-Kendall analysis for the period 2012–2016 yielded a Kendall's tau value of 0.20 with a p-value of 0.8065. This indicates a slight upward movement in annual fire counts during these years. However, the high p-value shows that the observed change is not statistically significant, meaning it may simply reflect normal year-to-year variability rather than a genuine increasing pattern. For the period 2016–2024, the Kendall's tau value was –0.0556 with a p-value of 0.91697. The negative tau suggests a very small decline in fire counts, but again the extremely high p-value indicates that this variation is not meaningful from a statistical standpoint. The historical data illustrate that the number of fire incident are maximum in the month of April and May.

The trained DNN model demonstrated strong predictive performance on the test dataset, achieving high accuracy and balanced precision-recall values. Besides the DNN, Random Forest (RF) and Support Vector Machine (SVM) were also applied to assess forest fire susceptibility in the Kailali District. The Random Forest model was efficient in managing nonlinear data relationships and identifying the significance of various environmental factors through its ensemble-based structure. Similarly, the Support Vector Machine showed strong performance in classifying complex datasets and handling multidimensional feature spaces. Nevertheless, the DNN was chosen as the main modeling technique since it provided relatively higher prediction accuracy and effectively captured complex spatial patterns and nonlinear dependencies among influencing factors. With its layered structure capable of learning detailed features from input data, the DNN proved more suitable for predicting forest fire susceptibility across the varied terrain of the Kailali District.

The predicted probability outputs were spatially mapped and classified into five forest fire susceptibility zones: very low, low, moderate, high, and very high. The spatial distribution of fire points within demonstrated that the northern, central, and southeastern regions of Kailali District show a very dense clustering of fire points, indicating these are the most fire-prone areas historically. Some southern and western areas have fewer fire points. In Kailali District, high and very high

susceptibility zones were primarily concentrated in low-elevation forested areas close to roads and settlements, reflecting the influence of anthropogenic activities on fire ignition. Validation using historical fire data revealed that approximately 91% of fire events occurred within high and very high susceptibility zones. When applied to Dang District, the model maintained robust performance, with 88% of historical fire events falling within high-risk zones.

Table 2: Evaluation Matrix of DNN, RF and SVM model

Model / Evaluation Matrix	DNN	RF	SVM
Accuracy	0.93	0.91	0.9
Precision	0.92	0.91	0.9
Recall	0.93	0.91	0.9
F1-score	0.93	0.91	0.9

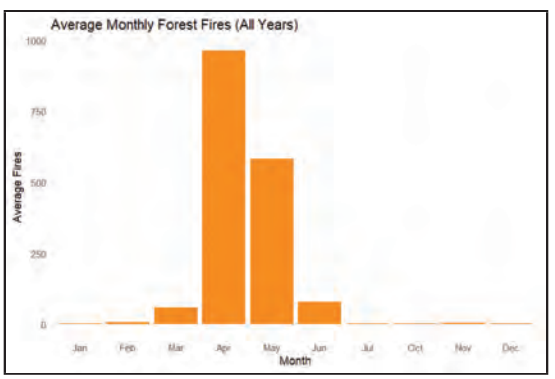

Figure 5: Average monthly forest fire in all years from 2012 to 2024

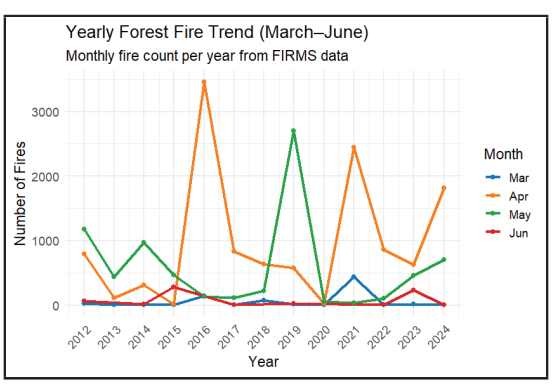

Figure 6: Monthly Forest fires count in March, April, May and June from 2012 to 2024

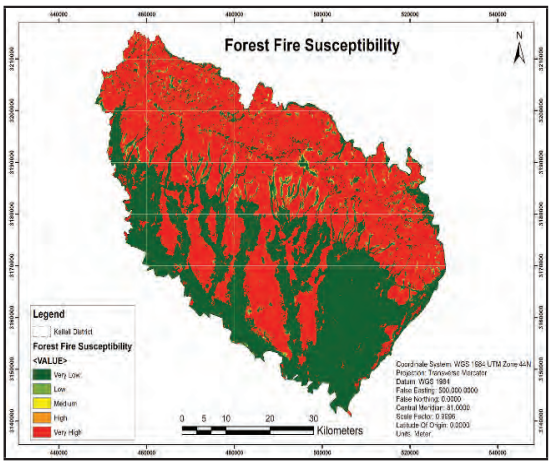

Figure 7: Forest fire susceptibility map of Kailali

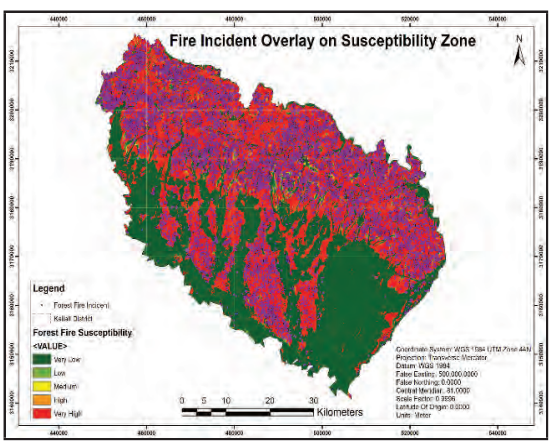

Figure 8: Fire incident overlay on susceptibility map in Kailali

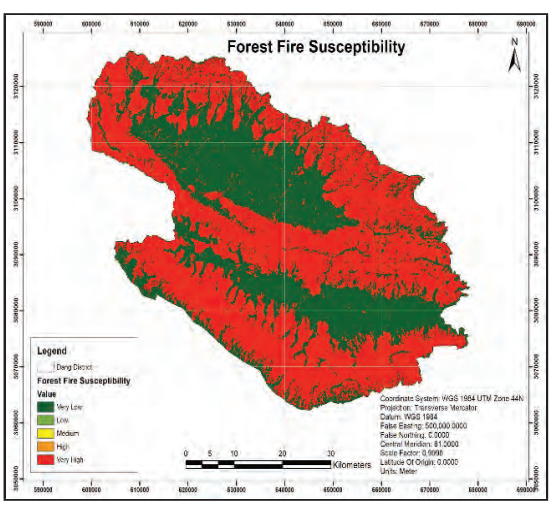

Figure 9: Forest fire susceptibility map of Dang

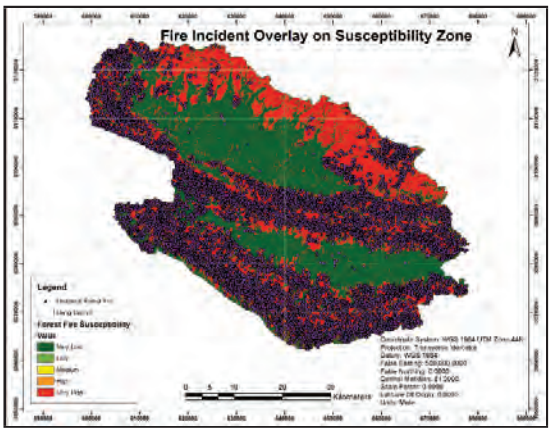

Figure 10: Fire incident overlay on susceptibility map in Dang

4.2 Discussion

The historical forest fire patterns are essential for accurate susceptibility modeling. In Kailali district, past fire events cluster seasonally and spatially, mostly during dry months from March to May. The yearly forest fire trend in Kailali shows an increase in the number of fire incidents in 2016, 2019, and 2021, with the highest number recorded in 2016. Also, number of fire incident are maximum in the month of April and May.

The selection and analysis of input variables are crucial for the performance of deep learning models in fire susceptibility mapping. Elevation, slope, aspect, population density, euclidean distance from river network, road network and settlement, annual precipitation, mean precipitation of driest quarter, land surface temperature, NDVI, land cover and historical fire data are used as input variables. Many other past research have also used these parameters for forest fire susceptibility mapping (Joshi et al., 2025; B. Mishra et al., 2023; Parajuli et al., 2020, 2023). The results provide high accuracy, with a score above 0.93, and the susceptibility maps generated aligned well with known fire hotspot.

To check if the model could perform well beyond the initial area, we tested it in the Dang district. Although the terrain and land use there are different, the model still did a good job pinpointing high-risk zones that aligned with historical fire records. The successful transfer of the model to Dang District highlights its generalizability and potential applicability to other fire-prone regions of Nepal.

5. CONCLUSION

This study explores the application of geospatial technology and machine learning approach to map forest fire susceptibility in Kailali and Dang district. In this study, elevation, slope, aspect, population density, Euclidean distance from river network, road network and settlement, annual precipitation, mean precipitation of driest quarter, land surface temperature, NDVI, land cover and historical fire data were used for forest fire susceptibility modeling. The deep learning approach was used to develop the forest fire susceptibility model of Kailali district. DNN was implemented for forest fire prediction in Kailali district. Then the developed model was extended for forest fire prediction in dang district. The successful application of this approach in Kailali and Dang districts demonstrates its potential for expansion to other fire-prone areas of Nepal, contributing to a national-level framework. Incorporating advanced techniques such as hybrid models that integrate deep learning, GIS, and ensemble methods can further enhance predictive performance. These types of research can be explored at local levels as well. A hybrid model combining deep learning with GIS analysis, ensemble learning utilizing different machine learning algorithms can be used for improved interpretability and robustness, especially in complex terrains or data-scarce regions.

REFERENCES

Banjade, R., & Dhungana, J. (2025). *The Consequences of Forest Fires in Nepal: A Comprehensive Review* [Dataset]. Zenodo. https://doi.org/10.5281/ZENODO.15617231

Bouhissi, M. E., Bouidjra, S. E. B., & Benabdeli, K. (2020). GIS, Forest Fire Prevention and Risk Matrix in the National Forest of Khoudida, Sidi Bel Abbes, Algeria. *Open Journal of Ecology*, *10*(6), Article 6. https://doi.org/10.4236/oje.2020.106022

Campo-Bescós, M., Muñoz-Carpena, R., Southworth, J., Zhu, L., Waylen, P., & Bunting, E. (2013). Combined Spatial and Temporal Effects of Environmental Controls on Long-Term Monthly NDVI in the Southern Africa Savanna. *Remote Sensing*, *5*(12), 6513–6538. https://doi.org/10.3390/rs5126513

Chen, F., Du, Y., Niu, S., & Zhao, J. (2015). Modeling Forest Lightning Fire Occurrence in the Daxinganling Mountains of Northeastern China with MAXENT. *Forests*, *6*(5), 1422–1438. https://doi.org/10.3390/f6051422

Eugenio, F. C., Dos Santos, A. R., Fiedler, N. C., Ribeiro, G. A., Da Silva, A. G., Dos Santos, Á. B., Paneto, G. G., & Schettino, V. R. (2016). Applying GIS to develop a model for forest fire risk: A case study in Espírito Santo, Brazil. *Journal of Environmental Management*, *173*, 65–71. https://doi.org/10.1016/j.jenvman.2016.02.021

DFRS. (2015). *State of Nepal's forests*. Department of Forest Research and Survey, Forest Resource Assessment (FRA) Nepal.

ICIMOD. (2023). *SERVIR-HKH*. Retrieved August 20, 2025, from https://servir.icimod.org/press_releases/new-fire-risk-system-for-nepal/

Joshi, K. P., Giri, S., Kuinkel, D., Kuikel, S., Devkota, R., Pradhananga, D., Marahatta, S., & Pokharel, B. (2025). Forest fire dynamics in Nepal: Regional trends and socio-ecological drivers. *Trees, Forests and People*, *21*, 100942. https://doi.org/10.1016/j.tfp.2025.100942

Kingma, D. P., & Ba, J. (2014). *Adam: A Method for Stochastic Optimization* (Version 9). arXiv. https://doi.org/10.48550/ARXIV.1412.6980

Kumar, S., & Kumar, A. (2022). Hotspot and trend analysis of forest fires and its relation to climatic factors in the western Himalayas. *Natural Hazards*, *114*(3), 3529–3544. https://doi.org/10.1007/s11069-022-05530-5

Mishra, B., Panthi, S., Poudel, S., & Ghimire, B. R. (2023). Forest fire pattern and vulnerability mapping using deep learning in Nepal. *Fire Ecology*, *19*(1), 3. https://doi.org/10.1186/s42408-022-00162-3

Mishra, M., Guria, R., Baraj, B., Nanda, A. P., Santos, C. A. G., Silva, R. M. D., & Laksono, F. A. T. (2024). Spatial analysis and machine learning prediction of forest fire susceptibility: A comprehensive approach for effective management and mitigation. *Science of The Total Environment*, *926*, 171713. https://doi.org/10.1016/j.scitotenv.2024.171713

Mohajane, M., Costache, R., Karimi, F., Bao Pham, Q., Essahlaoui, A., Nguyen, H., Laneve, G., & Oudija, F. (2021). Application of remote sensing and machine learning algorithms for forest fire mapping in a Mediterranean area. *Ecological Indicators*, *129*, 107869. https://doi.org/10.1016/j.ecolind.2021.107869

Parajuli, A., Gautam, A. P., Sharma, S. P., Bhujel, K. B., Sharma, G., Thapa, P. B., Bist, B. S., & Poudel, S. (2020). Forest fire risk mapping using GIS and remote sensing in two major landscapes of Nepal. *Geomatics, Natural Hazards and Risk*, *11*(1), Article 1. https://doi.org/10.1080/19475705.2020.1853251

Parajuli, A., Manzoor, S. A., & Lukac, M. (2023). Areas of the Terai Arc landscape in Nepal at risk of forest fire identified by fuzzy analytic hierarchy process. *Environmental Development*, *45*, 100810. https://doi.org/10.1016/j.envdev.2023.100810

Pham, B. T., Jaafari, A., Avand, M., Al-Ansari, N., Dinh Du, T., Yen, H. P. H., Phong, T. V., Nguyen, D. H., Le, H. V., Mafi-Gholami, D., Prakash, I., Thi Thuy, H., & Tuyen, T. T. (2020). Performance Evaluation of Machine Learning Methods for Forest Fire Modeling and Prediction. *Symmetry*, *12*(6), 1022. https://doi.org/10.3390/sym12061022

Rokaya, M. B., Parajuli, B., & Timsina, B. (2024). Vegetation and Forest in Nepal. In M. B. Rokaya & S. R. Sigdel (Eds.), *Flora and Vegetation of Nepal* (Vol. 19, pp. 37–88). Springer International Publishing. https://doi.org/10.1007/978-3-031-50702-1_3

Shakya, P. R., Shrestha, S., Basnet, T. B., & Bhuju, U. R. (2007). *Nepal Biodiversity Resource Book* (0 ed.). International Centre for Integrated Mountain Development (ICIMOD). https://doi.org/10.53055/ICIMOD.475

Sharma, S., & Khanal, P. (2024). Forest Fire Prediction: A Spatial Machine Learning and Neural Network Approach. *Fire*, *7*(6), 205. https://doi.org/10.3390/fire7060205

Shi, C., & Zhang, F. (2023). A Forest Fire Susceptibility Modeling Approach Based on Integration Machine Learning Algorithm. *Forests*, *14*(7), 1506. https://doi.org/10.3390/f14071506

Tariq, A., Shu, H., Siddiqui, S., Mousa, B. G., Munir, I., Nasri, A., Waqas, H., Lu, L., & Baqa, M. F. (2021). Forest fire monitoring using spatial-statistical and Geo-spatial analysis of factors determining forest fire in Margalla Hills, Islamabad, Pakistan. *Geomatics, Natural Hazards and Risk*, *12*(1), 1212–1233. https://doi.org/10.1080/19475705.2021.1920477

Truong, T. X., Nhu, V.-H., Phuong, D. T. N., Nghi, L. T., Hung, N. N., Hoa, P. V., & Bui, D. T. (2023). A New Approach Based on TensorFlow Deep Neural Networks with ADAM Optimizer and GIS for Spatial Prediction of Forest Fire Danger in Tropical Areas. *Remote Sensing*, *15*(14), 3458. https://doi.org/10.3390/rs15143458

Vecín-Arias, D., Castedo-Dorado, F., Ordóñez, C., & Rodríguez-Pérez, J. R. (2016). Biophysical and lightning characteristics drive lightning-induced fire occurrence in the central plateau of the Iberian Peninsula. *Agricultural and Forest Meteorology*, *225*, 36–47. https://doi.org/10.1016/j.agrformet.2016.05.003

Wang, Y., Liu, J., Misic, J., Misic, V. B., Lv, S., & Chang, X. (2019). Assessing Optimizer Impact on DNN Model Sensitivity to Adversarial Examples. *IEEE Access*, *7*, 152766–152776. https://doi.org/10.1109/ACCESS.2019.2948658

Zhang, Y., Lim, H. S., Hu, C., & Zhang, R. (2024). Spatiotemporal dynamics of forest fires in the context of climate change: A review. *Environmental Science and Pollution Research*. https://doi.org/10.1007/s11356-024-33305-x

Author's Information

Name	:	Ganesh Pandey
Academic Qualification	:	MSc Geoinformatics
Organization	:	Survey Department
Current Designation	:	Survey Officer

Call for papers

The editorial board requests for papers related to geo-information science and earth observation for publication in the 26th issue of the Journal on Geoinformatics, Nepal. The last date of submission is 30th March 2027.

For more information, please contact editorial board editorial@dos.gov.np

Survey Department

P.O. Box 9435, Kathmandu Nepal

Tel: +977 1 4106508, 4106957, Fax: +977 1 4106757

email: info@dos.gov.np

Instruction and Guidelines for Authors Regarding Manuscript Preparation

- The Editorial Board reserves the right to accept, reject or edit the article in order to conform to the journal format.
- The contents and ideas of the article are solely of authors.
- The article must be submitted in Microsoft Word by email.
- The Editorial Board has no obligation to print chart/ figure/table in multi color, in JPEG/TIFF format, the figure/picture should be scanned in a high resolution.
- Authors are also requested to send us a written intimation that the same articles are not sent for publication in another magazine/journal.
- Standard template for the journal paper submission can be requested through editorial@dos.gov.np

Page size: A4

Format: Single line spacing with two columns.

Margin: upper 1", left 1.15", right 1", bottom 1".

Length of manuscript: The article should be limited up to 15 pages including figures and references.

Body text font: Times New Roman "11".

Title: The title should be centrally justified appearing near the top of 1st page in Cambria, “20” point (Bold).

Authors Name: Author’s name should be in Times New Roman “10” with Upper and lower casing, centrally justified. There should be a gap of one line with 11 pt. between the title and author's name.

Authors Email: Author’s email should be in Times New Roman “10” centrally justified. There should not be a gap between the name and email.

Keywords: Four to five keywords on paper theme

in Times New Roman "10" with two spacing under

the author's email was left justified.

Abstract: Single line spacing after keywords, limited to around 300 words in Italic, Times New Roman “10”.

Major heading (Level 1) should be flushed with the left margin in Times New Roman “10” bold font and with Upper casings. Color Dark blue. Numbering 1

Minor heading (Level 2) should be flushed with the left margin in Times New Roman “11” Bold font and with Upper and Lower Casing. Color Dark blue. Numbering 1.1

Minor heading (Level 3) should be flushed with the left margin in Times New Roman “11” Bold font, Italic and with Upper and Lower Casing. Color Dark blue. Numbering 1.1.1

Minor heading (Level 4) should be flushed with the left margin in Times New Roman “10” Italic and with Upper and Lower Casing. Color Dark blue. Numbering 1.1.1.1

Bullet Point: Use only (•).

Placement of photographs/tables: Photographs or tables should be pasted in appropriate place of manuscript pages with captions in their positions in Times new Roman ‘‘10” with Upper and lower casing.

Equations: All equations should be in Times New Roman, "11" and italic with consecutive equation numbers placed flush right throughout the paper.

References: References should be listed alphabetically APA7th standard.

Citation: All papers are to be cited following the APA 7th standard.

Primary Author's Information: The author should provide

Name,

Academic Qualification,

Organization,

Current Designation, and scanned copy of author's passport size photo

Note: "Author should send the picture of all the figures kept in paper as separate file."

Land Cover Change Analysis: A Case Study of Suryabinayak Municipality

Ram Kumar Basnet[1], David Nhemaphuki[1], Dr. Subash Ghimire[2], Dr. Pradeep Sapkota Upadhyaya[1], Dinesh Khatri[1]
ramkumarb699@gmail.com, davis10ge@gmail.com, subash_ghimire@ku.edu.np, pradeepsapkota@gmail.com, dineshkc7373@gmail.com
[1]Survey Department, [2]Kathmandu University

KEYWORDS

Land cover, Spatial pattern analysis, Urbanization, Remote sensing

ABSTRACT

This research examines how the Land cover (LC) have consistently changed in past eight years of timeframe from 2016 to 2024 in Suryabinayak Municipality with the help of remote sensing and GIS techniques. This study employed Sentinel-2 imagery, which underwent pre-processing, followed by the application of the random forest algorithm to classify land cover for the years 2016, 2020, and 2024 using Google Earth Engine. After classifying the images, accuracy assessments were conducted to evaluate the reliability of these classifications. Subsequently, spatial pattern analyses were performed on the classified images to examine land cover changes over time. Additionally, a literature review was conducted to identify the causes and impacts of urbanization within the study area, drawing from various research studies. The results show from 2016 to 2024, vegetation suffered the most loss, with built-up areas experiencing increase along the roads and minimal change in agricultural land. This analysis showed a conversion trend where vegetation was primarily transformed into agricultural land, which was then developed into urban areas. At the ward level, wards 2 & 3 (Balkot) and wards 5 & 6 (Katunje) exhibited pronounced urbanization, with built-up areas exceeding those of other wards. The rising number of parcels in Chitpol and Sipadol underscores the increasing demand for land, reflecting ongoing urban growth. Internal migration was identified as a key driver of urbanization, with individuals relocating to urban areas for better opportunities. This research underscores the significant changes in LC within the Suryabinayak Municipality, largely driven by urbanization. This rapid urban growth not only threatens environmental sustainability but also triggers demographic changes, resulting in a decline in rural populations.

1. INTRODUCTION

The rapid conversion of rural regions into low-density urban areas, often separated by undeveloped land, significantly impacts the socioeconomic and environmental sustainability of communities (Mubea et al., 2011). Land-use and land-cover (LULC) changes are central to global environmental change and sustainable development debates. These modifications can alter water and air quality, ecosystem functions, and the climate system through greenhouse gas fluxes (Lambin et al., 2003).

While land cover describes the physical state of the earth's surface—such as forests, wetlands, or human structures—land use refers to the purpose for which land is managed, such as agriculture or urban development (Ellis & Pontius, 2007). In developing countries like Nepal, major towns are experiencing a rapid shift where core areas, previously devoted to agriculture, are being transformed into built environments (Muzzini & Aparicio, 2013). Nepal is projected to be one of the top ten rapidly urbanizing countries by 2050, with its urbanization level expected to exceed 30% (Desa, 2015). The Kathmandu Valley, including Suryabinayak Municipality, serves as a primary hub for this intense population concentration and urban growth.

Increasing population and economic activities drive unprecedented land-use changes that are often neglected by administrations (Nepal et al., 2020). In Suryabinayak Municipality, rapid urban sprawl is occurring in an unplanned manner, leading to the loss of natural vegetation and agricultural land. This study is necessary to provide data for future urban planning and decision-making. The primary goal of this research is to identify and analyze land cover (LC) changes within Suryabinayak Municipality between 2016 and 2024.

2. DATASETS AND PREPROCESSING

2.1 Datasets

This study utilized multispectral satellite imagery from European Space Agency's Sentinel-2 (Level-2A) products for the years 2016, 2020, and 2024 to analyze temporal land cover (LC) changes in Suryabinayak Municipality. The images (cloud cover <10%) include 12 spectral bands with spatial resolutions ranging from 10 m to 60 m. Additional data such as administrative boundaries were obtained from the Survey Department of Nepal, and parcel information from the Department of Land Management and Archive (DOLMA).

Table 1: Sentinel-2 images used

S.N.	Image	Resolution	Date
1	Sentinel-2	10 m	2016-04-13
2	Sentinel-2	10 m	2020-03-11
3	Sentinel-2	10 m	2024-03-05

2.2 Software Used

The analysis was carried out using Google Earth Engine, ArcGIS, and FRAGSTATS. Google Earth Engine was used for processing and analyzing satellite imagery in a cloud-based environment, ArcGIS supported spatial data management and map preparation, while FRAGSTATS was applied to compute landscape metrics for assessing spatial patterns and land cover structure (Singh et al., 2014).

2.3 Data pre-processing

Data preprocessing involved both spatial and spectral filtering to ensure accurate analysis. In the spatial filtering stage, Sentinel-2 images were clipped using the boundary of Suryabinayak Municipality to extract only the area of interest. In the spectral filtering stage, instead of using all available bands, only the most relevant bands—Band 2 (Blue), Band 3 (Green), Band 4 (Red), and Band 8 (Near-Infrared)—were selected, as these bands are particularly effective for distinguishing vegetation, water bodies, built-up areas, and other land cover types (Nhemaphuki, et. al., 2021).

3. METHODOLOGY

The initial phase involved the collection of essential remotely sensed datasets for the year 2016, 2020 and 2024. Also, primary field data was collected about the land cover for the verification of LC for the year 2024.

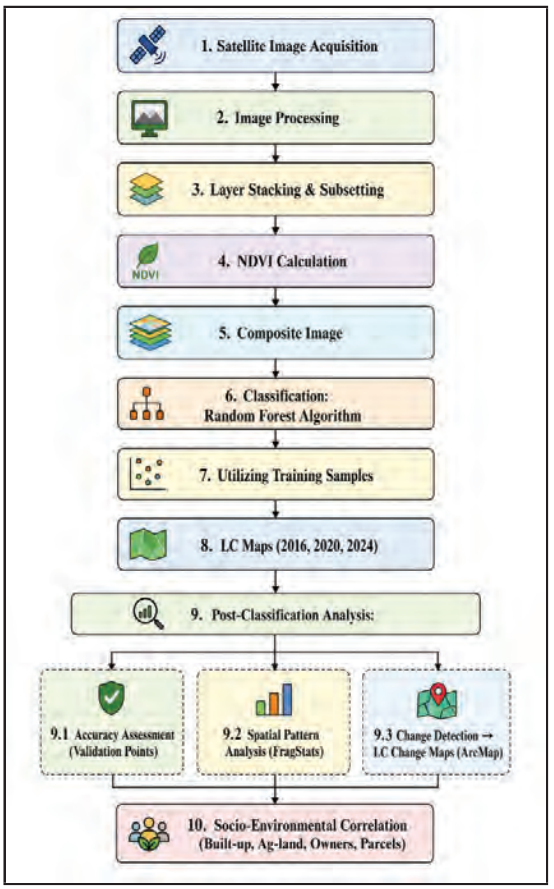

Figure 1: Research methodology

Google Earth Engine (GEE) which was used for processing and then the classification of satellite images using Random Forest Algorithm (RFA) to obtain LC for the corresponding year. It contains five classes which are agricultural land, built-up area, water body, vegetation and barren land. The accuracy assessment of these classifications was performed to ensure the quality, reliability of the data and its suitability for various applications. Change detection analysis was conducted for agricultural, built-up and vegetation area for three time periods: 2016 to 2020, to 2024, and the cumulative change from 2016 to 2024. Furthermore, Spatial Pattern Analysis (SPA) was conducted using Fragstat to gain a more comprehensive understanding of the changing landscape and how various LC categories were distributed and structured over the specified time periods (Weng, 2007).

3.1 Study area

The study area lies in Suryabinayak Municipality of Bhaktapur District, located on the eastern rim of the Kathmandu Valley in Nepal. Covering 42.45 km² with elevations ranging from about 1,372 m to 2,025 m.

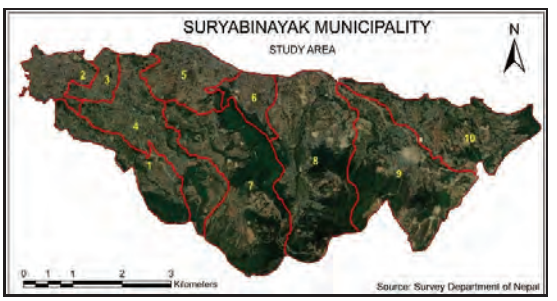

Figure 2: Study area

The municipality has experienced rapid urbanization and significant population growth, increasing from 78,845 in 2011 to 140,085 in 2021.

3.2 Data preparation

NDVI was calculated using Band 8 (Near-Infrared) and Band 4 (Red) from Sentinel-2 imagery through the standard formula

$$NDVI = (NIR - Red) / (NIR + Red)$$

which helps distinguish vegetation from non-vegetated surfaces based on reflectance characteristics. After computing NDVI for each study year, composite images were generated by stacking the selected spectral bands—Blue (B2), Green (B3), Red (B4), and NIR (B8)—together with the derived NDVI layer. These multi-band composite images enhanced the spectral information and were used as the final input dataset for land cover classification (Gitelson et al, 1996).

3.3 Land cover classification

Land cover classification in this study was performed using the Random Forest algorithm, an ensemble machine learning technique widely applied in remote sensing analysis (Naghibi et al., 2017). The model constructs multiple decision trees from randomly

selected training samples and input features, and the final classification is determined by aggregating the predictions of all trees, thereby improving accuracy and reducing overfitting. Due to its ability to handle high-dimensional multispectral data and capture complex nonlinear relationships (Zhang et al., 2021), Random Forest is well suited for LULC mapping (Congalton & Green, 2019). In this research, the model was trained using 20 trees with default feature settings and applied to classify land cover for the years 2016, 2020, and 2024.

3.4 Spatial pattern analysis

LC patterns were analyzed using spatial metrics to calculate metrics at patch, class, and landscape levels in order to assess spatial and temporal changes. In this study, six key metrics were used: Number of Patches (NP), Class Area (CA), Patch Density (PD), Largest Patch Index (LPI), Edge Density (ED), and Mean Patch Area (AREA_MN). CA measures the total area occupied by a specific land cover class, while NP and PD describe the fragmentation and spatial distribution of patches. ED reflects the extent of edges between different land cover types, indicating landscape complexity. LPI identifies the dominance of the largest patch within the landscape, and AREA_MN represents the average size of patches, helping to understand changes in landscape structure over time.

3.5 LC change analysis

LC change analysis was carried out for the periods 2016–2020, 2020–2024, and the overall span from 2016–2024 to assess both short-term and long-term transformations in the study area. Change detection maps were generated to examine micro-level changes within specific locations as well as macro-level trends (Kafi et al., 2014) across the entire municipality. The analysis particularly focused on agricultural land, vegetation, and built-up areas, identifying patterns such as urban expansion, agricultural fragmentation, and vegetation loss. This approach provided a comprehensive understanding of the extent, direction, and intensity of land cover transitions over time.

4. RESULT AND DISCUSSION

LC analysis for 2016, 2020, and 2024 reveals that agricultural land consistently dominated the study area, covering 53.53% (22.82 km²) in 2016, 56.39% (24.04 km²) in 2020, and 56.91% (24.26 km²) in 2024. Vegetation showed a gradual decline from 34.32% (14.56 km²) in 2016 to 27.66% (11.79 km²) in 2024, while built-up areas increased steadily from 10.38% (4.42 km²) to 13.71% (5.84 km²) over the same period.

Table 2: Land cover for different year

Land Cover Type	2016 Area (km²)	2020 Area (km²)	2024 Area (km²)
Vegetation	14.56	12.14	11.79
Agricultural Land	22.82	24.04	24.26
Water Body	0.08	0.14	0.01
Built-up Area	4.42	5.06	5.84
Barren Land	0.54	1.05	0.51

Change detection analysis (2016–2024) highlights that the major land transitions occurred between agricultural land and built-up areas.

Table 3: Change from other LC to built-up

Change Type	2016-2020	2020–2024	2016–2024
Vegetation → Built-up	0.22	0.22	0.42
Agriculture → Built-up	3.78	3.15	4.02
Water → Built-up	0.00	0.10	0.03
Barren → Built-up	0.32	0.29	0.16

Table 4: Change from built-up to other LC

Change Type	2016–2020	2020–2024	2016–2024
Built-up → Vegetation	0.06	0.14	0.32
Built-up → Agriculture	1.29	2.59	2.62
Built-up → Water	0.05	0.00	0.01
Built-up → Barren	0.17	0.10	0.00

Approximately 4.02 km² of agricultural land was converted into built-up areas, demonstrating strong urban growth pressure. Conversely, 2.62 km² of built-up land reverted to agriculture, largely due to the reclassification of former brick factory areas as shown in Table 3 and Table 4. Vegetation loss was mainly driven by conversion to agriculture, while minor shifts occurred toward built-up land.

Table 5: Spatial metrics for the year 2016

TYPE	CA	NP	PD	LPI	ED
Agricultural Land	2485.67	1206	15.21	25.22	148.58
Barren Land	88.71	1354	17.08	0.05	19.5
Built up	264.63	4377	55.23	0.44	61.2
Vegetation	1424.88	2111	26.63	11.98	80.12
Water Body	1.87	123	1.5	0.00	0.8

Table 6: Spatial metrics for the year 2024

TYPE	CA	NP	PD	LPI	ED
Agricultural Land	2v437.39	2150	27.13	15.4469	215.63
Barren Land	51.67	1028	12.97	0.04	11.85
Built up	588.26	7366	92.95	1.0473	132.92
Vegetation	1187.34	5114	64.53	3.30	123.59
Water Body	1.1	104	1.3	0.00	0.5

Spatial metrics computed using FRAGSTATS (Table 5 and 6) shows increasing fragmentation of built-up and vegetation classes between 2016 and 2020, followed by partial consolidation in 2024. Agricultural land maintained the highest Largest Patch Index (LPI), confirming its dominance, whereas built-up areas exhibited high patch density, reflecting urban sprawl.

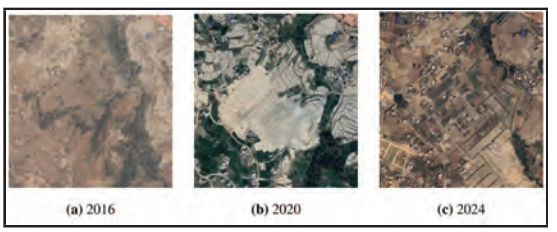

Figure 3: LC change in Sipadol region

Figure 3 illustrates satellite images of a portion of the Suryabinayak Municipality area in the Sipadol region, covering the years 2016, 2020, and 2024. The images clearly depict a transformation: agricultural land in 2016 was converted into barren land by 2020, as the area was cleared for housing development. By 2024, only a few plots have been developed with houses, while the remaining plots remain vacant and are being used for agricultural purposes.

Urban expansion was primarily concentrated in the northern part of Suryabinayak Municipality along the Araniko Highway, indicating a ribbon development pattern (Doan & Oduro, 2012).

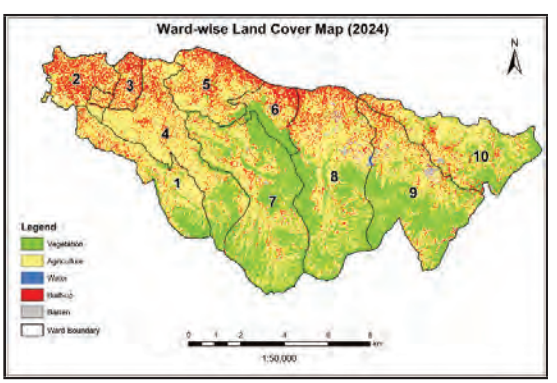

Figure 4: Ward-wise LC for 2024

Ward-wise analysis shows that Wards 2 and 3 (Balkot) and Wards 5 and 6 (Katunje) are highly urbanized, with greater built-up coverage than other areas, likely due to their proximity to the Araniko Highway as indicated earlier. In contrast, the southern wards (1, 4, 7, 8, and 9)

are less urbanized, with more vegetation and lower built-up presence.

Table 7: Ward-wise percentage coverage of built-up area

Ward	2016	2020	2024
1	3.22	6.40	10.39
2	16.73	33.44	43.55
3	13.32	34.67	41.94
4	2.97	9.04	11.86
5	15.21	21.55	27.15
6	15.45	24.96	26.18
7	1.27	6.12	12.45
8	3.92	8.22	12.07
9	3.38	5.27	9.26
10	8.73	11.16	12.10

Figure 5 (a) and 5 (b) shows the number of land owners and number of parcels from 2016 to 2024. In every location, both the number of land owners and the number of parcels shows an upward trend. Areas like Katunje, Dadhikot, and Sipadol consistently lead in both metrics, indicating they are the primary hubs of land activity and urbanization, whereas Sirutar remains the least active despite following the same upward trajectory.

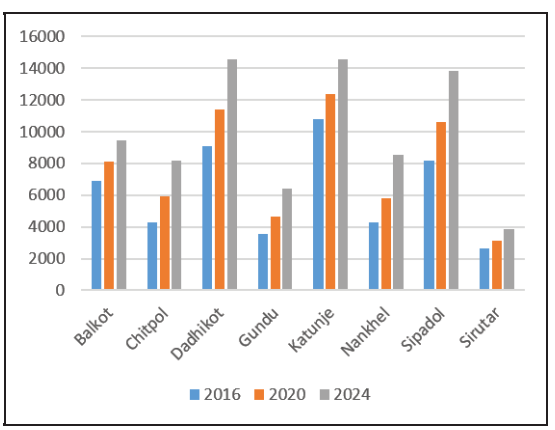

Figure 5 (a): Number of land owners

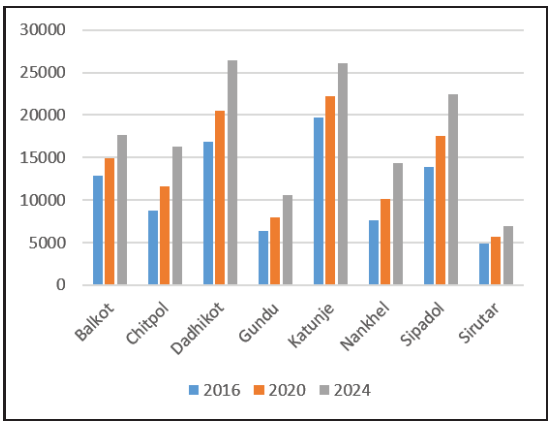

Figure 5 (b): Number of parcels

Furthermore, a strong positive correlation was observed between built-up area and number of parcels as well as land owners, confirming that land subdivision and ownership growth are closely linked to urbanization as shown in Table 8 below.

Table 8: Interrelationship between Parcels, Ownership, and Built-up Area

	Number of parcels	Owners	Built-up
Number of parcels	1		
Owners	0.99	1	
Built-up	0.75	0.76	1

Migration data further supports this trend, with higher inward migration recorded in rapidly urbanizing wards, demonstrating that population movement is a key driver of land cover transformation in the municipality as indicated by Twayana et al. (2021) in Banepa Municipality.

5. CONCLUSION

The study shows that Suryabinayak Municipality has undergone substantial land cover changes from 2016 to 2024, driven mainly by rapid urbanization along the Araniko Highway. Significant losses in vegetation and agricultural land were observed, with these areas progressively converting into built-up

zones. This transition follows a clear pathway vegetation converting into agriculture and agricultural land further transforming into urban areas. Wards 2, 3, 5, and 6 show the most intense urban growth, while the sharp increase in parcel numbers in Ward 8 and Ward 10 reflects rising land demand and active land development.

Specific locations such as Sipadol, Nankhel, and Chitpol have experienced notable transformations, including land reclamation from brick manufacturing sites and expansion of settlement areas. These shifts are strongly influenced by internal migration, political instability, and natural disasters, which have pushed people toward urban centers like Suryabinayak. As a result, rural areas face a declining and aging population, while urban expansion continues to put pressure on natural landscapes.

Overall, the findings highlight accelerating urban growth in Suryabinayak Municipality at the cost of vegetation and agricultural land, signaling urgent concerns for environmental sustainability and balanced regional development.

REFERENCES

Congalton, R. G., & Green, K. (2019). Assessing the accuracy of remotely sensed data: Principles and practices. CRC press.

Desa, U. (2015). World urbanization prospects: The 2014 revision. United Nations Department of Economics and Social Affairs. Population Division: New York, NY, USA, 41.

Doan, P., & Oduro, C. Y. (2012). Patterns of population growth in peri-urban Accra, Ghana. *International Journal of Urban and Regional Research*, *36*(6), 1306-1325.

Ellis, E., & Pontius, R. (2007). Land-use and land-cover change. *Encyclopedia of Earth*, 1, 1-4.

Gitelson, A. A., & Merzlyak, M. N. (1997). Remote estimation of chlorophyll content in higher plant leaves. *International Journal of Remote Sensing*, 18(12), 2691–2697

Kafi, K. M., Shafri, H. Z. M., & Shariff, A. B. M. (2014, June). An analysis of LULC change detection using remotely sensed data: A case study of Bauchi City. *In IOP conference series: Earth and environmental science* (Vol. 20, No. 1, p. 012056).

Lambin, E. F., Geist, H. J., & Lepers, E. (2003). Dynamics of land-use and land-cover change in tropical regions. *Annual Review of Environment and Resources*, 28(1), 205–241.

Mubea, K., Mundia, C., & Kuria, D. (2011). The use of Markov chain analysis in predicting land use/cover change in Nyeri. Working paper, Department of Civil Engineering, Kimathi University College, Kenya.

Muzzini, E., & Aparicio, G. (2013). *Urban growth and spatial transition in Nepal: An initial assessment.* International Bank for Reconstruction and Development/The World Bank.

Naghibi, S. A., Ahmadi, K., & Daneshi, A. (2017). Application of support vector machine, random forest, and genetic algorithm optimized random forest models in groundwater potential mapping. *Water Resources Management*, 31, 2761–2775.

Nepal, P., Khanal, N. R., Zhang, Y., Paudel, B., & Liu, L. (2020). Land use policies in Nepal: An overview. *Land Degradation & Development*, 31(16), 2203-2212.

Nhemaphuki, D., Chetri, K. T., & Shrestha, S. (2021). Fusion of radar and optical data for land cover classification using machine learning approach. *Journal on Geoinformatics, Nepal*, 20(1), 39-45.

Singh, S. K., Pandey, A. C., & Singh, D. (2014). Land use fragmentation analysis using remote sensing and Fragstats. *Remote Sensing Applications in Environmental Research* (pp. 151-176).

Twayana, R., Bhandari, S., & Shrestha, R. (2021). Analyzing urban growth pattern and driving factors using remote sensing and GIS: A case study of Banepa municipality, Nepal. *Journal on Geoinformatics, Nepal*, 20 (1), 9–18

Weng, Y. C. (2007). Spatiotemporal changes of landscape pattern in response to urbanization. *Landscape and urban planning*, 81(4), 341-353.

Zhang, X., Xu, J., Chen, Y., Xu, K., & Wang, D. (2021). Coastal wetland classification with gf-3 polarimetric SAR imagery by using object-oriented random forest algorithm. *Sensors*, 21(10), 3395.

Author's Information

Name	:	Ram Kumar Basnet
Academic Qualification	:	MSc in Land Administration
Organization	:	Survey Department
Current Designation	:	Chief Survey Officer

Mapping Sovereignty: Cartographic Evidence in Resolving International Boundary Disputes

Susheel Dangol
susheel.dangol@nepal.gov.com
Survey Department

KEYWORDS

Maps, International boundary, Dispute resolution, Cartographic evidence, Boundary dispute

ABSTRACT

This paper examines the role of cartographic evidence in resolving international boundary disputes and its efficacy in addressing the issue. Review of adjudicated cases from the ICJ, PCA, and UNCLOS tribunals, focusing on disputes where maps played a decisive role identified the patterns in map usages. Four cases settled down by ICJ is selected for the study which includes Preah Vihear case between Thailand and Cambodia, Aouzou strip case between Chad and Libya, boundary dispute between Burkina Faso and Mali, and the case of enclave between the Netherlands and Belgium. The study underscores the dual nature of maps as both technical tools and instruments of territorial claim-making, highlighting the need for standardized cartographic guidelines to mitigate historical discrepancies. The findings contribute to the discourse on conflict resolution by empirically validating the conditional effectiveness of cartographic evidence.

1. INTRODUCTION

International boundary disputes remain a persistent challenge in global geopolitics, often rooted in historical uncertainties, colonial legacies, and competing territorial claims. Among the tools employed to resolve such conflicts, cartographic evidence occupies a unique position as a technical instrument for delimitation, demarcation, and management of boundaries (Blake, 1995). The relationship between maps and sovereignty has long been recognized in international relations (Branch, 2014), yet the conditions under which cartographic evidence effectively contributes to dispute resolution remain underexplored. This paper addresses this gap by systematically analyzing the role of maps in adjudicated and negotiated boundary disputes.

The significance of cartography in boundary disputes is not only simple representation; maps often serve as active participants in territorial claim-making (Weissberg, 1963). For instance, historical maps have been instrumental in cases like the Northwest Passage dispute between US and Canada, where competing cartographic narratives expanded over conflicting sovereignty claims (Tsiouvalas & Solski, 2023). However, the reliability of such

evidence varies significantly across contexts. Maritime disputes, governed by frameworks like United Nations Convention on the Law of the Sea (UNCLOS), tend to resolve more predictably with cartographic input, whereas terrestrial conflicts-especially in post-colonial regions frequently resist with discrepancies between legal boundaries and lived realities (Saliternik, 2017). This divergence raises critical questions about the contextual efficacy of maps and the need for adaptive resolution mechanisms.

The role of cartographic evidence in international boundary disputes has been extensively examined through multiple disciplinary lenses, including international law, political geography, and conflict resolution studies (Saliternik, 2017). Early scholarship emphasized maps as passive representations of territorial claims, but contemporary research increasingly recognizes their active role in shaping geopolitical narratives (Blake, 1995). This shift reflects broader theoretical movements in critical cartography, which interrogate how maps construct rather than simply reflect spatial realities (Weissberg, 1963).

In legal contexts, the importance of maps varies significantly. While some tribunals, such as those under UNCLOS, have treated cartographic evidence as pivotal in maritime delimitation cases (Mboce *et al.*, 2025), others caution against overreliance on maps due to their exposure to political manipulation. The ICJ's legal philosophy often subordinates cartographic evidence to treaty texts, particularly in terrestrial disputes (Saliternik, 2017). This tension between cartographic fairness and political partiality underscores the need for methodological clarification in map analysis.

Cultural and historical factors further complicate map usage. Research on maritime disputes highlights how national perceptions of sovereignty, influenced by power distance, affect the acceptability of arbitration outcomes where low power-distance countries like Australia and New Zealand have resolved boundary issues amicably through negotiation, whereas high power-distance states often reject unfavorable arbitration, as seen in the South China Sea arbitration between Philippines and China (Casetta, 2025).

Technological advancements have introduced new dimensions to cartographic evidence. Participatory GIS (PGIS) frameworks, such as the "butterfly model" for customary land conflict resolution, demonstrate how inclusive mapping can reconcile technical precision with community legitimacy (Gyamera *et al.*, 2017). While ICJ defines the value of maps depends on their technical reliability and the neutrality in relation to the dispute, international tribunals treats maps as important, significant evidence in determining boundary lines (Lee, 2005). In this context, ‘base map’ with physical geographic data with topography and natural features becomes the base for dispute resolution if the both parties in a dispute have confidence that the base map does not favor one side at the expense of other (Wood, 2000).

Unlike prior works that treat maps as either neutral tools or political instruments, this study identifies its role in resolving conflicts. While international law provides the structural framework for boundary determination, cartography supplies the visual language through which territorial claims acquire tangible form (Rajkovic, 2018). Large-scale maps assume evidentiary primacy in boundary demarcation cases due to their granular detail, as seen in the 2002 ICJ ruling on Cameroon v. Nigeria (ICJ, 2002; Merrills, 2003). Cases such as the Bangladesh v. India maritime boundary dispute were analyzed to understand how modern geospatial technologies, including bathymetric data and satellite-derived

baselines, influenced adjudication outcomes (Kałduński, 2015; PCA, 2014; Ramnath, 2022).

The remainder of this paper is organized as follows: Section 2 discuss about the methods adopted for this study. Section 3 dissect on the results of the study with discussion and section 4 concludes the paper.

2. STUDY DESIGN AND METHODS

This study employs a multi-method approach to systematically analyze the role of cartographic evidence in international boundary dispute resolution. The research design integrates qualitative and comparative legal analysis with geospatial evaluation techniques, allowing for a nuanced examination of how maps function across different dispute contexts and resolution frameworks. The study focuses on adjudicated cases from primary sources of ICJ with other examples from PCA, and tribunals operating under the UNCLOS cases, with selection based on explicit references to cartographic evidence, ensuring that the analysis captures disputes where maps played a substantive role. Both maritime and terrestrial disputes were studied to enable comparative analysis. A qualitative content analysis was conducted to identify how maps are used and interpreted in boundary disputes.

3. RESULTS AND DISCUSSION

The findings presented in this section emerge from a systematic analysis of cartographic evidence across adjudicated boundary disputes, revealing distinct patterns in map usage, and legal influence. These results highlight the conditional efficacy of maps in resolving conflicts, with notable variations between maritime and terrestrial contexts.

3.1. Overview of key findings

The systematic review of cases from the ICJ, PCA, and UNCLOS tribunals reveals that cartographic evidence functions as a double-edged sword in international boundary dispute resolution simultaneously facilitating impartial demarcation while also serving as an instrument of political disagreement. Clear legal framework governing maritime boundary particularly Article 15 and 74 of UNCLOS (UN, 1982) provide clearer standards for map evaluation than the often-ambiguous principles applied to land borders (Blake, 1995).

In the case between Eritrea vs. Yemen handled by PCA in 1998, bathymetric charts and equidistance calculations enabled precise maritime delimitation (UN, 2006), whereas terrestrial disputes such as the Indonesia-Malaysia conflict over Sipadan and Ligitan islands was hindered in competing historical map interpretations (Butcher, 2013). Differences in evidentiary weight of large-scale maps Vs. “sketch-like” maps are seen the boundary related cases as in the case between Nicaragua Vs. Colombia where ICJ rejected Spain’s 1825 Carta Esferica due to its sketch like nature despite Nicaragua’s insistence on its relevance. Conversely, modern technologies like the use of satellite imagery data receives instance acceptance if metadata on different parameters like projection system and accuracy are provided along with as in the case of Ghana and Cote d’Ivoire maritime dispute (ITLOS, 2017).

The results collectively demonstrate that while cartographic evidence has become indispensable in boundary dispute resolution, its effectiveness remains contingent on dispute type, technological modernity, and the degree to which mapping processes accommodate pluralistic territorial conceptions.

3.2. Case specific analysis of boundary disputes

Four cases on international boundary dispute were analyzed where cartographic evidence played a pivotal role in shaping dispute resolution outcomes, revealing how maps

influence legal reasoning across different geopolitical contexts. All the cases selected were from ICJ only. Case of Preah Vihear was selected since clashes are still happening today, in spite of the decisions made centuries back. Two of the cases were selected from the African nations colonized by European. One was selected from the European countries who colonized African countries.

3.2.1. Preah Vihear case between Thailand and Cambodia

The temple of Preah Vihear case between Cambodia and Thailand is the most prominent example of and international boundary dispute resolved primarily on the basis of maps in which the ICJ awarded the temple and surrounding territory to Cambodia, using a French produced map as the decisive evidence (ICJ, 1962). A 1904 treaty between France and Siam (now Thailand) stated the border should follow the watershed line of the Dangrek mountains while in 1907 treaty, French surveyors produced a map (*Figure 1*) annexed to the treaty that deviated from the natural watershed line to place the temple within Cambodian territory (Ciorciari, n.a.).

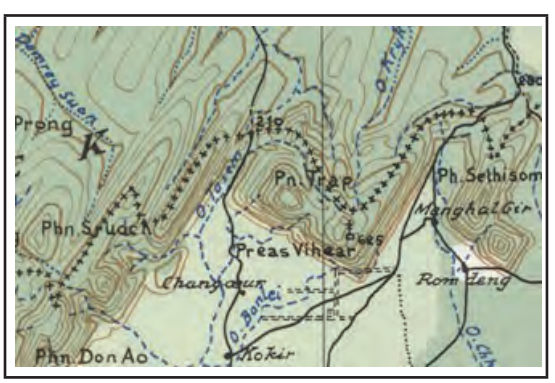

Figure 1: Map showing the location of temple. (Source: https://en.wikipedia.org/)

In this context, Thailand argued that the map was technically inaccurate and therefore not binding. However, ICJ ruled that because Thailand had used this map for decades, and never officially protested it and had legally agreed by silence to the boundary depicted in the map and hence ICJ concluded that the map, even with its technical errors, had become the legally binding definition to the border (ICJ, 1962).

3.2.2. Case of Aouzou strip between Chad and Libya

Case between Chad and Libiya regarding Aouzou strip occupied by Libiya was settled by the ICJ in 1994, awarding the strip to Chad based on 1955 colonial-era treaty (Al-Tahir, 2021; McKoeon, 1991; Rademacher, 2020; Stebek, 2009). The ICJ ruling on 1994 determined the Chad-Libya boundary based on the 1955 Treaty of Friendship and Good Neighborliness (Figure 2).

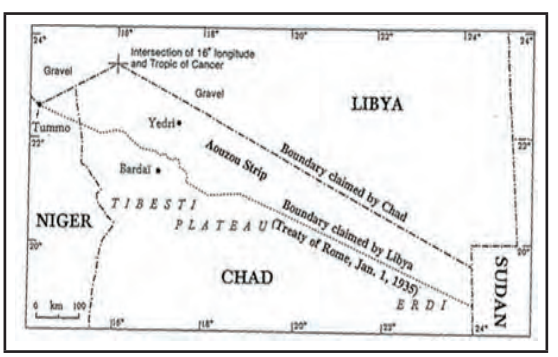

Figure 2:Strip of Aouzou strip claimed by Chad and Libya. (Source: (Al-Tahir, 2021)

Though no any maps were attached to the treaty, ICJ provided its own Sketch Map No. 4 (Figure 3) on the basis of frontier noted in 1955 treaty to illustrate the boundary and confirmed the boundary aligned with the Aouzou Strip's northern limit, largely following the line established in the 1919 Franco-Italian convention, rejecting Libya's claim to the region (Blake, 1994). The ICJ ruled that because article 3 of the treaty specified the frontiers defining the boundaries even a new physical map wasn't drawn for the 1955 document itself (ICJ, 1994).

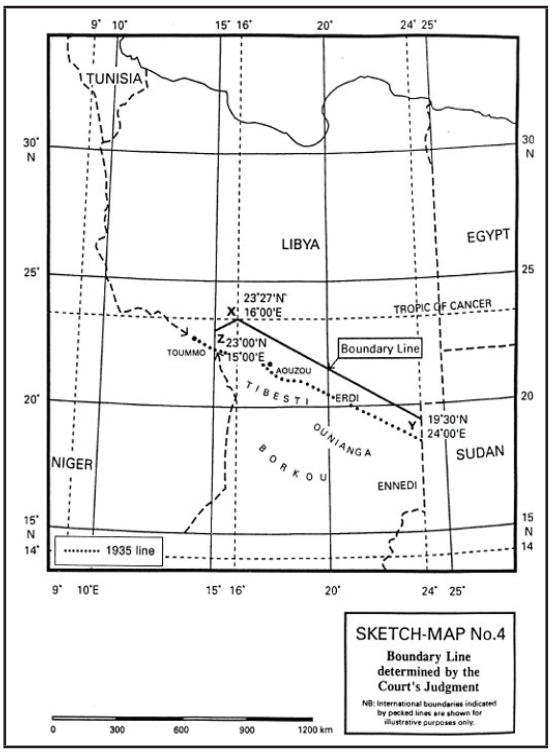

Figure 3:Sketch-Map no 4 by ICJ (Source: (Blake, 1994)

3.2.3. Case between Burkina Faso and Mali

The next case was the boundary dispute between Burkina Faso and Mali resolved by ICJ in 1986 using colonial-era administrative maps applying the principle of *uti possidetis juris* respecting existing colonial boundaries (Leigh, 1987). ICJ marked the line of frontier for illustrative purpose on the map of the scale 1:200000 which was also annexed to the same judgement (ICJ, 1986a).

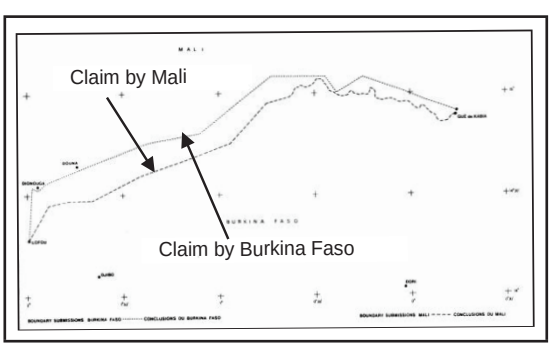

Figure 4:Boundary claim by Mali and Burkina Faso (Source: (ICJ, 1986b))

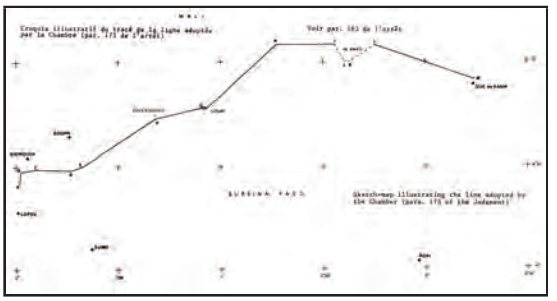

Figure 5:Boundary finalized by ICJ. (Source: (ICJ, 1986b)

The dispute between Burkina Faso and Mali is over 275 km long and 30 km wide Agacher strip of land along the border in northern Burkina Faso (Salliot, 2010), whose claim from both the countries are shown in Figure 4. Judgement of the chamber published in communique of ICJ dated 22 December 1986 shows the boundary claim of the Burkina Faso and Mali and the final decided boundary line (Figure 5) by ICJ (ICJ, 1986b).

According to clause 171 of case concerning frontier dispute, Mali submitted map of 1:1000000 scale published in 1927 showing its claim of boundary alignment and clause 172 clarifies that Burkina Faso submitted map of scale 1:200000 map published in 1969 showing its claim of the boundary (ICJ, 1986a). Looking at both the maps Chamber of the ICJ fixed the line of the frontier between the two countries which was agreed by both parties and the dispute was peacefully settled (ICJ, 1986b).

3.2.4. Case between Netherlands and Belgium

In 1959, the ICJ addressed territorial disputes on sovereignty over frontier land between Belgium and the Netherlands. The dispute was basically on the sovereignty over two plots of land as number of enclaves were formed by Belgian commune and Netherlands commune (ICJ, 1959b). A Communal Minute drafted between 1836 and 1841 assigned the plots to Baarle-Nassau, while a Descriptive Minute and accompanying map annexed to the 1843

Boundary Convention attributed them to Baerle-Duc (ICJ, 1959b). Belgium relied on the Descriptive Minute and the official maps annexed to the 1843 convention, which explicitly qualified the plots to the Belgian commune while Netherlands argued that the 1843 convention was intended only to maintain the status quo.

Figure 6: Enclaves of Netherlands and Belgium (Source: https://amproehl.com/)

After reviewing the evidence, ICJ found that the maps and Descriptive minute were integral part of the 1843 Treaty and carried out the same legal weight as the treaty and hence the Court concluded in its judgment of 20 June 1959 that sovereignty over the two disputed plots rested with Belgium (ICJ, 1959a).

3.3. International boundary of Nepal

Nepal shares its international boundary with China at the North and India at East, South and West. Sugauli treaty on 4th March 1816, supplementary treaty of Sugauli treaty on11th December 1816, 1st November 1860 and 7 January 1875 defined the present-day boundary between Nepal and India (Baral, 2018). Nepal-China boundary agreement was signed on 21 March 1960 to scientifically demarcate the traditional boundary between the two countries. The boundary treaty was signed on 5 October 1961 which also included maps of scale 1:500000 showing entire boundary line, and 1:50000 scale maps showing the location of temporary boundary markers to be erected. On the basis of the treaty, boundary delimitation was conducted and first boundary protocol between Nepal and China was signed on 20 January 1963 resolving all the issues between the two countries and defined the present-day boundary alignment between Nepal and China (Shrestha, 2013).

In the context of Nepal and India, the issue concerning the Kalapani–Limpiyadhura and Susta regions remain unresolved (Baral, 2018; Shrestha, 2013). Differences in views regarding the source of the Kali River gave rise to the Kalapani–Limpiyadhura dispute, with Nepal and India each presenting different sets of maps, which prevented the two sides from reaching an agreement (Shrestha, 2013).

In case of Susta region, change in course of the Narayani river is the main reason for the dispute where no pillars were constructed along the river course (Shrestha, 2013). Anticipating such difficulties, both sides agreed to apply the fixed-boundary principle in areas where rivers form the international boundary between Nepal and India, relying on the boundary lines indicated on the base maps jointly agreed upon and prepared after the Sugauli Treaty, while the two sides could not agree on the single base map in this case as well and hence the issue is still pending (Shrestha, 2013).

As the two sides were unable to reach a technical consensus, the Third Joint Commission (JC) meeting, led by the foreign ministers of both countries and held in Kathmandu, Nepal, from 25 to 27 July 2014, recorded the Susta and Limpiyadhura–Kalapani–Lipulekh issues as outstanding and directed a foreign secretary–level mechanism to address them, with technical inputs from the Boundary Working Group (BWG) comprising Director General–level officials from the Survey Departments of both sides.

As discussed in Section Three, and as demonstrated by the Nepal–China boundary case where maps annexed to the treaty facilitated the resolution of boundary disputes, the Nepal–India boundary could similarly have been settled had maps been attached to the treaty. Nonetheless, with the establishment of a permanent Boundary Working Group (BWG) mechanism and continued joint engagement by both sides in boundary activities, the issue may be resolved through appropriate dispute-resolution mechanisms.

4. CONCLUSION

This study has examined the role of cartographic evidence in international boundary dispute resolution, revealing its conditional efficacy. The findings demonstrate that maps function not merely as technical tools but as dynamic instruments of territorial governance, with their legal weight contingent on dispute type, and technological modernity. While maritime disputes benefit from standardized frameworks under UNCLOS and the relative stability of hydrographic features, terrestrial conflicts remain hampered by historical cartographic ambiguities and the politicization of spatial representations.

Ubay (2011) argues that though maps are generally regarded as secondary evidence, they appear to be the most compelling form of documentary evidence in territorial sovereignty disputes. Further, Robertson (2013) too argues that, while maps offer clarity as to the location of boundary lines, their application in delimitation of boundary must be evaluated against established legal precedents governing evidence of sovereignty. Maps are a complex form of evidence, yet they hold significant potential in cases where recognized coordinates and boundary pillars are absent, as they are connected to the real world by depicting physical details and superimposing boundaries onto reference data (Srebro & Shoshany, 2013). Nevertheless, an examination of the cases studied clearly demonstrates that maps can play a crucial role in resolving boundary disputes.

REFERENCES

Al-Tahir, A. (2021). Border conflict in Africa: Part 3 — Aouzou strip. Retrieved 4/25/2026, from https://blnews.net/2021/04/border-conflict-in-africa-part-3-aouzou-strip/

Baral, T. N. (2018). Border disputes and its impact on bilateral relation: a case of Nepal-India international border management. *Journal of APF Command and Staff College*, *1*(1), 28-36.

Blake, G. (1994). A note on the International Court of Justice ruling on the Chad-Libiya dispute. *IBRU Boundary and SEcurity Bulletin*, 80-83.

Blake, G. (1995). The mapping of international boundaries. *Bulletin-Society of University Cartographers*, *28*(2), 1-7.

Branch, J. (2014). *The cartographic state: Maps, territory, and the origins of sovereignty*. Cambridge University Press.

Butcher, J. G. (2013). The International Court of Justice and the territorial dispute between Indonesia and Malaysia in the Sulawesi Sea. *Contemporary Southeast Asia*, 235-257.

Casetta, S. D. (2025). Ownership of the sea: Evaluating how culture affects the success of dispute resolution techniques in resolving maritime boundary conflicts. *Journal of International Dispute Settlement*, *16*(2). https://doi.org/10.1093/jnlids/idaf009

Ciorciari, J. D. (n.a.). *Thailand and Cambodia: The Battle for Preah Vihear*. Stanford Program on International and Cross-Cultural Educattion (SPICE). Retrieved 4/24/2026 from https://spice.fsi.stanford.edu/

Gyamera, E., Arko-Adjei, A., Duncan, E. E., & Kuma, J. (2017). Modelling participatory geographic information system for customary land conflict resolution. *ISPRS Annals of the Photogrammetry, Remote Sensing and Spatial Information Sciences*, *4*, 249-254.

ICJ. (1959a). *Reports of judgments, advisory opinions and orders: Case concerning sovereignty over certain frontier land (Belgium/Netherland)*. International Court of Justice

ICJ. (1959b). *Sovereignty over certain frontier land (Belgium/Netherlands)*. International Court of Justice. Retrieved 4/25/2026 from https://www.icj-cij.org/case/38

ICJ. (1962). *Communique 62/16*. International Courte of Justice

ICJ. (1986a). *Case concerning the frontier dispute (Burkina Faso/Republic of Mali)*. International Courte of Justice

ICJ. (1986b). *Frontier dispute (Burkina Faso/Mali): Judgement of the chamber*. International Court of Justice

ICJ. (1994). Case concerning the territorial dispute (Libyan Arab Jamahiriya/Chad). In *Summaries of Judgements, Advisory Opinions and Orders of the International Court of Justice*. International Court of Justice.

ICJ. (2002). *Land and maritime boundary between Cameroon and Nigeria*. International Court of Justice: ICJ

ITLOS. (2017). *Dispute concerning delimitation of the maritime boundary between Ghana and Cote D'Ivoire in the Atlantic Ocean*. I. T. f. t. L. o. Sea.

Kałduński, M. (2015). A commentary on maritime boundary arbitration between Bangladesh and India concerning the bay of Bengal. *Leiden Journal of International Law*, *28*(4), 799-848.

Lee, H. K. (2005). Mapping the law of legalizing maps: The implications of the emerging rule of map evidence in international law. *Washington International Law Journal*, *14*(1), 159-188.

Leigh, M. (1987). Case concerning the frontier dispute (Burkina Faso/Republic of Mali). *American journal of international law*, *81*(2), 411-414.

Mboce, N., Muigua, K., Momanyi, A., & Munyi, P. (2025). Efficacy of the international framework for settling disputes on maritime boundaries in Africa: A view through the Somalia v. Kenya maritime boundary dispute. *African Journal of International and Comparative Law*, *33*(2), 235-256.

McKoeon, R. W. (1991). The Aouzou Strip: Adjudication of competing territorial claims in Africa by the International Court of Justice. *Case Western Reserve Journal of International Law*, *23*(1), 147-170, Article 6.

Merrills, J. G. (2003). Land and maritime boundary between Cameroon and Nigeria (Cameroon v Nigeria:: Equatorial Guinea Intervening), Merits, Judgment of 10 October 2002. *The International and Comparative Law Quarterly*, *52*(3), 788-797.

PCA. (2014). *In the matter of the Bay of Bengal maritime boundary arbitration between the People's Republic of Bangladesh and the Republic of India*. Permanent Court of Arbitration, The Hague.

Rademacher, Y. (2020). Chad and Libya: Case Concerning the Territorial Dispute [1994]. In K. W. Gray (Ed.), *Global Encyclopedia of Territorial Rights* (pp. 1-10). Springer International Publishing. https://doi.org/10.1007/978-3-319-68846-6_592-1

Rajkovic, N. M. (2018). The visual conquest of international law: Brute boundaries, the map, and the legacy of cartogenesis. *Leiden Journal of International Law*, *31*(2), 267-288.

Ramnath, K. (2022). Making maritime boundaries in the Bay of Bengal. *Law and History Review*, *40*(3), 561-578.

Robertson, W. A. (2013). Contributions of and challenges for surveyors in the establishment of international boundaries-Cases in Africa. In H. Srebro (Ed.), *International boundary making* (pp. 39-50). FIG.

Saliternik, M. (2017). Expanding the boundaries of boundary dispute settlement: International law and critical geography at the crossroads. *Vanderbilt Journal of Transnational Law*, *50*, 113.

Salliot, E. (2010). *A review of past security events in the Sahel 1967–2007*. The OECD's Sahel and West Africa Club Secretariat.

Shrestha, B. N. (2013). Demarcation of the international boundaries of Nepal. In H. Srebro (Ed.), *International boundary making* (pp. 149-182). FIG.

Srebro, H., & Shoshany, M. (2013). The order of precedence of boundary definition. In H. Srebro (Ed.), *International boundary making* (pp. 39-50). FIG.

Stebek, E. N. (2009). ICJ Judgment (1994) on the Libya/Chad Territorial Dispute: A Brief Overview and Observations. *Mizan Law Review*, *3*, 167.

Tsiouvalas, A., & Solski, J. J. (2023). 'One map to rule them all'? Revisiting legalities through cartographic representations of the Northwest Passage. *Ocean Development & International Law*, *54*(4), 393-420.

Ubay, R. R. (2011). Evidence in international adjudication: Map evidence in territorial sovereignty dispute cases. *Aegean Review of the Law of the Sea and Maritime Law*, *1*(2), 287-300.

UN. (1982). *United Nations Convention on the law of the sea*. United Nations.

UN. (2006). Territorial sovereignty and scope of the dispute (Eritrea and Yemen). *Reports on International Arbitral Awards*, *XXII*, 209-332.

Weissberg, G. (1963). Maps as evidence in international boundary disputes: A reappraisal. *American journal of international law*, *57*(4), 781-803.

Wood, W. B. (2000). GIS as a tool for territorial negotiations. *IBRU Boundary and SEcurity Bulletin*, *8*(3), 72-78.

Author's Information

Name	:	Susheel Dangol
Academic Qualification	:	MSc in Geoinformation Science and Earth Observation for Land Administration
Organization	:	Survey Department
Current Designation	:	Deputy Director General

Price of Aerial Photograph

Data	Size	NRs. Rate	Remarks
Aerial Photo (Scan Copy)	23cm X 23cm	300	

Price of Image Data

Image of Topographic Map	NRs. Rate	Remarks
Digital orthoimage (at scale 1:5000)	Rs 3125	
Digital orthoimage (at scale 1:10000)	Rs 5000	
District Map (150 dpi in JPEG file)	Rs 200	
VDC Map (150 dpi in JPEG file)	Rs 50	

Price of Land Use Digital Data

District Level Data	Unit	Rate
Present Land Use	Per sq. Km.	5
GIS Data for Land Resource (Except Land Use Zoning Data)	Per sq. Km.	5
Profile	per district	200

Local Level Data	Unit	Rate
Present Land Use	Per sq.Km.	50
Soil Map Data	Per sq.Km.	50
Land Capability Data	Per sq.Km.	50
Profile	Per local level	1000

Price of LiDAR Data

Type	Unit	Rate
Point Cloud Data	Per sq. Km.	Rs 15000
Contour Data	Per sq. Km.	Rs 3000
Digital Surface Model Data	Per sq. Km.	Rs 4000

Type	Unit	Rate
Digital Terrain Model Data	Per sq. Km.	Rs 5000
Orthomosaic Data (RGB)	Per sq. Km.	Rs 6000
Full Data	Per sq. Km.	Rs 25000

Orthomosaic of Kathmandu Valley (39 sq. km) in RGB	Rs 5000 per sheet

Price of Digital Topographic Data Layers

LAYER	Rs/Sheet
Administrative	100.00
Transportation	200.00
Building	60.00
Landcover	300.00
Hydrographic	240.00
Contour	240.00
Utility	20.00
Designated Area	20.00
Full Sheet	1000.00

S.N	Data	Price
1	Seamless Data whole Country	
1.1	Digital data of all layers	Rs. 300000.00
1.2	Digital data compiled at scale 1:1000000	Free
2	Digital data of all layers compilled at scale 1:500000	Rs 1000 per sheet
3	Generalized Districtwise Data Layers	
3.1	Administrative Boundary	Free
3.2	Building	Rs. 15000.00
3.3	Contour	Rs. 65000.00
3.4	Transportation	Rs. 60000.00
3.5	Hydrographic	Rs. 70000.00
3.6	Landcover	Rs. 87000.00
3.7	Utility Line	Rs. 2000.00
3.8	Designated Area	Rs. 1000.00
3.9	Full Sheet	Rs. 2000.00
4	Rural Municipality (Gaunpalika) unitwise- all layers	Rs. 1000.00
5	Municipality (Nagarpalika) unitwise- all layers	Rs. 2000.00

Price of Printed maps

S.No	Maps	Unit	Rate (In NRs)
1	Political and Administrative Map of Nepal (2019)	Whole Nepal	150
2	Topographic Base Map (1992-2001)	Sheet	150
3	Topographic Map (1950s)	Sheet	50
4	District Map (1980s)	Sheet	50
5	Land Utilization Map (LRMP)	Sheet	50
6	Land Capability Map (LRMP)	Sheet	50
7	Land System Map (LRMP)	Sheet	50
8	Pysiographic Map of Nepal		50

Price of SOTER Data	Whole Nepal	NRs : 1000.00.

NeLIS: System Architecture and Transparency

Suresh Manandhar[1], Susheel Dangol[1]
sureshmdhr@gmail.com, susheel.dangol@nepal.gov.np
[1]Survey Department

KEYWORDS

NeLIS, LIS, Transparency, Architecture

ABSTRACT

Land Information Systems (LIS) are critical tools for effective land administration, promoting efficiency, tenure security, and strategic urban planning. This paper examines the development and implementation of the Nepal Land Information System (NeLIS) and its public portal, MeroKitta. We detail NeLIS's system, business, and information architectures, which utilize a modified three-tier client-server model to securely separate internal cadastral operations from external citizen services. Transitioning to this centralized architecture required rigorous spatial and attribute data harmonization to resolve topological errors, schema drift, and linguistic variations in legacy decentralized databases. Furthermore, the study highlights how NeLIS enhances functional transparency and accountability. Through real-time transaction tracking, Lead Time Velocity monitoring, automated SMS notifications, and integration with the Revenue Management Information System (RMIS), the system clarifies responsibilities and reduces bottlenecks. Ultimately, this standardized LIS architecture streamlines workflows, secures land records, and empowers citizens with accessible, trustworthy information, laying the groundwork for sustainable land governance.

1. LAND INFORMATION SYSTEM (LIS)

Information System (IS) is the set of components to collect, analyze and disseminate information to the user which is discussed as the interaction between people, processes, data and technology in general (Gupta, 2013). Land Information System (LIS) is the special type of IS which capture, process, store, analyze disseminate and share information about the land. It is designed to collect, store, reference, process, and retrieve land-related information, comprising four key components: data, processes, technology, and human resources.

"The International Federation of Surveyors (FIG) defined a land information system as a tool for legal, administrative and economic decision-making and an aid for planning and development. A land information system consists of a database containing spatially referenced land-related data for a defined area including procedures and techniques for the systematic collection, updating, processing and distribution of the data" (UN, 2005). LIS supports cadaster and land registration activities as well as land use planning, land valuation, and broader land resource management. (Tuan, 2006).

An LIS consists of a spatially referenced land-related database for a defined area, along with procedures and techniques for the systematic collection, updating, processing, and dissemination of data (Tuan, 2006). More specifically, an LIS comprises essential components that support land transactions, namely data sets, processes or functions, hardware and software, and people (Tuladhar, 2005).

The cadaster, which acts as the comprehensive registry of individual land parcels, constitutes the primary component of an LIS (Dhal, 2002; Zhao, 2010). A LIS facilitates quick, reliable, and streamlined land transactions through a one-stop service, while also supporting urban planning, infrastructure development, land reform, dispute reduction, and related initiatives. Broadly, the advantages of a LIS can be examined in terms of efficiency, effectiveness, and the creation of competitive advantage.

LIS reduces labor demands, minimizes the need for physical storage of analog documents, enables automated control processes that facilitate data sharing, and ultimately delivers higher-quality services. It also supports land administration functions such as alienation, transfer, valuation, development, and utilization of land, while also enhancing land tenure security by delivering current and reliable information and services at the lowest possible cost (Tuladhar, 2004). *Figure 1* shows the concept of LIS and its components.

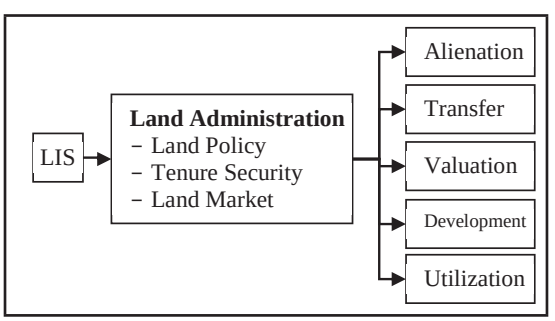

Figure 1: Land Information System.(Tuladhar, 2004)

To discuss some examples, The Korean Land Information System (KLIS) is an online application that provides electronic transaction services and essential information through kiosks. It comprises individual parcel maps digitized from paper records, continuous cadastral maps created by edge-matching individual parcels, and edited cadastral maps produced by transforming continuous cadastral maps to overlay on topographic maps (Kim & Lee, 2014). Landgate of Western Australia is the web-based LIS to provide information about land and property to the users (Kalantari et al., 2005). At the regional level, European Land Information System (EULIS) is the LIS which deals beyond the border in Europe which provide access to land information across the border and also support property market.

In context of Nepal, Nepal Land Information System (NeLIS) is the web-based application for the management of cadastral data and perform all the cadastral data related operations for land administration services and also, it maintains all the cadastral data at centralized database system considering security of the data while considering the fast, reliable and effective service delivery (Karmacharya et al., 2022). Complementing this spatial framework, the complete Nepal's LIS also constitutes the Land Records Information Management System (LRIMS), which manages textual ownership records and deed registrations.

2. INFORMATION SYSTEM ARCHITECTURE

Architecture represents a system by defining its components, the relationships among them, and the resulting product. It should be designed in a manner that ensures adoption by both government organizations and citizens. The components of the architecture must be interconnected, the data utilized should be interoperable, and the mechanisms for delivering information need to be clearly established. Effective information sharing among organizations is essential for enhancing efficiency and service quality, reducing labor costs, and minimizing data redundancy (Hobson et al., 2011). Moreover, it contributes to greater transparency in service delivery.

Among different architectures, The Open Group Architecture Framework (TOGAF) provides a complete framework for development of architecture discussed under four different vies as business, data, system and technical architecture (Jin et al., 2010). According to Jin et al. (2010), business architecture identifies the functions, process, and information flow for accomplishing the task of organization, data architecture defines structure of data being used by the system, system architecture is the factor which determine the adoption of the system by users and technology architecture defines how different systems within the system are connected with each other.

2.1. NeLIS system architecture

Dangol (2012) has proposed business architecture, information architecture, and system architecture for the development of e-government-based LIS for Nepal. The proposed system architecture was three-tier client server concept with application server, web server and database server. The same architecture concept was adopted to develop the NeLIS with some modification in connectivity (Figure 2).

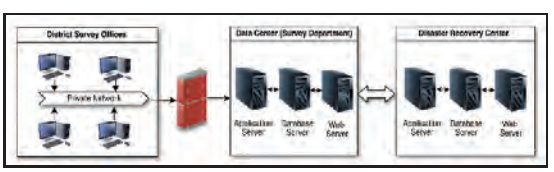

Figure 2: NeLIS system architecture (Modified) (Dangol et al., 2021))

The system architecture was slightly modified with separate web server for providing online map printing services for the customers through *MeroKitta* system. All the three servers are hosted at the Data Center (DC) of Survey Department. District survey offices connect to the DC through the private network with restriction through web access. All the servers are collocated at the Disaster Recovery (DR) center maintained at Hetauda by Integrated Data Management Center (IDMC), Government of Nepal. All the transactions are simultaneously updated and backed up at the DR site.

2.2. NeLIS business and information architecture

For the land transaction services and information delivery, two categories of users are maintained. The internal users are the NeLIS system users at district survey office and Survey Department. Internal users from the department use the system to monitor the system, provide technical support to the district offices and managing administration of the system. Internal users at the survey office use the system to provide all cadastral related services of the land administration services at the district level.

The external users are the individual persons and institutional users like financial organizations and the local level municipalities. The external users can get the cadastral services like map print, fieldbook/ plot register print, request for field survey and also pay the revenue for the services through the e-payment gateways. These services are provided through the *Merokitta* system. This is the web-based system; however, it does not have direct connection with the database server to ensure the security of the NeLIS (Figure 3).

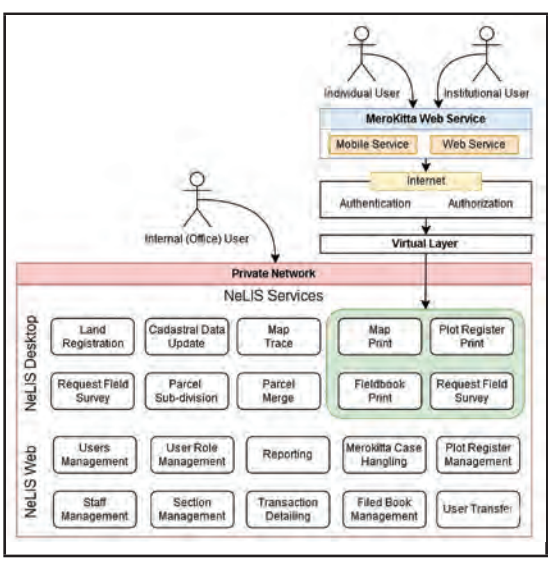

Figure 3: Business and information architecture.

Only major services are shown in the NeLIS services. NeLIS has two modules: NeLIS desktop and NeLIS web. The desktop module conducts all core land administration activities, which involves directly editing, updating, and processing the spatial and attribute data of the cadaster. In contrast, the NeLIS web module focuses primarily on overarching system administration and monitoring.

Merokitta provides online platform for the external users for requesting services like map print, field book/plot register print, field survey request. This platform is connected with Revenue Management Information System (RMIS) for online revenue payment by the users. The virtual layer is created for restricting direct access to the cadastral database by the external users.

3. NELIS SUPPORT MECHANISM

3.1. System implementation

The existing cadastral geodatabase of the district offices are the base of the cadastral data in NeLIS. Those databases are migrated to the NeLIS database with necessary data cleaning and harmonization.

3.2. Attribute data cleaning

The existing geodatabases are checked for how effectively the attributes align with the NeLIS database framework. These legacy databases were created using the Spatial Application Extension (SAEx), a decentralized digital cadastral service delivery tool used in Nepal for the past two decades. Over time, these SAEx databases have exhibited significant schema drift, such as missing columns, renamed fields, and non-standard data types (Paudyal, 2007). Required fields in parcel layer of the geodatabase including DISTRICT, VDC, WARDNO, GRIDS1, PARCELTY, and PARCELNO must be present and properly structured.

The 9-digit geocode (GRIDS1) must be generated for the free sheet maps and validated for all parcels. The NeLIS geocode format (Prefix + Scale + Ward + Sheet + Part) is specific to Nepal's administrative hierarchy.

Nepal's cadastral maps use Devanagari script for sheet identification, with transliterations varying significantly across survey offices. These linguistic variations need to be normalized and mapped to the standardized NeLIS geocoding schema (Karmacharya et al., 2022).

Attribute validation must be performed to ensure data integrity. District codes must be present and within valid range (1-77). VDC codes, ward numbers, and parcel numbers must be valid and within appropriate ranges. Sheet number mismatches between folder names and database entries need correction. Parcel type fields must be verified for correct entries. Legacy data often has incomplete attribute information that needs to be identified and filled from available sources (Tuladhar, 2004).

Database-level checks are also essential. Database version conflicts may exist where multiple databases of the same location contain different branching edits. Database fragmentation from accumulated scratch layers increases file size and slows loading time, requiring compaction (A. M. Tuladhar, 2005). Cross-boundary databases in trig sheet areas may contain parcels from multiple wards, causing data duplication during migration (Dangol et al., 2021).

3.3. Spatial data cleaning

Spatial properties of the geodatabase are also checked with different specified rules. The topological integrity of cadastral data is the foundation of any Land Information System (LIS) (Lemmen et al., 2015). A topologically correct cadastral map must satisfy two fundamental rules: (1) No Overlaps—the intersection of the interiors of any two distinct parcel polygons must be empty, and (2) No Gaps—the union of all parcel polygons in a

continuous block must form a seamless surface without unintended voids.

Existing data digitized using the Spatial Application Extension (SAEx) often violates these rules due to manual digitization errors, "double-digitizing" of shared boundaries, and floating-point precision errors (Paudyal, 2007). Micro-gaps and sliver overlaps must be resolved. Sliver polygons, which are thin unwanted polygons created during digitization, can be identified using the Circularity Index ($4\pi A/P^2$) combined with area thresholds. Geometry validity must be verified where self-intersecting polygons, unclosed rings, and null geometries must be corrected.

Multi-polygons, which are parcel features consisting of multiple disconnected parts, are not supported in NeLIS and must be separated into individual features. Spatially displaced sheets, where database corners are digitized in wrong locations, can be identified using background satellite imagery. Sheet extent mismatches, where adjacent sheet corners do not align, require geometric adjustment. Residual parcels, which are remaining areas left as single features during digitization, should be identified and removed. Roads that continue across sheet or ward boundaries must be properly segmented (Sapkota, 2012).

Duplicate features must be removed as they cause topological errors and database bloat. Attribute-geometry linkage must be preserved during any spatial correction to maintain cadastral integrity (Enemark et al., 2014). A review mechanism must be established for complex cases as large overlaps may indicate genuine boundary disputes requiring human judgment.

3.4. Service delivery support

Technical support mechanism through different medium is adopted to provide continuous support to ensure efficient service delivery at district survey offices (Koroso et al., 2013). The central Survey Department provides constant phone support to address technical issues faced by district offices. Remote desktop support using VNC and Any Desk software enables technical staff to directly troubleshoot problems on district office computers, reducing the need for physical visits and minimizing service disruption.

Training programs are conducted regularly to enhance the technical capacity of survey office staff (Karmacharya et al., 2022). These programs cover system operation, data management procedures, and troubleshooting techniques, ensuring that local staff can handle routine issues independently while complex problems are escalated to the central support team.

Network monitoring is essential for uninterrupted connectivity between district offices and the central data center. All district offices are connected through redundant private networks to ensure continuous service availability (Dangol et al., 2021). Continuous monitoring systems track network performance and alert administrators to potential issues before they affect service delivery.

System monitoring is implemented to track the health and performance of NeLIS servers and applications. Real-time monitoring of server resources, database performance, and application response times helps identify and resolve issues proactively (Cheng, 2013). This ensures high availability of the system for both internal users at survey offices and external users accessing services through *MeroKitta*.

Continuous updates to the system and software are deployed to improve functionality, security, and user experience. Regular software updates address bug fixes, introduce new features, and enhance system performance based on user feedback and operational requirements (Arshad et al., 2025). These updates are managed centrally to ensure consistency across all district offices while minimizing disruption to ongoing services.

3.5. Network monitoring

All district offices are connected to the DC with two separate private networks so that even if one network fails to work, then next one will continue the service. In spite of redundant private network, continuous monitoring of the network is essential for uninterrupted connectivity (Karmacharya et al., 2022).

4. FUNCTIONALITY FOR TRANSPARENCY

Transparency is one of the keywords of contemporary governance which implies to access to public information and hence, it is often assumed that increase in transparency leads to increased citizens trust in government (Erkkilä, 2020). Access to information is one of the major elements of transparency along with public participation and institutional reforms (TI, 2004). From a functional perspective, transparency focuses on the clarity of information—specifically addressing questions such as: Who does what? Who is responsible for what? Who processes applications? and Who makes decisions? (Cheng, 2013). Ontime information during land transaction supports in effective and efficient service delivery (Koroso et al., 2013).

To enhance the transparency in service delivery through NeLIS and *MeroKitta* system, different ways for providing information regarding land transaction has been developed.

4.1. Administrative monitoring and accountability

Figure 4 illustrates the Lead Time Velocity Timeline, which provides a granular breakdown of the time elapsed between each stage of a *MeroKitta* transaction. This visualization serves as a critical monitoring tool for the department, enabling administrators to identify specific bottlenecks and outliers in real-time. By analyzing these data points, the central authority can proactively intervene in cases exceeding standard processing times, requesting justifications from the respective survey offices to ensure accountability and maintain a high standard of service delivery.

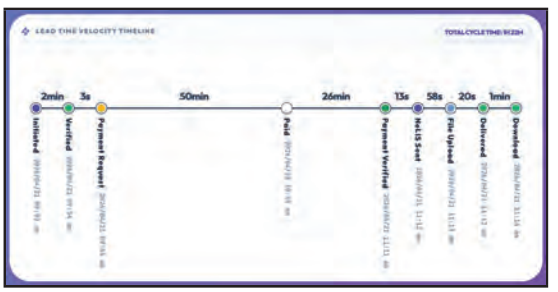

Figure 4: Lead time velocity timeline for MeroKitta transaction processing

4.2. Real-time transaction tracking

To provide clarity to the public, Figure 5 shows the current status of the transaction in NeLIS. CaseID is the unique number of every transaction in NeLIS all over the country. Concerned landowner with this ID can check the status of the transaction online. Transaction status is shown for every step completed at the survey office. For each step, whether it is initiated, checked or approved is shown with date and time stamp and the staff of the survey office who conducted the specific step of the transaction.

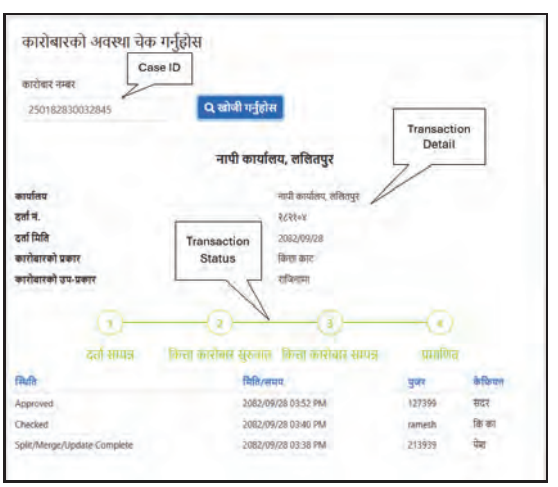

Figure 5: Live status of land transaction.

Additionally, Figure 6 shows the list of the transaction that is being handled at the survey office at the time. This shows the details of transaction with caseID, section, date,

transaction detail, cadastral detail and the status of the transaction. This is displayed in the television screen connected with NeLIS to provide information about the transaction status to the customers at the waiting lobby.

Figure 6: Transaction status shown at TV.

4.3. Proactive citizen communication and e-services

Transparency is further enhanced through proactive updates. Figure 7 shows the information through SMS service regarding initiation of the service request through *MeroKitta* system. While requesting for the online services through the *MeroKitta*, One Time Password (OTP) is provided to the customer and he/she will get SMS for every process completed by the Survey Office.

Figure 7: Mobile message about map print initiated status for citizen.

Once the data for the online services is verified by the survey office, the customer will receive SMS for revenue payment. The message includes the total amount to be paid and the links for all compatible payment gateways (Figure 8). All these payment gateways are linked with the Revenue Management Information System (RMIS) through which the revenue is directly deposited to the central treasury.

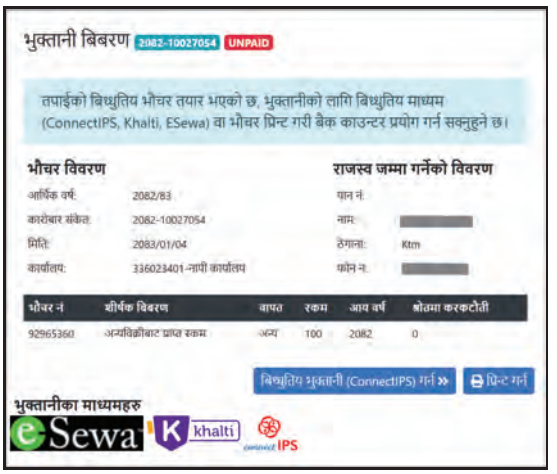

Figure 8: Online payment gateway options for revenue payment of map print.

Finally, once the customer completes the revenue payment, they will then receive the SMS for downloading the requested services (Figure 9). The customer can download the PDF version of the requested services, the link for download which will be available for fifteen days.

Figure 9: Final message for map download link.

5. CONCLUSION

Transparency has three main aspects as legal, structural and functional aspect. LIS explicitly

supports in functional transparency. As the LIS is developed with some standard architecture and workflow, it supports in enhancing transparency and hence enhance efficiency and effectiveness in the land administration services. In the context of LIS in Nepal, NeLIS has also been developed and deployed with standard system architecture.

Further, the establishment of a LIS built upon a standard system architecture is a cornerstone for modern land governance. By ensuring interoperability, consistency, and reliability across processes, such a system enhances transparency in land records and transactions. Moreover, it streamlines workflows, reduces duplication, and supports efficient service delivery in land administration. Ultimately, adopting a standardized architecture not only strengthens institutional accountability but also empowers citizens with accessible, trustworthy, and timely land information—laying the foundation for sustainable and equitable land management.

REFERENCES

Arshad, N., Butt, T., & Iqbal, M. (2025). A comprehensive framework for Intelligent, Scalable, and Performance-Optimized software development. *IEEE Access*. 13, 74062-74077.

Cheng, B. (2013). *Workflow database modeling in a workflow management system for better land transaction transparency.* [MSC Thesis, University of Twente]. The Netherlands, Enschede.

Dangol, S. (2012). *E-government based land information system architecture: A case of Nepal* A thesis submitted for the degree of Master of science in Geo-information Science and Earth Observation for Land Administration. ITC, The Netherlands, Enschede.

Dangol, S., Joshi, P., & Dahal, T. P. (2021). Online Service Delivery in Survey Offices: Step towards e-Land Administration. *Journal on Geoinformatics, Nepal*, 20(1), 67–74. https://doi.org/10.3126/njg.v20i1.39480

Dhal, N. (2002). Land Information System (LIS)-A Cae Study in Orissa. *Indian Cartographer*, *2*, 295–298.

Enemark, S., Bell, K. C., Lemmen, C., & McLaren, R. (2014). *Fit-for-purpose land administration*. International Federation of Surveyors (FIG).

Erkkilä, T. (2020). Transparency in public administration. In *Oxford research encyclopedia of politics*. Oxford University Press.

Gupta, E. (2013). Information system. In *Entrepreneurship and SMEs: Building Competencies* (pp. 97–102). Adhyayan Publishers & Distributors.

Hobson, S. F., Anand, R., Yang, J., & Lee, J. (2011). Towards Interoperability in Municipal Government: A Study of Information Sharing Practices. Conference Proceedings: IFIP Conference on Human-Computer Interaction, Portugal, September 5-9, 2011.

Jin, M., Kung, D., & Peng, W. (2010). Research of Information system Technology Architecture. Conference Proceedings: 2010 2nd International Conference on Industrial and Information Systems, Dalian, China 10 - 11 July 2010.

Kalantari, M., Rajabifard, A., Wallace, J., & Williamson, I. (2005). Toward e-land administration: Australian online land information services. Proceedings of SSC 2005 Spatial Intelligence, Innovation and Praxis: The national biennial Conference of the Spatial Sciences Institute, September, 2005. Melbourne.

Karmacharya, A., Pradhan, G., Niraula, P., Ghimire, P., Rajbhandari, S. P., Manandhar, S., Bhandari, S., & Dangol, S. (2022). Online Service Delivery in Survey Offices of Nepal. *Journal on Geoinformatics, Nepal*, 21(1), 43–50. https://doi.org/10.3126/njg.v21i1.50881

Kim, M., & Lee, K. H. (2014). *Korea Land Information System*. Korea Research Institute for Human Settlements (KRIHS).

Koroso, N. H., Van der Molen, P., Tuladhar, A. M., & Zevenbergen, J. A. (2013). Does the Chinese market for urban land use rights meet good governance principles? *Land use policy*, *30*(1), 417–426.

Lemmen, C., Van Oosterom, P., & Bennett, R. (2015). The land administration domain model. *Land use policy*, *49*, 535–545.

Paudyal, D. R. (2007). Assessment of the digital cadastre in Nepal from the cadastre 2014 vision. *Journal on Geoinformatics, Nepal*, 6(1), 9–15.

Sapkota, R. K. (2012). LIS Activities in Nepal: An Overview in prospect of DoLIA. *Journal on Geoinformatics, Nepal*, *11*, 23–28.

TI. (2004). *Tools to support transparency in local governance*. Transparency International, UN-HABITAT.

Tuan, V. A. (2006). *Reengineering of a land information system LIS for the Vietnamese land administration* [MSc Thesis, ITC]. Enschede, The Netherlands.

Tuladhar, A. (2005). Institutional and Technical Aspects of Cadastral Systems: Experiences and Reflections. In: Map India.

Tuladhar, A. M. (2004). Parcel-based geo-information system: concepts and guidelines.

Tuladhar, A. M. (2005). *Institutional and Technical Aspects of Cadastral Systems: Experiences and Reflections* Map India 2005,

UN. (2005). *Land Administration in the UNECE Region: Development trends and main principles*. United Nations.

Zhao, Y. (2010). "One Map"-Based Land Information System: Towards E-government for Land Management. Conference Proceedings: 2010 International Conference on E-Business and E-Government, Guangzhou, China, May, 2010.

Author's Information

Name	:	Suresh Manandhar
Academic Qualification	:	BE in Geomatics Engineering
Organization	:	Survey Department
Current Designation	:	Survey Officer

Price of Maps

S.No.	Description	Scale	Coverage	No. of sheets	Price per sheet (NRs)
1.	Topo Maps	1:25 000	Terai and mid mountain region of Nepal	590	150
2.	Topo Maps	1:50 000	HIgh Mountain and Himalayan region of Nepal	116	150
3.	Land Utilization maps	1:50 000	Whole Nepal	266	40
4.	Land Capibility maps	1:50 000	Whole Nepal	266	40
5.	Land System maps	1:50 000	Whole Nepal	266	40
6.	Geological maps	1:125 000	Whole Nepal	81	40
7.	Districts maps Nepali	1:125 000	Whole Nepal	76	50
8.	Zonal maps (Nepali)	1:250 000	Whole Nepal	15	50
9.	Region maps (Nepali)	1:500 000	Whole Nepal	5	50
10.	Nepal (English)	1:500 000	Whole Nepal	3	50
11.	Nepal Map (Nepali)	1:1000 000	Nepal	1	50
12.	Nepal Map (Nepali)	1:2000 000	Nepal	1	15
13.	Nepal Map (English)	1:1000 000	Nepal	1	50
14.	Nepal Map (English)	1:2000 000	Nepal	1	15
15.	Physiographic Map	1:2000 000	Nepal	1	15
16.	Relief Map	1:2000 000	Nepal	1	15
17.	Photo Map			1	150
18.	Wall Map (loosesheet)		Nepal	1 set	50
19	VDC/Municipality Maps (Colour)		Whole Nepal	4181	50
20.	VDC/Municipality Maps A4 Size		Whole Nepal	4181	5
21.	VDC/Municipality Maps A3 Size		Whole Nepal	4181	10
22.	Orthophoto Map		Urban Area (1:5000) and Semi Urban Area (1:10000)	-	1 000
23.	Outlined Administrative Map A4 size		Nepal	1	5

Price of Co-ordinates of Control Points

Type	Control Points	Price per point
Trig.Point	First Order	Rs 3 000.00
Trig. Point	Second Order	Rs 2 500.00
Trig. Point	Third Order	Rs 1 500.00
Trig. Point	Fourth Order	Rs 1000.00
Bench Mark	First & Second Order	Rs 1000.00
Bench Mark	Third Order	Rs 250.00
Gravity Point	-	Rs 1 000.00

Price of CORS Station Data

Type	Price
24 hr CORS Rinex data with 1 sec frequency for post processing	Rs 200
24 hr CORS Rinex data with 15 sec frequency for post processing	Rs 100
1 hr CORS Rinex data with 1 sec frequency for post processing	Rs 10
1 hr CORS Rinex data with 15 sec frequency for post processing	Rs 5
RTK Correction Service Unlimited Subscription 1 month	Rs 10000
RTK Correction Service Unlimited Subscription 3 months	Rs 27000
RTK Correction Service Unlimited Subscription 12 months	Rs 96000
GNSS Post-processing Service per point per hour data	Rs 10

Price of Geoid Data

Type	Price	Remarks
Geoid N-Sepration (per point)	Rs 200	
Geoid Determined Orthometric Height (per point)	Rs 1000	
Geoid Data (per 100 sq. km)	Rs 10000	Minimum 100 sq.km and multiple of 100 sq.km

Optimized Deep Learning Model for LULC Classification in the Terai Region: Comparing U-Net and Resunet With Spectral Index Fusion and Cross-Area Fine-Tuning

Hiralal Pardhe[1], Uma Shankar Panday[2] & Sanjeevan Shrestha[3]
hiralalpardhe@gmail.com, uspanday@ku.edu.np, shr.sanjeevan@gmail.com
[1]Survey Office Kalanki, [2]Department of Geomatics Engineering, Kathmandu University,
[3]Ministry of Land Management, Co-operatives, Federal Affairs and General Administration

KEYWORDS

Deep learning, U-Net, ResNet-50, Cross-area fine-tuning, Hyperparameter optimization, Spectral indices, GIS, Environmental monitoring

ABSTRACT

Accurate and up-to-date Land Use/Land Cover (LULC) mapping is crucial for environmental management and regional planning, but its development is often limited by insufficient labeled data, spectral similarity between land-cover classes, and difficulties in transferring models across regions. This study developed an optimized deep learning framework for LULC classification in Dhanusha District using cross-area fine-tuning with U-Net and a ResUNet-style architecture based on a ResNet-50 encoder backbone. The approach aimed to improve model transferability by adapting models trained in a data-rich source area (Mahottari District) to a target area (Dhanusha District) with limited labeled samples. Sentinel-2 Level-2A imagery from March 2021 was preprocessed and five LULC classes - Water Bodies, Cropland, Built-Up, Tree Cover, and Others were manually digitized from Google Earth imagery and converted into raster masks. Along with RGB imagery, spectral-index composites including NDVI, SAVI, EVI, MSAVI, GNDVI, NDWI, and NDBI were generated to improve class separability. Image and mask datasets were tiled into sizes of 128×128, 256×256, and 512×512 pixels and divided into training and testing sets. Hyperparameters such as batch size, dropout, L2 regularization, learning-rate scheduling, and early stopping were systematically optimized. Results demonstrated strong segmentation performance after cross-area adaptation. ResNet-50 consistently outperformed U-Net, achieving overall accuracies of up to 0.96 in Mahottari and 0.95 in Dhanusha, while U-Net achieved up to 0.95 and 0.94, respectively. Spectral-index composites reduced confusion among challenging classes, especially water bodies and built-up areas. Intermediate tile sizes (256×256) provided the best balance between spatial context, computational efficiency, and stable model convergence, resulting in improved generalization across districts.

1. INTRODUCTION

1.1 Background

Land Use/Land Cover (LULC) classification is a fundamental aspect of environmental monitoring, urban planning, and natural resource management. It involves categorizing Earth's surface into distinct classes such as forests, agricultural land, urban areas, water bodies, and barren land (Turner et al., 2007). Accurate LULC mapping is crucial for understanding ecological changes, assessing climate impacts, and formulating sustainable land management policies. Remote sensing (RS) and Geographic Information Systems (GIS) have revolutionized LULC studies by enabling large-scale, cost-effective monitoring through satellite imagery such as Landsat and Sentinel-2 (Drusch et al., 2012).

Nepal has experienced significant LULC changes due to rapid urbanization, agricultural expansion, and deforestation (Uddin et al., 2015).The Terai region, including Dhanusha District, has seen dramatic transformations, with forests converted to farmland (Paudel et al., 2018). These changes have ecological consequences, including biodiversity loss, soil degradation, and increased flood risks. Monitoring these trends is essential for sustainable development, yet traditional field surveys are labor-intensive and have limited scope.

Optical remote sensing has been widely used for LULC studies, leveraging platforms like Landsat (30m resolution) and Sentinel-2 (10m/20m resolution). Early studies employed pixel-based classification methods such as Maximum Likelihood and ISODATA (Richards & Jia, 1999), but these struggled with spectral complexity in heterogeneous landscapes. Machine learning (ML) techniques, including Random Forest (RF) and Support Vector Machines (SVM), improved accuracy by handling non-linear data relationships (Mountrakis et al., 2011). However, deep learning (DL) approaches, particularly Convolutional Neural Networks (CNNs), have recently outperformed traditional ML methods in LULC classification (Zhang et al., 2019).

Earlier approaches primarily relied on pixel-based classification methods such as Maximum Likelihood, which often struggled in heterogeneous landscapes (Richards & Jia, 1999). More recent studies have adopted machine learning algorithms such as Random Forest and Support Vector Machines to improve classification accuracy; however, these methods still depend heavily on handcrafted features and large labeled datasets (Mountrakis et al., 2011).

Despite these advancements, several limitations remain. Many Nepal-based studies have not fully leveraged deep learning techniques capable of capturing spatial context, and the scarcity of labeled data continues to hinder model performance. Furthermore, most existing research focuses on single-region analysis, with limited attention to model transferability across geographically similar areas. This study addresses these gaps by employing cross-area fine-tuning to transfer learned representations between similar regions, thereby reducing dependence on extensive training data while improving generalization (Tuia et al., 2016; Yuan et al., 2020). Additionally, the integration of hyperparameter optimization enhances model efficiency and predictive performance (Akiba et al., 2019). Together, these approaches provide a robust and scalable framework for accurate LULC classification in data-constrained environments like Nepal.

Among deep learning architectures, U-Net (Ronneberger et al., 2015) has emerged as a leading model for semantic segmentation in remote sensing. Its encoder-decoder structure with skip connections preserves spatial details, making it ideal for precise land cover mapping. ResUNet, an extension of

U-Net with residual blocks (Diakogiannis et al., 2020), further enhances feature learning by mitigating vanishing gradients in deep networks. These models have demonstrated superior performance in complex landscapes, achieving over 90% accuracy in LULC classifications (Maggiori et al., 2017).

In this study, a model initially trained on the Mahottari district, which shares comparable agro-ecological and climatic characteristics, is fine-tuned for Dhanusha district. This approach significantly reduces the dependency on extensive ground-truth data while preserving classification accuracy. Previous studies have demonstrated that spatially informed fine-tuning strategies substantially improve LULC mapping performance in data-scarce regions, especially when source and target areas exhibit similar land-use patterns and phenological behavior (Zhu et al., 2017;Gevaert & García-Haro, 2015).

Complementing cross-area fine-tuning, hyperparameter optimization (HPO) plays a critical role in maximizing model efficiency and predictive performance. Key hyperparameters-such as learning rate, batch size, and network depth, strongly influence convergence speed and classification accuracy (Bergstra & Bengio, 2012). Manual tuning is often inefficient and suboptimal; therefore, automated HPO techniques such as Bayesian Optimization and evolutionary search methods, implemented through open-source frameworks like Optuna, allow systematic and computationally efficient exploration of the hyperparameter space (Akiba et al., 2019). The combined use of cross-area fine-tuning and HPO forms a robust framework that enhances model adaptability, accuracy, and computational efficiency for LULC classification in data-constrained remote sensing applications. By utilizing freely available Sentinel-2 imagery and its corresponding composites of spectral indices and Deep learning architectures, this research provides a cost-effective solution for land cover mapping in Nepal.

1.2 Objectives

The primary objective of this study is to develop an **optimized cross-area fine-tuning model** for Land Use/Land Cover (LULC) classification in the **Dhanusha district** using **U-Net and ResUNet** architectures enhanced with **hyperparameter optimization**. The secondary objectives are as follows:

- To access the baseline classification accuracy of U-Net and ResNet-50 models trained on the Mahottari district prior to cross-area fine-tuning.
- To measure the accuracy loss of both models after fine-tuning on the spatially distinct Dhanusha dataset.

2. MATERIALS AND METHODS

2.1 Study area

The study was conducted in the neighboring districts of Mahottari and Dhanusha in Madhesh Province, southeastern Nepal, located in the Terai region. These districts were selected to evaluate the cross-area fine-tuning capability of deep learning–based Land Use Land Cover (LULC) classification models, with Mahottari used as the training area and Dhanusha as the testing area. Their similar climate, topography, and land-use patterns make them suitable for assessing model transferability and generalization.

Mahottari District covers about 1,002 km² and consists mainly of flat Terai plains with diverse land-cover features such as agricultural land, forests, settlements, water bodies, and built-up areas, making it suitable for model training. Dhanusha District, covering approximately 1,180 km², shares similar environmental and land-use characteristics with Mahottari, making it an appropriate region for testing the performance of the transferred deep learning models.

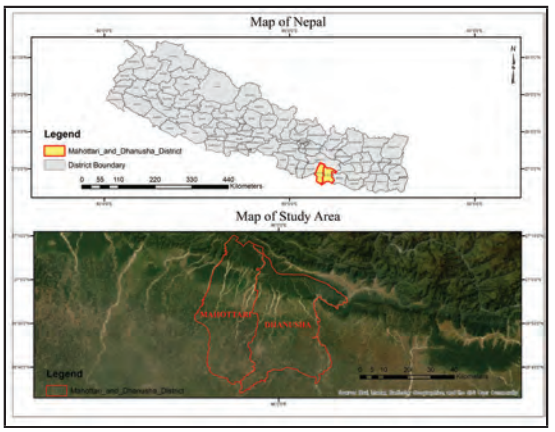

Figure 1: Study area

2.2 Methodology

The overall methodology of the study is presented in *Figure 2.*

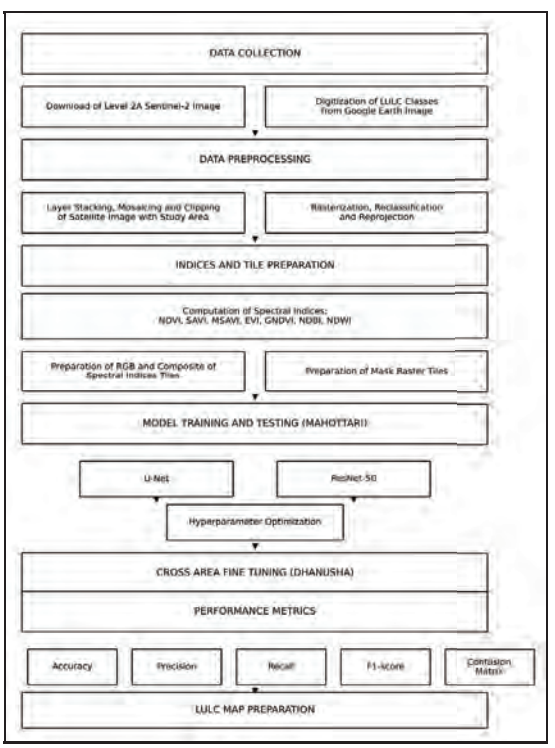

Figure 2: Overall methodology of the study

2.2.1 Data collection

The data acquisition process for Sentinel-2A imagery of March 2021 for Mahottari and Dhanusha districts involves the collection of high-resolution multispectral satellite images capturedbytheEuropeanSpaceAgency's(ESA) Copernicus Sentinel-2 mission. These images, available at a 10-meter spatial resolution, were downloaded from the Copernicus Open Access Hub. The selection of the March 2021-time frame ensures minimal cloud cover and optimal visibility conditions for surface feature extraction during the dry season. In this study, Sentinel-2 satellite imageries of the year 2021 March of the study area were used. For Mahottari, two imageries tiles (T45RUK and T45RVK) were downloaded. Similarly, three S2 imageries tiles (T45RUK, T45RUL and T45RVK) were downloaded for Dhanusha district. The acquired imagery includes multiple spectral bands, particularly those in the visible, near-infrared (NIR), and short-wave infrared (SWIR) ranges, which are essential for computing spectral indices such as NDVI (Normalized Difference Vegetation Index), NDWI (Normalized Difference Water Index), and NDBI (Normalized Difference Built-up Index). The systematic acquisition of these images serves as the foundational step for further analysis and the development of deep learning-based classification models for accurate LULC mapping.

The labelled dataset for LULC classification in Mahottari and Dhanusha districts was prepared primarily through manual digitization of high-resolution Google Earth imagery from the year 2021. High-resolution Google Earth imagery was visually interpreted to delineate detailed land cover features such as built-up areas, cropped areas, water bodies, tree cover, and other relevant classes. The number of samples for each class is presented in *Table 1*.

Table 1:Classwise Samples of both districts

Class	No of Samples			
	Mahottari		Dhanusha	
	Train	Test	Train	Test
Water Bodies	276	69	152	38
Cropland	1680	420	960	240
Built-Up	1760	440	952	238
Tree Cover	1200	300	720	180
Others	880	220	480	120

2.2.2 Pre-processing

Data preprocessing is a critical stage in the methodology, as it ensures the quality, consistency, and spatial compatibility of both satellite imagery and reference data prior to deep learning-based analysis. All preprocessing operations were carefully performed to minimize noise, reduce geometric discrepancies, and prepare datasets for accurate pixel-wise classification. Initially, the downloaded Sentinel-2 Level-2A multispectral imageries are processed by selecting the relevant spectral bands required for LULC classification.

In parallel, the reference LULC data obtained through manual digitization from Google Earth imagery are prepared for model training. Since deep learning-based semantic segmentation requires pixel-level labels, the vector-based LULC polygons are converted into raster format through rasterization. During rasterization, each pixel is assigned a class label corresponding to the underlying LULC category. The rasterized LULC data are then subjected to reclassification, where original class codes are standardized and harmonized to maintain consistency across the dataset and avoid ambiguities during training.

2.2.2.1 Computation of spectral indices

To enhance feature discrimination among different land cover classes, various **spectral indices** are computed from the preprocessed Sentinel-2 bands. These indices include **NDVI, SAVI, MSAVI, EVI, GNDVI, NDBI, and NDWI**, each designed to emphasize specific surface characteristics such as vegetation vigor, soil influence, built-up areas, and water bodies. The inclusion of these indices improves the deep learning model's ability to distinguish between spectrally similar classes. The derived indices were stacked together to form multi-band composite images, providing comprehensive spectral information for subsequent model training and classification. This composite dataset served as the input for both traditional and deep learning algorithms in the LULC classification process. *Table 2* shows the spectral indices used in the study.

2.2.2.2 Generation of image and mask tiles

Following the steps mentioned above, all three generated tile sizes for the year 2021 were split into training and testing subsets. Twenty percent of the total dataset was kept for validating the performance of the model, and the rest was used for the training of the model. Similarly, the tiles corresponding to the Dhanusha district were separated in the same manner to facilitate fine-tuning and testing of performances of models.

2.2.3 Model training and testing

Model training and testing were performed using labeled samples from the Mahottari district, which served as the source area for subsequent cross-area fine-tuning. The available dataset was divided into training and testing subsets to ensure reliable model development and unbiased performance assessment. Training was carried out iteratively by optimizing model parameters to minimize classification error, with training progress monitored to ensure stable convergence. To enhance generalization under limited data conditions, appropriate regularization strategies and a controlled learning rate were applied during training.

2.2.3.1 U-net

The implemented model is based on the **U-Net architecture**, a fully convolutional neural network (FCN) that has proven highly effective for **semantic segmentation tasks.** U-Net is specifically designed to identify and classify each pixel into distinct land-cover categories such as, water, built-up areas, cropland, and tree cover. The architecture follows a **symmetric encoder - decoder structure** with skip connections that bridge corresponding layers between the encoder and decoder, ensuring that detailed spatial information is preserved while the network learns broader contextual features.

The **encoder (contracting path)** extracts increasingly abstract spatial spectral features from the input images through successive convolutional blocks, with filter depths of 32, 64, 128, and 256. Each block is composed of two convolutional layers followed by batch normalization, **ReLU activation**, **dropout**, and **max pooling** for downsampling. The **dropout rate** was optimized between **0.05 and 0.1** to balance regularization and feature learning, preventing overfitting without hindering model convergence. The **bottleneck layer**, consisting of 512 filters, captures deep and compact feature representations of the image.

The **decoder (expansive path)** restores the spatial dimensions using **transposed convolutions (up-convolutions)** and concatenates the corresponding encoder outputs through skip connections, enabling the network to reconstruct high-resolution segmentation maps with accurate boundary delineation. The final 1*1 convolution layer with a **softmax activation function** generates a five-channel output, representing the probability of each pixel belonging to one of the land-cover classes (Ronneberger et al., 2015).

Table 2: Spectral indices used in the study

Indices	Full Name	Formula	Purpose	References
NDVI	Normalized Difference Vegetation Index	$\frac{\text{NIR-RED}}{\text{NIR+RED}}$	Separates vegetation from non- vegetation classes	(Rouse et al., 1973)
SAVI	Soil Adjusted Vegetation Index	$\frac{(NIR - Red)}{(NIR + Red + L)} \times (1 + L)$, where $L = 0.5$	Improves vegetation detection in sparse or soil-exposed areas	(Huete, 1988)
EVI	Enhanced Vegetation Index	$2.5 \times \frac{(NIR - Red)}{(NIR + 6 \times Red - 7.5 \times Blue + 1)}$	Enhances dense vegetation mapping and reduces atmospheric noise	(Huete et al., 2002)
MSAVI	Modified Soil Adjusted Vegetation Index	$\frac{2 \times NIR + 1 - \sqrt{(2 \times NIR + 1)^2 - 8 \times (NIR - Red)}}{2}$	Distinguishes vegetation in mixed soil-vegetation pixels	(Qi et al., 1994)
GNDVI	Green Normalized Difference Vegetation Index	$\frac{\text{NIR-GREEN}}{\text{NIR+GREEN}}$	Detects vegetation health variations and crop conditions	(Gitelson et al., 1996)
NDWI	Normalized Difference Water Index	$\frac{\text{GREEN-NIR}}{\text{GREEN+NIR}}$	Extracts water bodies and separates water from land	(McFEETERS, 1996)
NDBI	Normalized Difference Built-Up Index	$\frac{\text{SWIR-NIR}}{\text{SWIR+NIR}}$	Identifies built-up/urban areas from vegetation and water	(Zha et al., 2003)

2.2.3.2 ResNet-50

The **ResNet-50 architecture** was conceptually integrated into the study as a potential **encoder backbone** for enhanced feature extraction in future work. **ResNet-50 (Residual Network with 50 layers)** introduces the principle of **residual learning**, where shortcut (identity) connections allow gradients to flow efficiently through the network, mitigating the vanishing gradient problem commonly observed in deep models.

The network is composed of an initial convolutional stem followed by four stages of **bottleneck residual blocks**, with filter depths increasing from 256 to 2048 (conv2_x to conv5_x). Each residual block contains a series of 1×1, 3×3, and 1×1 convolutions, enabling effective dimensionality reduction and hierarchical feature learning. ResNet-50 models are often **pretrained on large-scale datasets such as ImageNet**, providing robust initial feature representations that can be fine-tuned for specific tasks like land-cover classification. When integrated as the encoder in a U-Net configuration (forming a **ResU-Net**), it combines the spatial precision of U-Net's decoder with the deep semantic understanding of ResNet's encoder, enhancing segmentation performance and generalization across diverse landscapes (He et al., 2016).

2.2.4 Hyperparameter optimization

Prior to training, the dataset was divided into training and testing subsets using stratified sampling to preserve the proportional representation of all land-cover categories. Stratification was based on the dominant class within each image tile, ensuring balanced class distribution across both subsets. The training data were used to optimize model weights, while the validation data provided an unbiased measure of model generalization. This process was initially applied to the Mahottari dataset, which served as the base dataset for model training. The network was compiled using the Adam optimizer (Kingma & Ba, 2014) with a base learning rate of $1*10^{-4}$, and a decay constant of 10^{-4} was introduced to gradually reduce the learning rate as training progressed, promoting stable convergence. To further refine this process, a ReduceLROnPlateau callback was employed, automatically reducing the learning rate when validation loss plateaued, thereby facilitating more efficient optimization.

Hyperparameter optimization played a crucial role in achieving an optimal trade-off between computational efficiency, segmentation accuracy, and training stability. Three tile sizes (128*128, 256*256, and 512*512) pixels were tested to evaluate their influence on spatial context and computational demand. Similarly, various batch sizes (4, 8, and 16) were experimented with to determine optimal memory–convergence trade-offs. The dropout rate was fine-tuned between 0.05 and 0.1, where 0.1 provided slightly better regularization. The learning rate was dynamically adjusted using the ReduceLROnPlateau scheduler, which reduced the learning rate by half whenever the validation loss stagnated, ensuring smoother convergence. Furthermore, early stopping was used to terminate training once no further improvement in validation performance was observed, preventing overfitting and unnecessary computation (Bergstra & Bengio, 2012; Akiba et al., 2019).

2.2.5 Cross-area fine-tuning

Cross-area fine-tuning (CAFT) is a transfer learning approach that adapts a deep learning model trained in one geographic region (Mahottari) to another similar region (Dhanusha) with limited labeled data. The model initially learns general spatial and spectral features such as edges, shapes, vegetation textures, water bodies, and built-up patterns, which are largely transferable across regions. When applied to a new dataset, differences in spectral response, texture, and illumination may arise, but the pre-trained model provides a strong starting point. This

leads to faster convergence, reduced risk of overfitting, and improved classification performance, especially when the target dataset is small or less diverse (Pan & Yang, 2010; Shin et al., 2016).

The fine-tuning process is carried out in two phases to effectively adapt the model to the Dhanusha dataset. In the first phase, a significant portion of the network (mainly the encoder) is frozen, and only the decoder is trained, allowing the model to map previously learned generic features to new land cover classes without losing important spatial representations. In the second phase, all layers are unfrozen and trained together using a smaller learning rate, enabling subtle adjustments across the entire network. This controlled update helps the model adapt to local variations such as soil color, vegetation reflectance, and urban patterns, while preserving the valuable knowledge learned from the source region.

2.2.6 Performance evaluation

The evaluation focuses on several quantitative metrics -Accuracy, Precision, Recall, F1-Score, as well as qualitative assessments through visual inspection of output maps and confusion matrices. Together, these approaches help determine whether the model is robust enough for operational LULC monitoring and decision-making applications in the Dhanusha district.

Accuracy measures the overall proportion of correctly classified pixels relative to the total number of pixels in the validation dataset. It provides a general sense of model performance but can be misleading in cases where certain land cover classes dominate the dataset (Powers, 2011). To address this, Precision and Recall are calculated to evaluate class-specific performance. Precision quantifies the percentage of correctly predicted pixels among all pixels predicted for a particular class, reflecting the model's ability to avoid false positives (Sokolova & Lapalme, 2009). Recall, on the other hand, measures the percentage of correctly identified true class pixels out of all actual pixels of that class, indicating how effectively the model detects specific features such as forest, water, or urban areas (Sokolova & Lapalme, 2009). Together, they provide insight into both the reliability and sensitivity of the model's predictions.

The F1-Score, computed as the harmonic mean of Precision and Recall, balances the trade-off between the two metrics, making it particularly useful for imbalanced datasets where some land cover types are underrepresented (Sokolova & Lapalme, 2009).

2.2.7 LULC map preparation

Finally, the optimized models generate comprehensive **LULC classified tiles** providing actionable insights for agricultural planning, flood risk management, and urban development across both districts. The workflow's geographic specialization - training on Mahottari's landscapes and fine-tuning for Dhanusha's unique conditions ensures high accuracy while demonstrating how residual connections in ResUNet improve feature learning for complex terrain compared to standard U-Net implementations.

3. RESULTS AND DISCUSSIONS

3.1 U-net segmentation

This study implemented a U-Net–based semantic segmentation framework for Land Use Land Cover (LULC) classification using a cross-area fine-tuning approach, where a model trained on Mahottari district was adapted and evaluated on Dhanusha district to assess spatial transferability and generalization capability (Tuia et al., 2016). Five LULC classes were classified using both RGB Sentinel imagery and composite spectral indices, which improved feature representation by capturing vegetation, moisture, soil, and built-up characteristics (Stoian et al., 2019). The overall accuracy for each RGB and composite is presented in *Table 3*.

For RGB-based segmentation, the U-Net model was trained using multiple tile sizes

and batch sizes with the Adam optimizer, dropout regularization, and L2 weight decay to reduce overfitting (Kingma & Ba, 2014; Srivastava et al., 2014). Results showed that larger tile sizes provided better spatial context for segmentation, with the 512×512 tile size achieving the highest accuracies of 0.95 in Mahottari and 0.94 after fine-tuning on Dhanusha. Cropland and Tree Cover classes achieved the highest precision and F1-scores, while Water Bodies and Built-Up classes showed lower recall due to spectral mixing and smaller object sizes. *Figure 3* and *Figure 4* shows training and validation curves indicating stable convergence and effective overfitting control (Ronneberger et al., 2015). *Table 4* Per class precision,recall and F1 score for each class for RGB and composite.

For segmentation using composite spectral indices, the same U-Net architecture and cross-area fine-tuning strategy were applied. The integration of spectral indices improved the discrimination of complex land-cover classes by combining spectral and spatial information (Stoian et al., 2019). Adaptive learning-rate scheduling using ReduceLROnPlateau enhanced training stability. The best performance was achieved with the 256×256 tile size, reaching accuracies of 0.95 in Mahottari and 0.93 in Dhanusha. *Table 5* presents U-Net segmentation prediction for different tiles of Dhanusha district.

3.2 ResNet-50 segmentation

This study employed a ResNet-50–based semantic segmentation framework for Land Use Land Cover (LULC) classification using a cross-area fine-tuning approach. The model was trained on Mahottari district data and fine-tuned on Dhanusha district to evaluate spatial transferability and generalization. Five LULC classes -Water, Cropland, Built-Up, Tree Cover, and Others were classified using both RGB imagery and composite spectral indices. Training utilized different tile sizes (128×128, 256×256, and 512×512) and batch sizes, while optimization included ReduceLROnPlateau learning-rate scheduling, dropout regularization, L2 regularization, and early stopping to minimize overfitting.

For RGB-based segmentation, larger tile sizes improved performance by providing greater spatial context for identifying complex land-cover patterns. The best results were achieved with 512×512 tiles, producing accuracies of 0.96 in Mahottari and 0.95 after fine-tuning on Dhanusha that is presented in *Table 6*. Although slight performance reduction occurred due to regional spectral differences, the high accuracy demonstrated the effectiveness of cross-area fine-tuning for improving model generalization in regions with limited labeled data (Tuia et al., 2016). Cropland, Tree Cover, and Others classes achieved high precision, recall, and F1-scores above 0.95, while Water and Built-Up classes showed lower recall because of spectral confusion with surrounding land-cover types as shown in *Table 7*. Training and validation curves shows stable convergence and controlled overfitting as presented in *Figure 5* and *Figure 6*.

The study also integrated composite spectral indices into the ResNet-50 encoder within a U-Net segmentation framework. Residual connections enhanced deep spatial-spectral feature extraction and reduced gradient degradation during training. The 256×256 tile size achieved the best performance, with accuracies of 0.95 in Mahottari and 0.94 in Dhanusha, suggesting that moderate tile sizes provide a better balance between spatial context and training stability (Hoeser & Kuenzer, 2020). The integration of spectral indices significantly improved segmentation robustness and transferability across geographically distinct regions for remote sensing–based LULC classification (Persello et al., 2022). *Table 8* presents ResNet-50 segmentation prediction for tiles of Dhanusha district.

3.3 Discussions

This study examined the comparative performance of deep learning architectures,

U-Net and ResNet-50 for semantic segmentation of LULC from Sentinel-2 imagery, emphasizing cross-area fine-tuning, hyperparameter optimization, and spectral index fusion. The findings reveal that both architectures exhibit strong potential for automated LULC mapping across agro-ecologically similar districts in Nepal, with ResNet-50 outperforming U-Net in overall accuracy and generalization. However, the performance gap narrows when composite spectral indices are introduced, highlighting the importance of input spectral richness in deep feature extraction.

The analysis across tile sizes (128×128, 256×256, 512×512) revealed a consistent relationship between spatial context and model performance. Both U-Net and ResNet-50 achieved their best balance of accuracy and class sensitivity at 256×256, with larger tiles (512×512) slightly improving overall accuracy but degrading recall for minority classes such as Water and Built-Up. This supports findings by (Kattenborn et al., 2021) and (Mboga et al., 2017), who emphasized that intermediate receptive fields preserve both fine spatial detail and global context. Excessively small tiles limit contextual awareness, while excessively large one's blur class boundaries, particularly in heterogeneous landscapes.

Hyperparameter optimization was also critical for convergence stability. Learning rate 10^{-4} using **ReduceLROnPlateau scheduling, dropout rate of 0.1**, **L2 regularization of 10^{-4}** produced the most robust results. These configurations align with the optimization strategies described by (Goyal et al., 2017), where moderate dropout and controlled learning rates reduce overfitting in convolutional networks(Prechelt, 2012).

A major finding of this study was the significant improvement achieved when spectral indices were incorporated as composite inputs. The addition of these indices enhanced the discriminative capability of both architectures, particularly in separating Built-Up and Water classes from spectrally similar surfaces such as bare soil or vegetation. This improvement mirrors conclusions from (Stoian et al., 2019) and (Zhang et al., 2019), who reported that spectral index fusion provides complementary biophysical information such as vegetation vigor, moisture content, and urban reflectance thereby reducing class confusion.

For instance, NDWI and NDBI improved separability between urban and aquatic features (Xu, 2006: Zha et al., 2003; McFeeters, 1996), while NDVI and SAVI stabilized vegetation classification by mitigating soil background noise (Huete, 1988; Tucker, 1979). Consequently, the composite-based ResNet-50 achieved 0.94 overall accuracy and an average F1-score of 0.86, outperforming its RGB counterpart by approximately +0.02 in F1. This trend validates findings by (Phiri et al., 2020) and (Talukdar et al., 2020), who demonstrated that integrating spectral indices substantially enhances class-level precision in multispectral segmentation.

The U-Net architecture demonstrated strong performance (OA = 0.92–0.94) with robust generalization under cross-area fine-tuning. However, ResNet-50 consistently outperformed U-Net across both RGB and composite configurations, attaining peak accuracy of 0.95 with RGB and 0.94 with spectral indices. This superiority arises from ResNet's residual connections, which facilitate deeper feature propagation without gradient vanishing (He et al., 2016). The skip connections in ResNet-50 allowed for hierarchical learning of both local textures and global spatial dependencies, crucial for distinguishing spectrally overlapping classes such as Built-Up and Cropland. Similar conclusions were reported by (Audebert et al., 2016) and (Maggiori et al., 2017).

Cross-Area Fine-Tuning played a pivotal role in enhancing generalization between the Mahottari (source) and Dhanusha (target)

districts. Models pretrained on Mahottari imagery and fine-tuned on Dhanusha exhibited high transferability for vegetation-dominated classes, Cropland and Tree Cover achieving recall values above 0.95. This aligns with the observations of (Yosinski et al., 2014), who highlighted that feature reuse across similar domains accelerates convergence and mitigates overfitting. However, transfer performance declined for Water and Built-Up classes due to spatial heterogeneity and class imbalance, a common challenge in land-cover modeling (Castelluccio et al., 2015).

Misclassification between Water and Agriculture classes was mainly caused by similar spectral reflectance in shallow water, moist soil, and dry agricultural land (Qiu et al., 2020; Wurm et al., 2019). NDWI and EVI helped reduce this confusion by improving spectral contrast. In this study, bare land was mostly labeled as Cropland because it represented fallow farmland, while urban bare surfaces were classified as Built-Up. This created spectral ambiguity between Cropland and Built-Up classes, while shallow and sediment-rich water bodies reduced Water classification accuracy in heterogeneous rural landscapes.

Table 3: Overall accuracy U-net segmentation

Tile Size	Batch Size	Epochs	dropout	Overall Accuracy(RGB)		Overall Accuracy(Composite)	
				Model Trained and Tested on Mahottari	Model Fine Tuned on Dhanusha	Model Trained and Tested on Mahottari	Model Fine Tuned on Dhanusha
128*128	16	60	0.1	0.93	0.91	0.93	0.92
256*256	8	60	0.1	0.93	0.92	0.95	0.93
512*512	4	60	0.1	0.95	0.94	0.92	0.90

Table 4: Accuracy metrics U-net segmentation

S.N	Class	U-Net (RGB)			U-Net (Composite)		
		Precision	Recall	F1-Score	Precision	Recall	F1-Score
1	Water Bodies	0.65	0.57	0.61	0.74	0.64	0.69
2	Cropland	0.92	0.96	0.94	0.93	0.96	0.95
3	Built-Up	0.76	0.42	0.54	0.76	0.52	0.62
4	Tree Cover	0.92	0.97	0.94	0.93	0.98	0.96
5	Others	1.0	0.94	0.97	1.0	0.95	0.97

Table 5: U-net segmentation prediction

Tiles	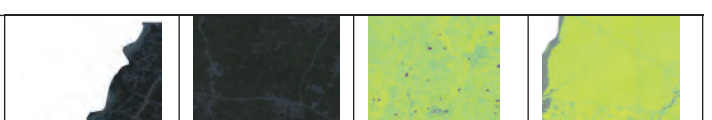
Masks	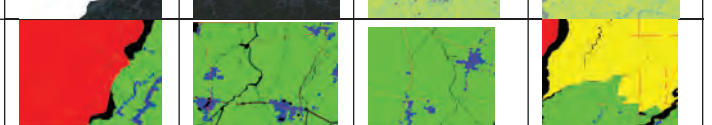
Prediction	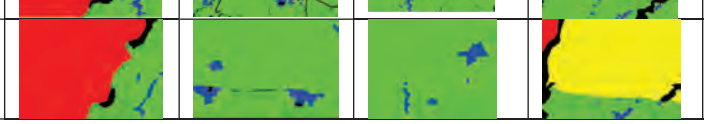

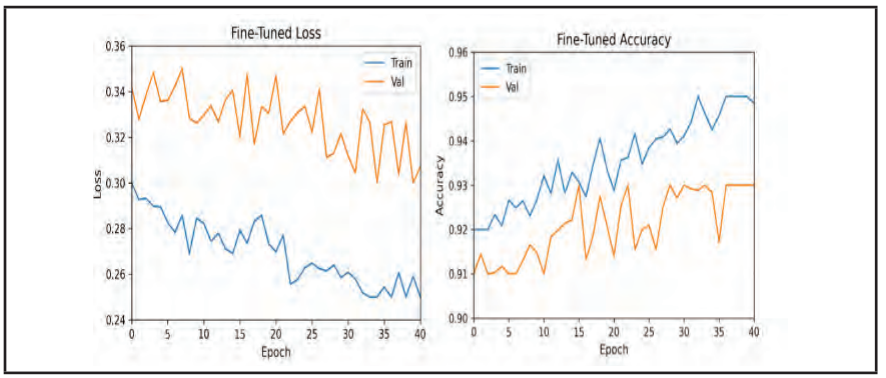

Figure 3 :Fine-Tuned loss and accuracy (RGB) U-net

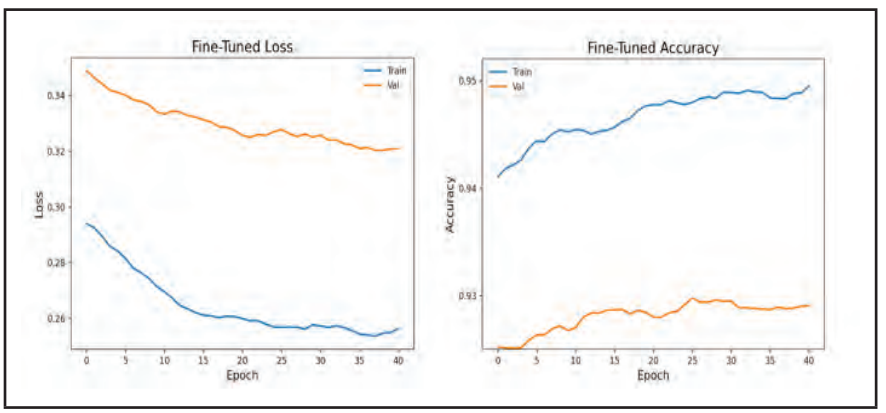

Figure 4 :Fine-tuned loss and accuracy (Composite) U-Net

Table 6: Overall accuracy ResNet-50 segmentation

Tile Size	Batch Size	Epochs	dropout	Overall Accuracy(RGB)		Overall Accuracy(Composite)	
				Model Trained and Tested on Mahottari	Model Fine Tuned on Dhanusha	Model Trained and Tested on Mahottari	Model Fine Tuned on Dhanusha
128*128	16	60	0.1	0.93	0.92	0.93	0.92
256*256	8	60	0.1	0.95	0.93	0.95	0.94
512*512	4	60	0.1	0.96	0.95	0.89	0.87

Table 7: Accuracy metrics Res-net-50 segmentation

		ResNet-50 (RGB)			ResNet-50 (Composite)		
S.N	**Class**	**Precision**	**Recall**	**F1-Score**	**Precision**	**Recall**	**F1-Score**
1	Water Bodies	0.85	0.56	0.67	0.82	0.68	0.74
2	Cropland	0.92	0.98	0.95	0.94	0.98	0.96
3	Built-Up	0.79	0.52	0.63	0.77	0.60	0.67
4	Tree Cover	0.95	0.98	0.96	0.95	0.99	0.97
5	Others	1.0	0.98	0.99	1.0	0.95	0.97

Table 8: ResNet-50 segmentation prediction

Tiles	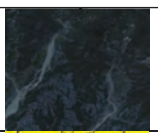	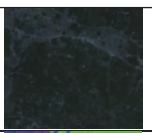	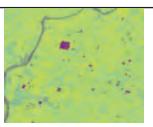	
Masks	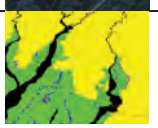	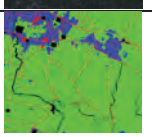	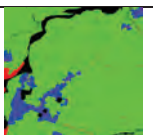	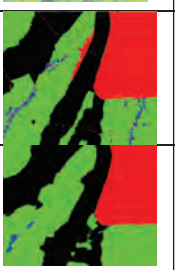
Prediction	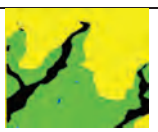		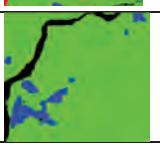	

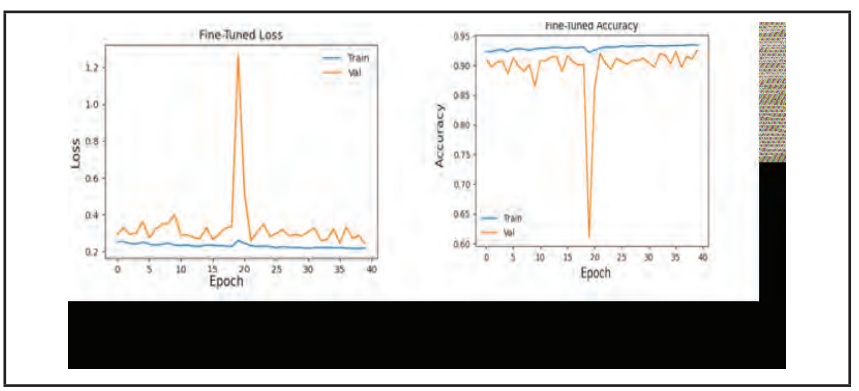

Figure 5:Fine-tuned loss and accuracy (RGB) ResNet-50

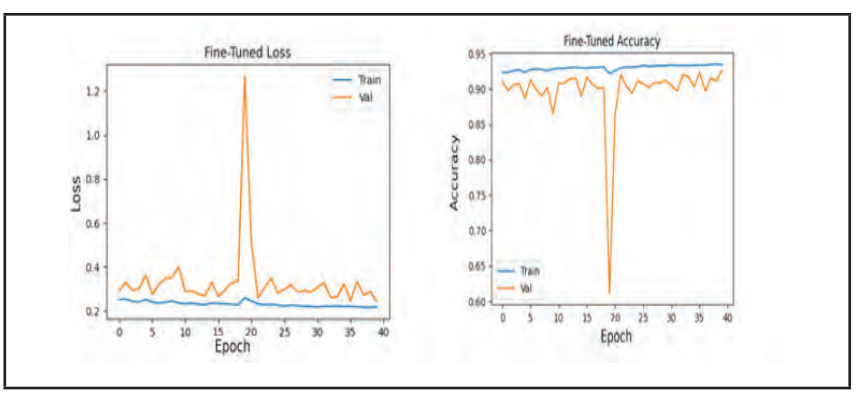

Figure 6: Fine-tuned loss and accuracy (Composite) ResNet-50

4. CONCLUIONS AND RECOMMENDATIONS

This study developed an optimized deep learning framework for Land Use/Land Cover (LULC) classification in the Terai districts of Mahottari and Dhanusha, Nepal, by integrating cross-area fine-tuning, hyperparameter optimization, and spectral-index fusion using Sentinel-2 imagery. Among the tested models, ResNet-50 outperformed U-Net, achieving an overall accuracy of 0.94 and an average F1-score of 0.86, while U-Net achieved an overall accuracy of 0.93 and an F1-score of 0.84. The inclusion of spectral indices such as NDVI, NDWI, and NDBI improved class separability, particularly for vegetation and water-related classes. The optimal training configuration (256×256 tile size, batch size 8, dropout 0.1, and learning rate of 10^{-4}) provided stable convergence and balanced computational efficiency.

The study concludes that combining cross-area fine-tuning with spectral-index integration and optimized training strategies offers a scalable and data-efficient solution for LULC mapping in data-scarce regions. However, limitations such as the use of single-date imagery, limited field data for minority classes, and computational constraints affected model generalization and exploration. Future research should incorporate automated hyperparameter optimization methods, additional data sources such as SWIR bands, topographic information, and multi-temporal imagery, as well as advanced architectures including ResUNet, DeepLabv3+, and Transformer-based models to further improve classification accuracy and large-scale environmental monitoring.

REFERENCES

Akiba, T., Sano, S., Yanase, T., Ohta, T., & Koyama, M. (2019). *Optuna: A Next-generation Hyperparameter Optimization Framework* (Version1)

Audebert, N., Saux, B. L., & Lefèvre, S. (2016). *Semantic Segmentation of Earth Observation Data Using Multimodal and Multi-scale Deep Networks* (Version 1).

Bergstra, J., & Bengio, Y. (2012). Random Search for Hyper-Parameter Optimization. *Journal of Machine Learning Research*, *13*(10), 281–305.

Castelluccio, M., Poggi, G., Sansone, C., & Verdoliva, L. (2015). *Land Use Classification in Remote Sensing Images by Convolutional Neural Networks* (Version 1).

Diakogiannis, F. I., Waldner, F., Caccetta, P., & Wu, C. (2020). ResUNet-a: A deep learning framework for semantic segmentation of remotely sensed data. *ISPRS Journal of Photogrammetry and Remote Sensing*, *162*, 94–114.

Drusch, M., Del Bello, U., Carlier, S., Colin, O., Fernandez, V., Gascon, F., Hoersch, B., Isola, C., Laberinti, P., Martimort, P., Meygret, A., Spoto, F., Sy, O., Marchese, F., & Bargellini, P. (2012). Sentinel-2: ESA's Optical High-Resolution Mission for GMES Operational Services. *Remote Sensing of Environment*, *120*, 25–36.

Gevaert, C. M., & García-Haro, F. J. (2015). A comparison of STARFM and an unmixing-based algorithm for Landsat and MODIS data fusion. *Remote Sensing of Environment*, *156*, 34–44.

Gitelson, A. A., Kaufman, Y. J., & Merzlyak, M. N. (1996). Use of a green channel in remote sensing of global vegetation from EOS-MODIS. *Remote Sensing of Environment*, *58*(3), 289–298.

Goyal, P., Dollár, P., Girshick, R., Noordhuis, P., Wesolowski, L., Kyrola, A., Tulloch, A., Jia, Y., & He, K. (2017a). *Accurate, Large Minibatch SGD: Training ImageNet in 1 Hour* (Version 2).

He, K., Zhang, X., Ren, S., & Sun, J. (2016). Deep Residual Learning for Image Recognition. *2016 IEEE Conference on Computer Vision and Pattern Recognition (CVPR)*, 770–778.

Huete, A., Didan, K., Miura, T., Rodriguez, E. P., Gao, X., & Ferreira, L. G. (2002). Overview of the radiometric and biophysical performance of the MODIS vegetation indices. *Remote Sensing of Environment*, *83*(1–2), 195–213.

Huete, A. R. (1988). A soil-adjusted vegetation index (SAVI). *Remote Sensing of Environment*, *25*(3), 295–309.

Hoeser, T., & Kuenzer, C. (2020). Object Detection and Image Segmentation with Deep Learning on Earth Observation Data: A Review-Part I: Evolution and Recent Trends. Remote Sensing, 12(10), 1667.

Kattenborn, T., Leitloff, J., Schiefer, F., & Hinz, S. (2021). Review on Convolutional Neural Networks (CNN) in vegetation remote sensing. *ISPRS Journal of*

Photogrammetry and Remote Sensing, *173*, 24–49.

Kingma, D. P., & Ba, J. (2014). *Adam: A Method for Stochastic Optimization* (Version 9).

Ma, L., Liu, Y., Zhang, X., Ye, Y., Yin, G., & Johnson, B. A. (2019). Deep learning in remote sensing applications: A meta-analysis and review. *ISPRS Journal of Photogrammetry and Remote Sensing*, *152*, *166–177*.

Maggiori, E., Tarabalka, Y., Charpiat, G., & Alliez, P. (2017). Convolutional Neural Networks for Large-Scale Remote-Sensing Image Classification. *IEEE Transactions on Geoscience and Remote Sensing*, *55*(2), 645–657.

Mboga, N., Persello, C., Bergado, J., & Stein, A. (2017). Detection of Informal Settlements from VHR Images Using Convolutional Neural Networks. *Remote Sensing*, *9*(11), 1106.

McFeeters, S. K. (1996). The use of the Normalized Difference Water Index (NDWI) in the delineation of open water features. *International Journal of Remote Sensing*, *17*(7), 1425–1432.

Mountrakis, G., Im, J., & Ogole, C. (2011). Support vector machines in remote sensing: A review. *ISPRS Journal of Photogrammetry and Remote Sensing*, *66*(3), 247–259.

Pan, S. J., & Yang, Q. (2010). A survey on transfer learning. *IEEE Transactions on Knowledge and Data Engineering*, *22*(10), 1345–1359.

Paudel, B., Zhang, Y., Li, S., & Liu, L. (2018). *Spatiotemporal changes in agricultural land cover in Nepal over the last 100 years*. *28*.

Persello, C., Wegner, J. D., Hansch, R., Tuia, D., Ghamisi, P., Koeva, M., & Camps-Valls, G. (2022). Deep Learning and Earth Observation to Support the Sustainable Development Goals: Current approaches, open challenges, and future opportunities. *IEEE Geoscience and Remote Sensing Magazine, 10(2), 172–200.*

Powers, D. M. W. (2011). Evaluation: From precision, recall and F-measure to ROC, informedness, markedness and correlation. *Journal of Machine Learning Technologies*, *2*(1), 37–63.

Prechelt, L. (2012). Early Stopping—But When? In G. Montavon, G. B. Orr, & K.-R. Müller (Eds.), *Neural Networks: Tricks of the Trade* (Vol. 7700, pp. 53–67).

Qiu, C., Schmitt, M., Geiß, C., Chen, T.-H. K., & Zhu, X. X. (2020). A framework for large-scale mapping of human settlement extent from Sentinel-2 images via fully convolutional neural networks. *ISPRS Journal of Photogrammetry and Remote Sensing*, *163*, 152–170.

Richards, J. A., & Jia, X. (1999). *Remote Sensing Digital Image Analysis: An Introduction*. Springer.

Rouse, J., Haas, R. H., Schell, J. A., & Deering, D. (1973). *Monitoring vegetation systems in the great plains with ERTS*.

Shin, H. C., Roth, H. R., Gao, M., Lu, L., Xu, Z., Nogues, I., & Summers, R. M. (2016). Deep convolutional neural networks for computer-aided detection: CNN architectures, dataset characteristics and transfer learning. *IEEE Transactions on Medical Imaging*, *35*(5), 1285–1298.

Sokolova, M., & Lapalme, G. (2009). A systematic analysis of performance measures for classification tasks. *Information Processing & Management*, *45*(4), 427–437.

Srivastava, N., Hinton, G., Krizhevsky, A., Sutskever, I., & Salakhutdinov, R. (2014). Dropout: A Simple Way to Prevent Neural Networks from

Overfitting. *Journal of Machine Learning Research*, *15*(56), 1929–1958.

Stoian, A., Poulain, V., Inglada, J., Poughon, V., & Derksen, D. (2019). Land Cover Maps Production with High Resolution Satellite Image Time Series and Convolutional Neural Networks: Adaptations and Limits for Operational Systems. *Remote Sensing*, *11*(17), 1986.

Talukdar, S., Singha, P., Mahato, S., Shahfahad, Pal, S., Liou, Y.-A., & Rahman, A. (2020). Land-Use Land-Cover Classification by Machine Learning Classifiers for Satellite Observations—A Review. *Remote Sensing*, *12*(7), 1135

Tucker, C. J. (1979). Red and photographic infrared linear combinations for monitoring vegetation. *Remote Sensing of Environment*, *8*(2), 127–150.

Tuia, D., Persello, C., & Bruzzone, L. (2016). Domain Adaptation for the Classification of Remote Sensing Data: An Overview of Recent Advances. *IEEE Geoscience and Remote Sensing Magazine*, *4*(2), 41–57.

Uddin, K., Shrestha, H. L., Murthy, M. S. R., Bajracharya, B., Shrestha, B., Gilani, H., Pradhan, S., & Dangol, B. (2015). Development of 2010 national land cover database for the Nepal. *Journal of Environmental Management*, *148*, 82–90.

Wurm, M., Stark, T., Zhu, X. X., Weigand, M., & Taubenböck, H. (2019). Semantic segmentation of slums in satellite images using transfer learning on fully convolutional neural networks. *ISPRS Journal of Photogrammetry and Remote Sensing*, *150*, 59–69.

Xu, H. (2006). Modification of normalised difference water index (NDWI) to enhance open water features in remotely sensed imagery. *International Journal of Remote Sensing*, *27*(14), 3025–3033.

Yosinski, J., Clune, J., Bengio, Y., & Lipson, H. (2014). *How transferable are features in deep neural networks?*

Zha, Y., Gao, J., & Ni, S. (2003). Use of normalized difference built-up index in automatically mapping urban areas from TM imagery. *International Journal of Remote Sensing*, *24*(3), 583–594.

Zhang, C., Sargent, I., Pan, X., Li, H., Gardiner, A., Hare, J., & Atkinson, P. M. (2019). Joint Deep Learning for land cover and land use classification. *Remote Sensing of Environment*, *221*, 173–187.

Zhu, X. X., Tuia, D., Mou, L., Xia, G.-S., Zhang, L., Xu, F., & Fraundorfer, F. (2017). Deep Learning in Remote Sensing: A Comprehensive Review and List of Resources. *IEEE Geoscience and Remote Sensing Magazine*, *5*(4), 8–36.

Author's Information

Name	:	Hiralal Pardhe
Academic Qualification	:	M.E Geoinformatics
Organization	:	Survey Office Kalanki
Current Designation	:	Survey Officer

Obituary

All the officials of Survey Department pray to the almighty for eternal peace to the departed soul of the following officials of the department and this department will always remember the contribution they have made during their service period in this department.

Mahendra Chaudhary
Surveyor
18 August 2025

Umesh Prasad Kanu
Surveyor
25 September 2025

Devendra Nath Yadav
Then Survey Officer
15 October 2025

Tirtha Bahadur Pradhananga
Then Deputy Director General
10 November 2025

Rajendra Shrestha
Then Survey Officer
10 March 2026

Nepal Remote Sensing and Photogrammetric Society (NRSPS)

Executive Committee

Susheel Dangol, ***President***
susheeldangol@gmail.com

Er. Sanjeevan Shrestha, ***Vice President***
shr.sanjeevan@gmail.com

Er. Tina Baidar, ***Secretary***
tina.baidar13@gmail.com

Raj Kumar Thapa, ***Assistant Secretary***
thapark2013@gmail.com

Er. Girija Pokharel, ***Treasurer***
girija.pokhrel12@gmail.com

Members
Jagat Raj Poudel
jagatrajpoudel@hotmail.com

Roshani Sharma
anjarija@gmail.com

Er. Sushmita Timilsina
qust04sharma@gmail.com

Er. Dinesh Khatri
dineshkc7373@gmail.com

E-mail: nrspsociety@gmail.com

NRSPS conducted its **16th Annual General Meeting**, highlighted by the official launch of the **12th Earth Observation Newsletter** by esteemed chief guests.

The Society contributes as **Promotional Partner for CIPA Nepal Heritage School 2026** on "3D Surveying and Modelling Techniques for Cultural Heritage Documentation"

NRSPS organized a **technical seminar** on the "***Application of Photogrammetry for Cultural Heritage Mapping"*** in collaboration with the ISPRS Student Consortium which featured internationally renowned experts attracting a diverse audience of professionals, researchers, students, and enthusiasts in geomatics and cultural heritage.

The society officially signed the contract agreement for providing research grants to the winners of "**Research Grant Program**". The research grant was provided to one for the master's level and 2 for bachelor level research in the field of advanced photogrammetry and remote sensing techniques providing solutions to real field problems in context of Nepal.

Earth Observation
Editorial Board

Susheel Dangol, ***Advisor***
susheeldangol@gmail.com

Er. Pravesh Yagol, ***Chief Editor***
shrpravesh@gmail.com

Members

Er. Shankar K.C
Er. David Nhemaphuki
Er. Rajeev Gyawali

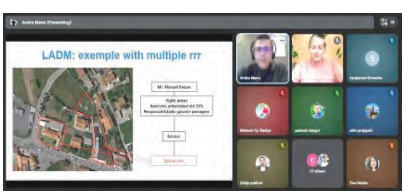

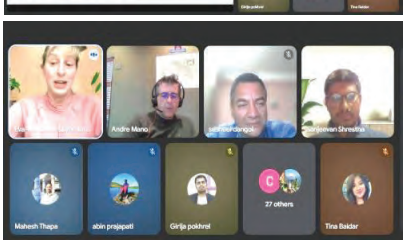

NRSPS launched its **Talk Series** with Episode 1, bringing together globally recognized expertise in land administration and Geoinformatics. This online knowledge-sharing session focuses on ***"Land Rights and Land Information with LADM and STDM"***, highlighting innovative frameworks and approaches shaping modern land governance. The event features distinguished speakers Dr. Eva-Maria Morscher-Unger from Kadaster International and Mr. André da Silva Mano from the University of Twente, offering valuable insights to professionals, researchers, and students engaged in geospatial sciences and land management.

Nepal Surveyor's Association (NESA)

NESA Central Executive Committee

President
Mr. Prakash Oli

Senior Vice President
Er. Sudarshan K. Gautam

Vice President
Mr. Uttam Khadka
Ms. Rupa Dotel Pudasaini

General Secretary
Mr. Dharma Raj Ojha

Secretary
Er. Ashok Kumar Rimal
Mr. Ram Kumar Shah
Mr. Rajiv Shrestha
Mr. Arjun Shrestha

Treasurer
Mr. Tilak Raj Joshi

Members
Mr. Arjun Dulal
Mr. Akash Kumar Chaudhary
Er. Rishi Acharya
Mr. Kali Bahadur Singh
Mr. Dipendra Khadka
Mr. Dipendra Pulami
Mr. Dipak B.K
Er. Naresh Bista
Mr. Prakash Kumar Karna
Mr. Mohan Datta Awasthi
Er. Rakesh Kumar Yadav
Mr. Raj Kumar Paudel
Mr. Roshan Bhandari
Ms. Sudha Shahi Adhikari
Mr. Harihar Chaulagain

Background

Following the restoration of multiparty democracy in 1990, the liberalization of civil society in Nepal facilitated the establishment of various professional and social entities. In this context, survey professionals across diverse sectors collaborated in 1991 to form the Nepal Surveyors' Association (NESA), which represents the first formally registered professional body for surveyors in the country.

Objectives

The primary mandate of the association is to formalize its status as a robust, operational platform for survey professionals across Nepal. To fulfill this mission, the organization pursues the following strategic objectives:

- **Public and Governmental Advocacy:** Sensitizing state actors and the general public to the critical nature of the surveying profession while mitigating risks associated with technical mismanagement.
- **Technological Advancement:** Enhancing service delivery by advising government agencies on the integration of contemporary geospatial tools and methodologies.
- **Professional Development:** Improving the technical competencies of members through domestic and international training, academic seminars, and expert consultations.
- **Socio-Economic Welfare:** Advocating for improved job security and career opportunities within both public and private sectors to elevate the standard of living for practitioners.
- **Equity and Professional Rights:** Safeguarding the rights of surveyors to ensure equitable access to opportunities and fostering an environment free from discrimination.
- **Educational Reform:** Contributing to the refinement of surveying and mapping curricula through targeted workshops and stakeholder interactions.
- **Reputational Management:** Actively addressing public misconceptions to enhance the social prestige and professional image of the surveying discipline.
- **Ethics and Integrity:** Enforcing a rigorous code of conduct to ensure practitioners maintain the highest standards of moral integrity and professional ethics.
- **Legislative Advocacy:** Lobbying for the ratification and implementation of the Survey Council Act and the Integrated Land Act to establish a comprehensive regulatory framework for national surveying activities.

Memberships Criteria

The association maintains specific eligibility criteria to ensure professional integrity and competence. Membership is open to any surveying professional who adheres to the established code of ethics and possesses a minimum of one year of formal vocational training in the field. The organizational structure categorizes its constituency into three distinct tiers: Life Members, General Members, and Honorary Members. As of the current reporting period, the association comprises a total of 2,031 registered members.

Nepal Geomatics Engineering Society (NGES)

website: www.nges.org.np email: contactgeomatics@gmail.com

Executive Committee

President
Er. Mahesh Thapa
Vice-President
Er. Bhuwan Singh Bisht
Secretary
Er. Ashok Shrestha
Joint-Secretary
Er. Pranjal Basnet
Treasurer
Er. Susmina Manandhar

Executive Members
Er. Binod Prasad Bhatta
Er. Gorkah Nath Pandey
Er. Samrat Acharya
Er. Sanisha Gharti Pun
Er. Vibek Dumre
Er. Dristi Bajimaya
Er. Sushil Subedi
Er. Kriti Kajol Chudal

Photo Feature

[Participants of Drone for Data talk program]

[Glimpse of online training for HOT mapping]

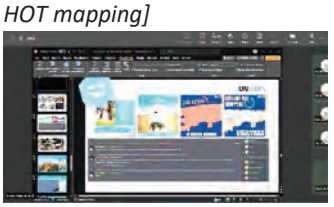

About NGES

Established on August 16, 2015, the Nepal Geomatics Engineering Society (NGES) serves as the premier umbrella organization for geomatics professionals across the country. NGES is dedicated to fostering the development of the discipline by connecting experts, promoting the application of geospatial technologies, enhancing professional skill sets, and safeguarding member rights. Through strategic advocacy, policy lobbying, and the execution of diverse professional programs, NGES actively cultivates an environment where geomatics engineering drives impactful contributions toward national development.

KEY EVENTS

Talk Program on "Drones for Data: Professional Applications and Lessons Learned in Nepal"

On June 6, 2025, NGES, in collaboration with the Nepal Engineers' Association, hosted a talk program at Pulchowk, Lalitpur, titled "Drones for Data: Professional Applications and Lessons Learned in Nepal." The event highlighted the vital role of drone technology in modern data acquisition, featuring expert insights from Er. Pravin Lamsal, Geomatics Engineer and Vice President of the Nepal Drone Association, who showcased applications ranging from surveying and mapping to wildlife monitoring. Additionally, Er. Ramesh Kumar Shah, Electronics Engineer and Inspector of the Nepal Police, detailed the integration of drones in critical security and search-and-rescue operations. Closing the session, NGES President Er. Mahesh Thapa emphasized the importance of expanding the adoption of drone technology as a highly effective method for geospatial data collection.

Orientation and Mock Test Programs

On July 8, 2025, NGES organized an orientation program and free mock tests for the Nepal Engineering Council (NEC) license examination to familiarize Geomatics Engineering graduates with the test's format and provide essential preparation guidance. Subsequently, on July 19, 2025, NGES conducted a specialized guidance program to support candidates preparing for the interview and group discussion stages of the survey officer examination.

Agricultural Waterways Mapping of Southern Maritania

In collaboration with UN Mappers, NGES participated in the Humanitarian OpenStreetMap Team (HOT) project to map agricultural waterways in Southern Mauritania. NGES launched a campaign and facilitated training for participants to contribute to this mapping initiative. On August 14, 2025, Michael Mantani, coordinator of the UN Mappers community, led an online training session to guide the project's technical execution.

HOT Mentorship Program

NGES collaborated with the Humanitarian Open Mapping Community Working Group to participate in the HOT Mentorship Program. Through this partnership, three NGES members served as mentors, providing guidance and support to participants within the global mapping community.

Felicitating academic excellence in Geomatics Engineering: Bachelor's toppers and a recent PhD graduate in the field-during the 9th Global Surveyors' Day, jointly organized by the Survey Department and NICS.

Observation at the CORS station

Expert team setting up the LiDAR sensor and receiver before conducting airborne LiDAR survey

Joint inspection of Nepal-India boundary field work

The first Nepal-India boundary Field Survey Team (FST) meeting held by Field Team 2 at Rasaul, India, on 24th March 2026.

Nepali delegation team from the Ministry of Land Management, Cooperatives and Poverty Alleviation, Survey Department, Department of Land Management and Archives, Land Management Training Center, and Ministry of Finance during a visit to Jakarta and Yogyakarta, Indonesia, from 11-15 August 2025.

Making Sense of Geo-spatial data for total solution in National and Local Development Activities

Available Maps and Data

- Geodetic Control Data
- CORS Station Data
- Geoid Data
- Aerial Photographs
- Topographic Base Maps
  - Terai and middle mountain at the scale of 1:25,000
  - High hills and Himalayas at the scale of 1:50,000
- Land Use Maps
- LiDAR Data
- Political and Administrative Map of Nepal
- Digital Topographic Data at scales 1:25,000 & 1:50,000
- Cadastral Plans
- Orthophoto Maps
- Image Data
- SOTER Data
- Topographic Digital Data at scales 1:100,000 1:250,000 1:500,000 1:1,000,000

Available Services

- Establishment of control points for various purposes of Surveying and Mapping
- Cadastral Surveying
- Surveying and mapping for development activities
- Topographic and large scale mapping
- Digital geo-spatial database support
- GIS Development

Price of some of the publications of Survey Department

- List of Geographical Names, Volume I to V – NRs 600/- per volume.
- The Population and Socio - Economic Atlas of Nepal, 2011 (HardCopy) NRs.2,500.00 (In Nepal), €200.00 (Outside Nepal)
- The Population and Socio - Economic Atlas of Nepal, 2011 (CDVersion) NRs.250/-

Contact Address:

SURVEY DEPARTMENT

Min Bhawan, Kathmandu, Nepal
Phone: +977-1 -4106508, Fax: +977-1 -4106757
E-mail: info@dos.gov.np
website: www.dos.gov.np

ISSN 2717-5022